CRUSTAL STRUCTURE OF THE EASTERN MEDITERRANEAN AND BLACK SEA BASINS FROM SATELLITE ALTIMETRY AND SHIPBORNE GRAVITY DATA

Doctor of Philosophy

Marine Geology and Geophysics
Middle East Technical University
Graduate School of Marine Sciences

by

Devrim TEZCAN

Mersin - TURKEY
February 2008

Approval of the thesis:

CRUSTAL STRUCTURE OF THE EASTERN MEDITERRANEAN AND BLACK SEA BASINS FROM SATELLITE ALTIMETRY AND SHIPBORNE GRAVITY DATA

submitted by Devrim TEZCAN in partial fulfillment of the requirements for the degree of Doctor of Philosophy in Marine Geology and Geophysics department, Institute of Marine Sciences, Middle East Technical University by,

Prof. Dr. Ferit BİNGEL
Director, Graduate School of Marine Sciences, METU   ———————————

Assoc. Prof. Dr. Semal YEMENİCİOĞLU
Head of Department, Marine Geology and Geophysics
Graduate School of Marine Sciences, METU   ———————————

Prof. Dr. Mahmut OKYAR
Supervisor, Department of Geophysics,
Süleyman Demirel University   ———————————

Examining Committee Members:

Prof. Dr. Özden BAŞTÜRK
Faculty of Fisheries, Mersin University   ———————————

Prof. Dr. Mahmut OKYAR
Department of Geophysics, Süleyman Demirel University   ———————————

Prof. Dr. Ferit BİNGEL
Graduate School of Marine Sciences, METU   ———————————

Prof. Dr. Süleyman TUĞRUL
Graduate School of Marine Sciences, METU   ———————————

Prof. Dr. Nilgün KUBİLAY
Graduate School of Marine Sciences, METU   ———————————

I hereby declare that all information in this document has been obtained and presented in accordance with academic rules and ethical conduct. I also declare that, as required by these rules and conduct, I have fully cited and referenced all material and results that are not original to this work.

Devrim TEZCAN

_____

ABSTRACT

Crustal Structure of the

Eastern Mediterranean and Black Sea Basins

From Satellite Altimetry And Shipborne Gravity Data

TEZCAN, Devrim

Ph.D. in Marine Geology and Geophysics

Supervisor: Prof. Dr. Mahmut OKYAR

February 2008, 106pp.

The crustal structures of the Black Sea and Eastern Mediterranean Sea are analyzed by gravity modeling method using satellite altimeter derived gravity data.

Firstly, the satellite gravity data were compared with available ship borne gravity data. It is considered that the satellite data is suitable for regional studies, however, for small-scale detailed studies, the satellite data have to be improved with new altimeter data.

Then, Free-air and Simple Bouguer Anomaly maps were compiled from the satellite gravity data for Black Sea and Eastern Mediterranean Sea. To calculate the Simple Bouguer anomalies the sea water density (1.03 g/cm^3) was replaced by average rock density (2.69 g/cm^3). From the maps, it is concluded that bathymetric features affect the anomalies in Eastern Mediterranean, but are not significant in Black Sea.

Finaly, the gravity models of the crust structures of the Black Sea and Eastern Mediterranean were constructed and gravity response of the models were calculated. From the model results that Moho rises up to 19 km in Black Sea, and 22 km in Eastern Mediterranean. The thinnest crust (~5km) exists in western Black Sea basin. In the Mediterranean Sea, the thickness of the crust ranges from 9 km in Levantine Basin and 25 km off the Anatolia.

Keywords: Black Sea, Eastern Mediterranean, gravity, satellite altimetry, Moho depth

ÖZ

Uydu ve Deniz Gravite Verileri ile
Doğu Akdeniz ve Karadeniz Havzalarının
Kabuk Yapısı

TEZCAN, Devrim
Doktora Tezi, Deniz Jeolojisi ve Jeofiziği
Tez Danışmanı: Prof. Dr. Mahmut OKYAR
Şubat 2008, 106 sayfa.

Karadeniz ve Doğu Akdeniz'in kabuk yapısı, uydu altimetri verisinden türetilen gravite verisi kullanılarak gravite modellemesi ile araştırılmıştır.

Öncelikle, uydu gravite verisi mevcut gemi gravite verisi ile karşılaştırılmıştır. Uydu verisinden türetilen gravite verisinin geniş alanlarda yapılacak çalışmalar için uygun, ancak küçük ölçekli, detay çalışmaları için, bu verilerin yeni altimetri verileri ile geliştirilmesi gerektiği düşünülmektedir.

İkinci olarak, uydu gravite verilerinden Karadeniz ve Doğu Akdeniz için Serbest-Hava ve Basit Bouguer Anomali haritaları oluşturulmuştur. Basit Bouguer haritası için suyun 1.03 g/cm^3 olan yoğunluğu, ortalama kayaç yoğunluğu kabul edilen 2.69 g/cm^3 ile değiştirilmiştir. Bu haritalardan deniz tabanındaki morfolojik yapıların Doğu Akdeniz'de gravite anomalisi yarattığı ama Karadeniz'de çok etkili olmadığı sonucuna varılmıştır.

Son olarak, Karadeniz ve Doğu Akdeniz'in kabuk yapılarının gravite modelleri yapılmış, ve bunların gravite cevapları hesaplanmıştır. Model sonuçlarına göre Moho derinliği Karadeniz'in altında 19 km'ye, Doğu Akdeniz'de 22 km'ye kadar yükseldiği tespit edilmiştir. En ince kabuk 5 km ile batı Karadeniz havzasının altında yer almaktadır. Doğu Akdeniz'de kabuk kalınlığı Levant Havzası'nda 9 km ile Anadolu açıklarında 25 km arasında değişmektedir.

Anahtar Kelimeler: Karadeniz, Doğu Akdeniz, gravite, uydu altimetri, Moho derinliği

ACKNOWLEDGMENTS

TABLE OF CONTENT

LIST OF TABLES

LIST OF FIGURES

1   Introduction

The eastern Mediterranean and the Black Sea area has been recognized as an excellent "natural laboratory" for studying the kinematics and dynamics of plate interactions because of the wide variety of tectonic processes, including continental collision, subduction, continental extension, continental escape, strike-slip faults and a variety of smaller-scale processes associated with African-Arabian-Eurasian plate interactions (Aksu et al., 2005a; McClusky et al., 2000; Robertson, 1998a). All these features made this relatively small region one of the most extensively studied areas of the world. Despite these extensive researches, different hypotheses, internally self-consistent, have been proposed to explain the crustal structure and tectonism of the area. This is because the complex deformation associated with plate interactions.

1.1   The study area

The study area covers the eastern part of the Mediterranean Sea, defined as the easternmost Mediterranean (east of 28°E longitude; Robertson 1998a), and the Black Sea (Figure 1.1).
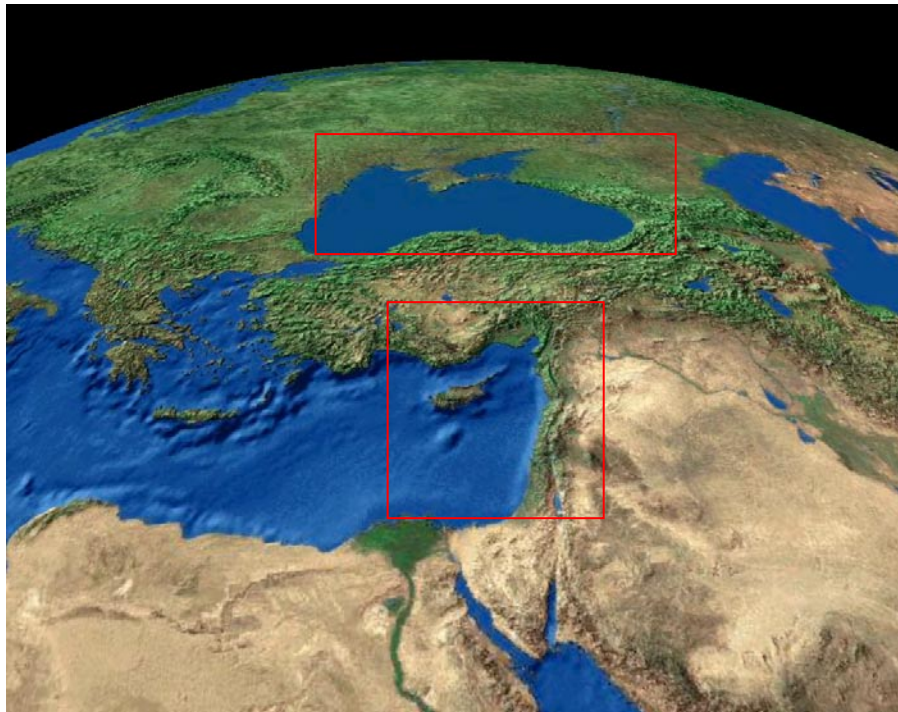
Figure 1.1 Study area.

1.1.1   Previous investigations in the study area

Eastern Mediterranean, as an excellent natural laboratory including several geodynamic mechanisms, has been investigated for a long time. Several authors (Vening-Meinesz, 1934; Cooper et al., 1952; Girdler and Harrison, 1957; Gass and Masson-Smith, 1963) studied the region with sparse gravity data.

With 1970s, several studies have been carried out to investigate the crustal structure of the eastern Mediterranean by utilizing extensive gravity data (Rabinowitz and Ryan, 1970; Woodside and Bowin, 1970; Özelçi, 1972; Finetti and Morelli, 1973; Morelli et al., 1975; Makris and Stobbe, 1984). Rabinowitz and Ryan (1970) were used the gravity profiles taken by R/V Conrad (Lamont Doherty Geological Observatory) in 1965 to determine the variation of surface sedimentary cover thickness.

Woodside and Bowin (1970) studied the crustal structure of the eastern Mediterranean using the gravity data compiled from Woods Hole Oceanographic cruises of the R/V Chain in 1964 and 1966. They constructed a crustal structure model along a north – south profile from free-air anomaly data to determine the Moho depth. Rabinowitz and Ryan (1970) and Woodside and Bowin (1970) published the free-air anomalies map of the Eastern Mediterranean.

Finetti and Morelli (1973), and Morelli et al. (1975) investigated the geophysics of the whole Mediterranean combining bathymetric, seismic, gravimetric and magnetic data.

Gravity studies in the Black Sea started in 1960s (Balavadze and Mindeli, 1965; Mindeli et al., 1965). In 1988, a special issue of Bollettino Di Geofisica on geological and geophysical properties of the Black Sea was published (Bocaletti et al., 1988a; Bocaletti and Manetti, 1988; Bocaletti et al., 1988b; Manetti et al., 1988; Eva et al., 1988; Dachev et al., 1988; Belousov et al., 1988; Finetti et al., 1988; Persoglia et al., 1988). Because of the hydrocarbon potentiality, a lot of studies including gravity have been carried out in the Black Sea (Spadini et al., 1996; Meredith and Egan, 2002; Nikishin et al., 2003; Rangin et al., 2002; Yegorova and Starostenko, 2002; Verzhbitsky et al., 2002; Starostenko et al., 2004).

1.1.2 The tectonic history of the study area

According to Hsü (1978), Black Sea and Mediterranean Sea are remnants of Tethys that was an ancient ocean located between Africa and Europe. Tethys Sea had connection both Atlantic Ocean and Indian Ocean. With the northward movement of the African plate some 20 millions years ago, the Tethys sea began to close off. Because of the collision of African plate and Asian plate, the eastern connection of the Tethys Sea with Indian Ocean was closed.

The collision with Europe gave rise to a long chain of mountains that includes the Alps, the Dinaric and Hellenic mountains of Yugoslavia, Albania and Greece, and the Taurus Mountains. Tethys was divided into two arms as a result of these mountains buildings; Mediterranean and Paratethys. The Paratethys extended from the Hungarian basin in the west to beyond the Aral Sea in the east including the present Black Sea and Caspian Sea. Connection between Mediterranean and Paratethys was cut off about 15 millions years ago because of the isolation of the Paratethys by mountains buildings.

About 6 millions years ago (Late Miocene), the continued northward progress of the African continental plate gave rise to mountain building on the Iberian Peninsula and in northwest corner of Africa that cut off the connection of the Mediterranean Sea with Atlantic Ocean. In spite of the rivers input, Mediterranean Sea had dried up for a millions years (Messinian) because of the high evaporation.

The drying of the Mediterranean affected the Paratethys as well. The Paratethys drained into the Mediterranean and both seas were reduced to a network of lakes. Black Sea was one of these lakes. Five millions years ago the Atlantic Ocean broke through at Gibraltar and the Mediterranean basin again became a sea. This event is accepted the finish of the Miocene, and the beginning of the Pliocene.

1.2 Black Sea

Black Sea is a semi-enclosed sea that is connected to the Mediterranean Sea through the narrow Bosphorus strait and to the Azov Sea through the shallow Kerch Strait. It is an elliptical basin that has a surface area of about 423.000 km^2. The average depth is 1271 m, and the maximum depth is up to 2200 m in the Euxine Abyssal plain (Ross et al., 1974).

The Black Sea basin has four main physiographic regions: shelf, basin slope, basin apron, and abyssal plain (Ross, 1974). The shelf varies in width. In the west of the Crimean Peninsula, the shelf exceeds 190 km, however along the mountainous coast of Turkey, Caucasia and south of the Crimean Peninsula the shelf is narrow and about 20 km wide (Ross et al., 1974). Off the Danube, the wide shelf is due to outbuildings by sediment carried by the numerous rivers (Danube, Dnestr, Bug and Dnepr). Two distinct types of basin slopes exist in Black Sea: a steep slope that is highly dissected by submarine canyons and a relatively smooth slope (Ross et al., 1974). Steep slope type is followed off most of the Turkish coast and part of the Caucasian coast. Smooth slope type occurs off Rumania and Bulgaria.

The basin apron, seaward of the basin slope, has a gradient varying from 1:40 to 1:1000; a gradient similar to that of continental rises. The most distinctive depositional feature of the basin apron is the Danube Fan that divides the abyssal plain into two unequal parts. Presently, no major deposition seems to be occurring on the Danube Fan (Ross, 1974). This fan is a relict Pleistocene depositional feature formed when sea level was lower than at present (Ross et al., 1974). Most basin aprons at the base of the slopes are continuous and are interrupted only locally by small hill-like features.

Black Sea exists in an E-W intermountain depression between two Alpine fold belts. The North Anatolian mountains are located at the south of the Black Sea, along the Turkish coastline. East of the Black Sea, the Caucasus Mountains occur with a maximum elevation of 4040 m. The western and northern coastal regions are relatively low (Ross et al., 1974; Ross., 1974).

The present-day tectonics of the area is dominated by the motion of Arabian plate northward relative to the Eurasian plate. The westward escape of the Anatolian plate along the North Anatolian Fault and the Great Caucus lineaments presently control the Black Sea tectonics (Ross et al., 1974; Ross., 1974).

GPS studies (McClusky et al., 2000; Tari et al., 2000) showed that a slight north-south shortening in the eastern half of southern Black Sea coast and a westward movement in the south western Black Sea coast occur. Recent geological and geophysical studies (Finetti et al., 1988; Meisner et al., 1995; Okay and Sahinturk, 1997; Barka and Reilinger, 1997) propose that the Eastern Black Sea is still under compressional tectonic regime.

1.2.1 Tectonic evolution

The Black Sea is a geologically unusual feature; it is a marine basin situated between Alpine Mountains systems. As a part of the Eastern mediterranean, the mechanism which caused the origin of the Black Sea is still debating (Figure 1.2).
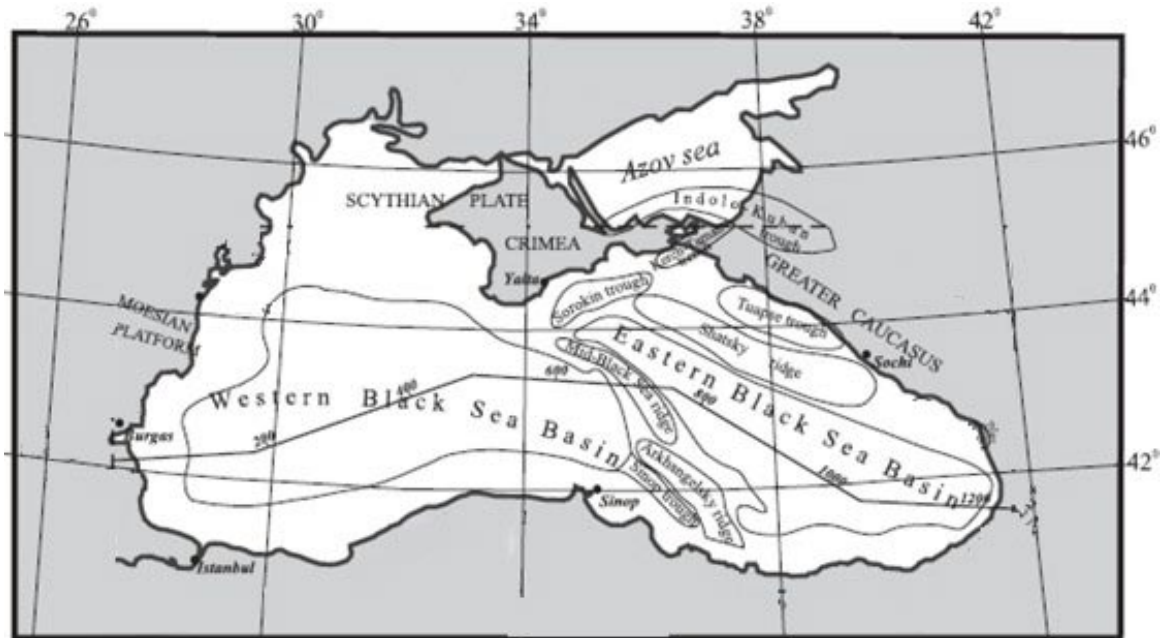
Figure 1.2 Tectonic outline of the Black Sea (modified from Starostenko et al., 2004).

The tectonic evolution of the Black Sea region has been discussed by many authors (Tugolesov et al., 1985; Görür, 1988; Finetti et al., 1988; Okay et al., 1994; Spadini et al., 1996; Robinson, 1997; Nikishin et al., 2001). At present, Black Sea is commonly regarded as Cretaceous-Palaeogene back-arc basin related to subduction of an ocean since closed in present-day Turkey (Görür, 1988; Finetti et al., 1988; Okay et al., 1994; Robinson, 1997; Nikishin et al., 2001; Starostenko et al., 2004). But there is no agreement on the internal structure because of its complex tectonic history.

Although the present day Black Sea basin floor appears to reflect a single basin, seismic studies have revealed that the basin consists mainly of two extensional subbasins in the Black Sea, eastern Black Sea basin and western Black Sea basin. These two basin are separated by the NW-SE trending Mid-Black Sea High (Figure 1.2).

One common disagreement is the opening time of these sub basins. Because of the absence of representative data on the structure of the lower part of the sedimentary fill of the basins, several models have been proposed for timing. Some authors propose that both sub basins have the same time of origin (Zonenshain and Le Pichon 1986; Finetti et al. 1988, Kazmin et al., 2000), and the others suggest that the western basin is older than the eastern basin (Okay et al., 1994; Robinson et al., 1995; 1996).

Western Black Sea Basin is considered to be beginning to open with the separation of a fragment from the Moesian Platform (Romania and Bulgaria) (Robinson et al., 1995; Spadini et al., 1996). The most recent interpretations based on stratigraphic evidences from the northern margin, suggest a mid-Cretaceous age for the opening of the western basin (Robinson et al., 1996; Rangin et al., 2002). According to the seismic data, this basin consists of up to 19 km of flat lying Upper Cretaceous to recent volcanics and sediments (Nikishin et al., 2003).

Eastern Black Sea Basin is considered to be opened between the Shatsky Ridge and the Mid-Black Sea high by rotation about a pole west of Crimea (Robinson et al., 1995; 1996; Spadini et al., 1996). The opening age is contentious but there are several lines of evidence supporting a Paleogene date (Robinson et al., 1996). The crust of the eastern Black Sea basin is considered to be oceanic or thinned continental. The basin is filled by 8 to 12 km of post rift sediments (Rangin et al., 2002).

NW-SE trending *Mid-Black Sea high* that consists of Andrusov and Archangelsky ridges is formed from continental crust and overlain by 5-6 km thickness of sedimentary cover (Tugolesov et al., 1985; Finetti et al., 1988; Robinson, 1997). *Archangelsky Ridge* starts off the Turkish coast and plunges northward. It is bounded by Paleocene aged normal faults that are overlain by recent sediments (Ivanov 1992, Çiftçi et al., 2002).

Shatsky Ridge is an uplifted continental block located between the over thrusts of the Greater Caucasus range and the deep Eastern Basin. The consolidated crust of the Shatsky Ridge is 20- to 25- km thick and it is underlain by thick (1.5-9 km) sediment cover (Ergün and Çifçi 1999).

1.3   Eastern Mediterranean

On the basis of physiography and crustal structure, the Mediterranean may be divided into western and eastern segments by a line connecting Italy, Sicily, and Tunisia (Vogt et al., 1971). The eastern segment is physiographically more complex than the western segment (Figure 1.3).

The most common view is that the eastern Mediterranean has been in a state of diachronous collision since the Late Crateceous (Robertson, 1998a; Aksu et al., 2005a). Today, the tectonism of the Eastern Mediterranean is controlled by the latest phase of diachronous collision between the African and Eurasian plates, and the displacements of the Arabian and Anatolian-Aegean microplates. Analysis of plate tectonic models (seafloor spreading, fault systems, earthquake slip vectors) point out that the African plate is moving in a N-NE direction relative to Eurasian plate at a rate of about 10 mm/yr, and the Arabian microplate is moving in a N-NW direction relative to Eurasian plate at a rate of about 18-25 mm/yr (McClusky et al., 2000; Figure 1.3). The sinistral Dead Sea transform fault accommodates the differential motion between the African plate and the Arabian microplate. The northward motion of Arabia results in continental collision along the Bitlis-Zagros fold-trust belt, intense earthquake activity, and high topography in eastern Turkey and the Caucasus Mountains, and westward extrusion of the Aegean-Anatolian microplate (Aksu et al., 2005a; McClusky et al., 2000; Reilinger et al., 1997). The westward extrusion of the Aegean-Anatolian microplate, which is accommodated by the dextral North Anatolian Fault (NAF) and the sinistral East Anatolian Fault (EAF) since the late Miocene-Pliocene (McKenzie, 1970; Şengör et al., 1985; Dewey et al., 1986), causes a collision with the Apulia-Adriatic platform (Underhill, 1989). It is also hypothesized that the Apulia-Adriatic platform forces the Agean-Anatolian microplate to rotate southwestwards (Aksu et al., 2005a). The leading edge of the African Plate is being subducted beneath the Eurasian plate along the South Aegean arc. Subduction of the African Plate is also thought to occur along the Cyprean arc (Aksu et al., 2005a; Bridge et al., 2005; McClusky et al., 2000).
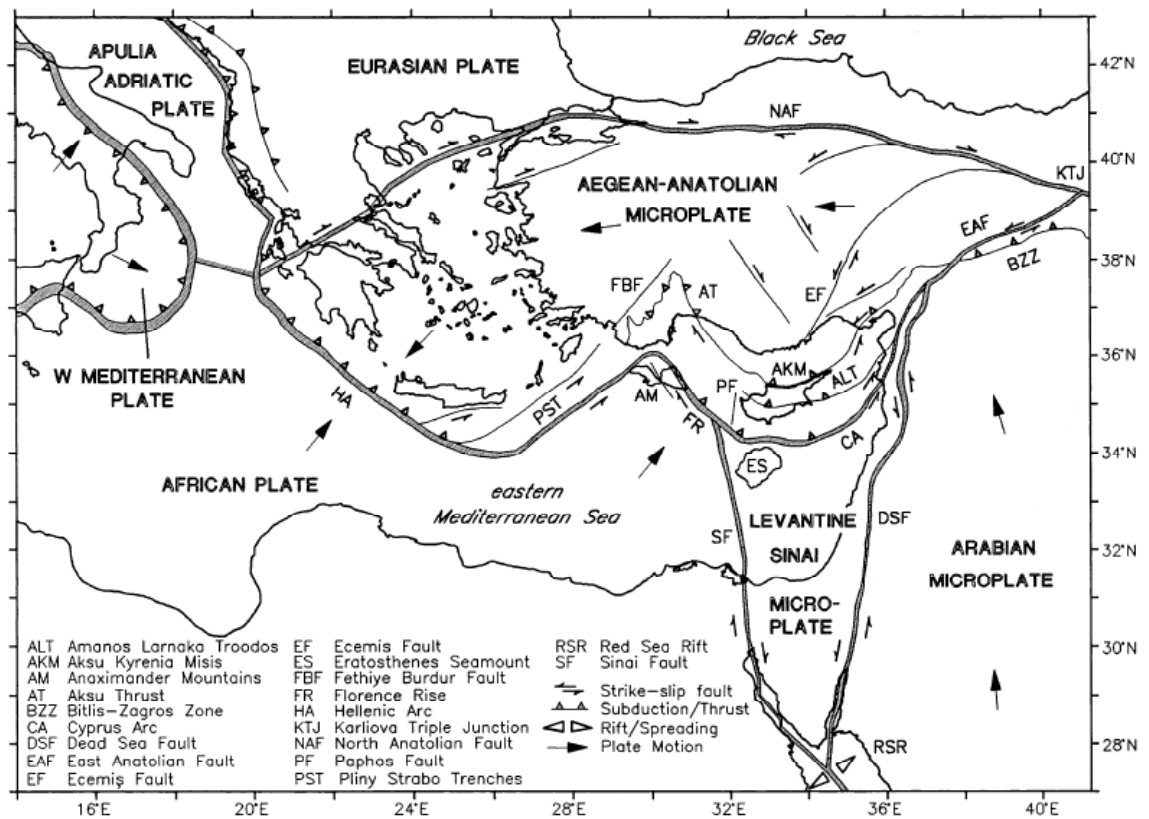
Figure 1.3 Simplified tectonic map of the eastern Mediterranean and surrounding region (from Aksu et al., 2005a).

1.3.1 Tectonic evolution

Although many different paleo-tectonic and –geographic reconstructions have been proposed for the eastern Mediterranean region, it is now widely accepted that the eastern Mediterranean Sea is a relic of a southerly Neotethyan (mainly Mesozoic) oceanic basin that formed part of a larger Tethyan ocean (Le Pichon, 1982; Robertson 1998a).

In a comprehensive review, Robertson (1998a) presented the three lines of evidence in support of the origin of the eastern Mediterranean comes from the Neotethyan oceanic basin. The three lines of evidence are as follows: the existence of the boundary between African and Eurasian plates based on seismic data (Kempler and Ben-Avraham, 1987; Anastasakis and Kelling, 1991); the existence of the oceanic crust based on seismic refraction, gravity and magnetic studies (Woodside, 1977; Makris et al., 1983; Ben-Avraham, 1986; Ben-Avraham and Tibor, 1994); and the existence of Mesozoic ophiolites in Cyprus and southwestern Turkey (Robertson

and Woodcock, 1979; Woodcock and Robertson, 1982; Hayward and Robertson, 1982).

Figure 1.4 Sea floor morphology of the easternmost Mediterranean Sea.

1.3.2 Location of the plate boundary

The junction of Aegean-Anatolian microplate with the African plate form the present day active plate boundary along the Eastern Mediterranean basin (Figure 1.3; Garfunkel, 1998). The zone of convergence is marked by two arcuate belts, the South Aegean Arc in the west, and the Cyprus Arc in the east (Hall et al., 2005a). The Cyprus Arc consists of several morphologic features, from west to east, the Anaximander Seamount, Florence Rise, the island of Cyprus and Girne-Larnaca-Latakia rises, respectively (Figure 1.4; Woodside et al., 2002).

Although the precise location of this plate boundary is controversial, it is suggested to be located between Cyprus island and Erathosthenes Seamount (Biju-Duval et al., 1978; Nur and Ben-Avraham, 1978; Riad et al., 1981; Rotstein and Kafka, 1982; Rotstein and Ben-Avraham, 1985; Robertson et al., 1994, 1995;

Anastasakis and Kelling, 1991; Ambraseys and Adams, 1993; Kempler and Garfunkel, 1994; Oral et al., 1995; Robertson, 1998a; Vidal et al., 2000b). The junction between the Levantine Basin and the Hecateus Rise is also considered to be plate boundary (Vidal et al., 2000b).

There is, however, no consensus on the location of plate boundaries for the eastern and western extensions of the Cyprus Arc.

To the west, the plate boundary is considered to be as a subduction dominated plate boundary segment linking the Florence Rise with the Cyprian Arc (Robertson, 1998a). However, Woodside et al. (2002) interpreted the eastern part of the Cyprus Arc as a typical transpressional feature, where the subduction stopped before the Messinian. Woodside et al. (2002) also regarded The Florence Rise (Figure 1.4) as a relic of prior subduction. On the other hand, based on earthquake data in the eastern part of the Cyprus Arc, Papazachos and Papaioannou (1999) mapped a NNE striking transform dextral fault, the Paphos Transform Fault.

To the east, the plate boundary is suggested to extend from south Cyprus to the İskenderun Bay, towards the junction of East Anatolian Fault (Biju-Duval et al., 1978; Nur and Ben-Avraham,1978; Riad et al., 1981; Rotstein and Kafka, 1982; Rotstein and Ben-Avraham, 1985; Robertson et al., 1994, 1995; Anastasakis and Kelling, 1991; Ambraseys and Adams, 1993; Kempler and Garfunkel, 1994; Oral et al., 1995; Ben-Avraham et al., 1995). However, its precise location and deformation mechanism is controversial. For example, Kempler and Garfunkel (1994), Ben-Avraham et al. (1995) and Robertson (1998b) proposed that the plate boundary is delineated by a single zone trending along the Hecataeus Rise, Latakia Ridge and Tartus Rigde (Figure 1.4). However, Vidal et al. (2000) regarded this boundary as two northeast-trending lineaments: the Latakia Ridge in the south and Larnaka Ridge in the north. Although the hypothesis about the migration of the plate boundary from north (Misis-Girne Ridge, Larnaka Ridge) to south (Latakia Rigde; Kempler and Ben Avraham, 1987; Ben Avraham et al., 1995) seems to be plausible the results of the study by Calon et al. (2005a) don't support this hypothesis.

1.3.3   Crust character

The crust type beneath the Levantine Basin is also controversial. Woodside (1977) suggest that the crust is more likely to be continental than oceanic. However,

Robertson (1998a) described the westward extension of the Levantine Basin filled by thick sediment deposition on an oceanic crust. This hypothesis is supported by lack of a distinctive high-velocity (6 km/s) layer in Levantine Basin (Ryan et al., 1973; Nur and Ben-Avraham, 1978; Makris et al., 1983; Makris and Stobbe, 1984). The strong negative magnetic anomaly in the Levantine basin is interpreted to be indicative of the oceanic basement (Makris et al., 1994).

On the other hand, ophiolite sequences, which are considered to be fragments of ancient oceanic lithospheres formed at constructive plate margins, are also found in the eastern Mediterranean (Figure 1.5). Mesozoic ophiolites and related allochthonous units in this area (Figure 1.5) are interpreted as the emplaced remnants of a southerly Neotethyan ocean basin (Robertson and Woodcock, 1979; Woodcock and Robertson, 1982; Whitechurch et al., 1984; Robertson 1998a)
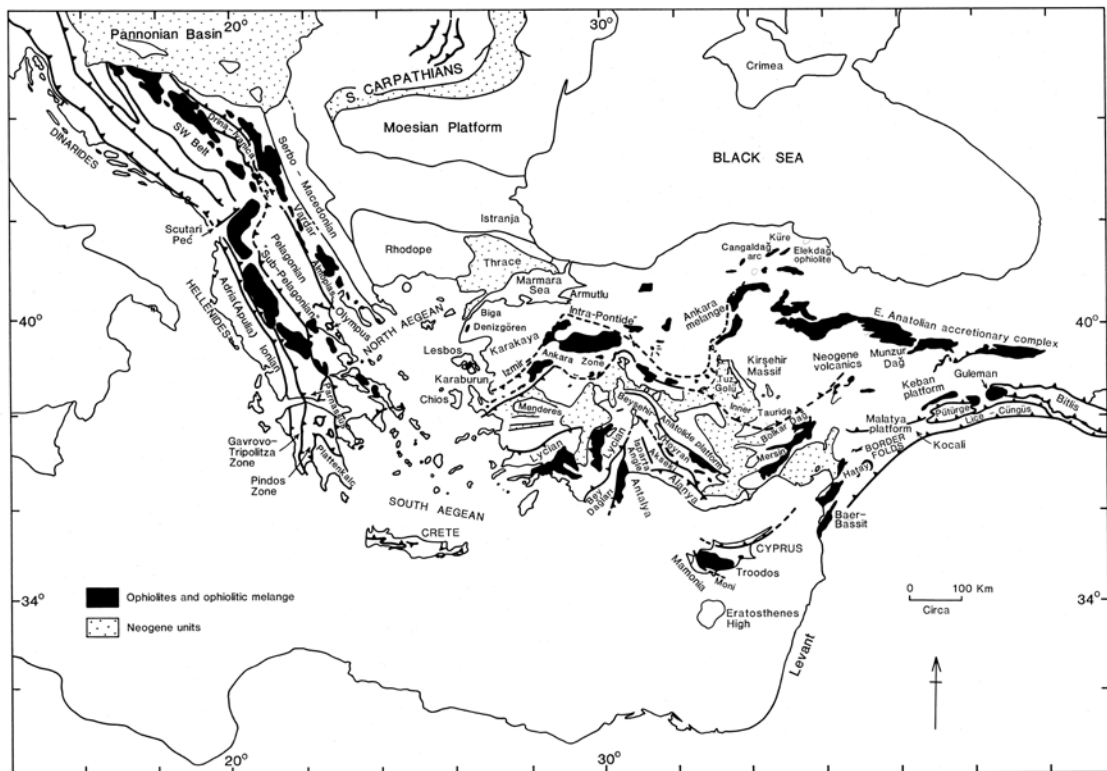
Figure 1.5 Ophiolite formations in the eastern Mediterranean area (after Robertson, 1998a).

1.3.4   Eastern Mediterranean basins

Eastern Mediterranean is shaped by several basins that separated from each other by natural frontiers such as rises and ridges. To better understand the properties, it is necessary to examine each basin separately.

Levantine Basin

Levantine basin is surrounded by Levant continental margin in the east, the Nil Cone in the south, Eratosthenes seamount in the west and the Cyprus Arc in the north (Figure 1.4).

Woodside (1977) claimed that Levantine Basin is underlain by stretched continental crust. However, other researchers have supported the view that the basin is floored with oceanic crust (Robertson, 1998a). Ben –Avraham et al. (2002) suggested that the crust is oceanic, but possibly modified during its history. On the contrary, Vidal et al. (2000a) proposed that Levantine Basin is underlain by a possible thinned or transitional continental crust.

Based on seismic data, Vidal et al. (2000a) reported that the Levantine Basin is filled by up to 10 km of sediments. The thickness of the Mesozoic sedimentary successions in the basin is about 6 km. Cenozoic sediments consist of about 1.5 km thick Messinian evaporites and 0.5 km thick Plio-Quaternary sedimentary sequences (Vidal et al., 2000a).

Levant continental margin is a passive margin situated off the coasts of Israel, Lebanon and Syria (Tibor and Ben-Avraham, 2005; Ben-Gai et al., 2005). Its formation was associated with the evolution of the Neo-Tethys Ocean (Tibor and Ben-Avraham, 2005). According to on seismic data, Levant Margin is underlain by continental crust that thins northward and westward (Ben-Avraham et al., 2002; Tibor and Ben-Avraham, 2005).

Erathosthenes seamount that rises over 1000 m above the sea floor separates the Levantine and Herodotus basins. It is suggested that Erathostenes seamount is a rifted continental fragment from the northern margin of the North African Plate in early Mesozoic time, associated with rift-related intrusions or extrusions of igneous rocks at depth (Woodside, 1977; Robertson 1998b; Hall et al., 2005b). It is generally agreed that the Erathostenes seamount is now in the process of collision with the

Cyprus active margin forming a part of regional Africa-Eurasia plate boundary (Robertson, 1998b).

Antalya Basin

Antalya basin is bounded to the west by the Beydağları Mountains and to the north by the Taurus Mountains and seaward by the Florence Rise to the south, the Anaximander Mountains to the west and the Anamur-Koruçam Rise to the east (Figure 1.4).

In spite of several investigations in the Eastern Mediterranean, only a few studies (Woodside, 1977, Özhan, 1988; Taviani and Rossi, 1989) had been performed to identify the deep structure of the Antalya Basin. Woodside (1977), using seismic data adjacent to the basin, mapped the Pliocene-Miocene boundary, representing top of the Messinian evaporites (Upper Miocene). Recent multibeam mapping and seismic profiling studies have been carried out, contributed to a better understanding of the tectonic evolution of the Antalya Basin. Woodside et al. (2002) presented detailed information on the nature of faulting and the morphology of the Florence Rise. Origin and evolution of the Anaximander Mountains have been discussed in detail by Zitter et al. (2003). İşler et al. (2005) investigated the structural and stratigraphic architecture of the Antalya Basin and defined three stratigraphic units. From base to top these are Plio-Quaternary, Late Miocene and Pre Messinian deposits. High resolution seismic reflection profiles collected from shallower water depths of 150 m in the Antalya Basin have revealed the presence of two distinct seismic units separated by major unconformities related to the last Quaternary sea level changes (Tezcan, 2001; Tezcan and Okyar; 2001, 2003 and 2006).

Antalya Basin is thought to be formed during the Miocene as an extensional basin (Robertson, 1998a). It is interpreted as the result of crustal extension behind a subduction zone linking the Florence Rise with the southern boundary of the Anaximander Seamount (Robertson, 1998a).

Florence Rise is a gently elevated submarine feature that connects the Cyprus to Anaximander Mountains. It is bordered by the Pytheus trench to the southwest. The Messinian reflector on seismic profiles that pinches out over the crest of the Florence Rise showed that it was already a topographic high by the Late Miocene

(Robertson 1998a). As explained previously, Woodside et al. (2002) concluded that Florence Rise is probably a relic of prior subduction.

Anaximander Mountain is located at the intersection of Antalya Basin, Turkish mainland and Rhodes. It is formed by three main submarine highs; Anaximander, Anaximenes and Anaxogoras, from west to east (Robertson 1998a). Despite some older hypotheses (Ryan et al., 1973; Woodside 1977; Nesteroff et al., 1977; Rotstein and Ben-Avraham, 1985), it was suggested that the Anaximander Mountains form the offshore continuation of structural units exposed onshore in southwest Turkey (Woodside and Dumont, 1997; tenVeen et al., 2004).

Latakia Basin and Cyprus Basin

The eastern segment of the Cyprus arc is formed by three submarine lineaments; Kyneria Range, Larnaka and Latakia ridges (Figure 1.4). The subduction zone related to the plate boundary between African and Anatolian plate is considered to be located in this region. Vidal et al., (2000b) proposed that the deformation occurs in a wide zone between the Larnaka and Latakia ridges rather than a single zone (Kempler and Garfunkel, 1994; Ben-Avraham et al., 1995; Robertson 1998a).

Latakia Basin locating between the Larnaka Ridge in the south and the Girne Ridge in the north, it is thought to be developed in an extensional basin setting during the Miocene (Robertson 1998a). It contains about 1 km thick Plio-Quaternary sediments on a thick evaporite layer.

Larnaka Ridge is an arcuate structure extending between southeastern Cyprus and the Amanos Mountains in SE Turkey. It merges in the east with the northern portion of the Tartus Ridge at the Syrian.

Cyprus Basin is located between the Latakia and Larnaka ridges. Cyprus Basin separates the Hecateaus Rise from the Cyprus Island. The basin has about 1 km thick post-Miocene sediments (Ben-Avraham et al., 1995).

Latakia Ridge is a structure that extends from Hecateaus Rise in the west to the northern Levantine coast in the east. Vidal et al. (2000b) showed that the sedimentary sequences of the Levantine Basin terminate abruptly towards the ridge, and thus they interpreted the ridge as the southern expression of the plate boundary.

Hecateaus Rise is located south of Cyprus (Figure 1.4) and is regarded as a rifted continental fragment of North African Plate (Robertson, 1998a). However, Vidal et al. (2000b) considered the Hecateaus Rise as a continental fragment belonging to south of Cyprus continental crust. Vidal et al. (2000b) also explained a presence of strike slip plate boundary between the Hecateaus Rise and the Levantine basin.

Çukurova Basin and İskenderun Basin

Çukurova basin and İskenderun basin are located between Turkey and Cyprus (Figure 1.4). Two basins are separated by Misis-Kyrenia Range (Aksu et al., 1992a).

Çukurova basin and its onshore extension Adana basin are bounded by Taurus Mountains in the north, Cyprus Island in the south, Misis-Girne Range in the east and the N–S trending Anamur–Koruçam zone in the west. Çukurova basin is dominated by the siliclastic sediment transported by four major rivers; Ceyhan, Seyhan, Tarsus and Göksu rivers (Aksu et al., 2005b). The morphology of the basin is controled by these rivers (Aksu et al., 2005b).

İskenderun basin is a small marine basin located between Misis Mountains and Amanos Mountains. The plio-Quaternary sediments are thickest in the southwestern edge of the basin, but thin northeast along the basin axis defining a wedge (Aksu et al., 2005c).

Adana-Çukurova and İskenderun basins collectively form a large semi-enclosed depocentre (Aksu et al., 1992a).

1.3.5 Crust elements

Although the composition of the crust beneath the eastern Mediterranean Sea varies spatially, it can be separated into several layers that have different density values.

Plio-Quaternary sediments

The youngest layer of the crust contains sediments that have been deposited for about five million years, in other words, since Pliocene time. Obviously, the Plio-Quaternary sediment layer is the most investigated part of the crust because of its age and its relatively shallower thickness. The upper boundary forms the present seafloor and its base is marked by a strong and distinctive regional reflector, the upper

boundary of Messian evaporites, which identified in the eastern Mediterranean as the "M-Reflector" (Ryan, 1969).

The thickness and distribution of the Plio-Quaternary sediments over the whole Mediterranean had been mapped and published by IOC in 1993 (Figure 1.6). In this study, to construct the crust model, the initial values for the Plio-Quaternary sediments were taken from this map.
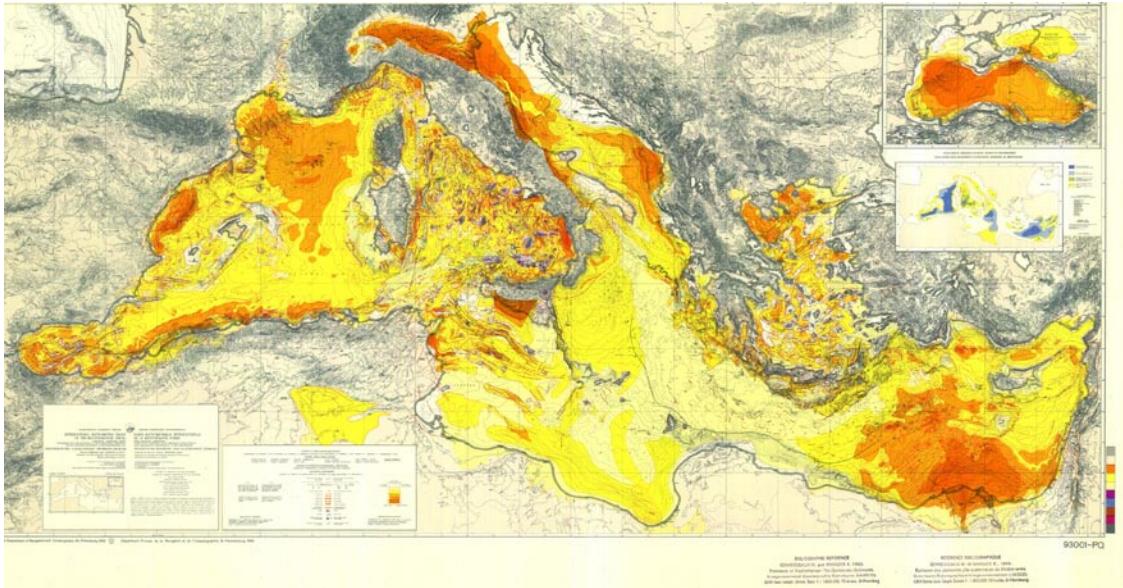
Figure 1.6 Plio-Quaternary sediment thickness map of the Mediterranean (IBCM-PQ, 1993).

Variations in sediment thickness divide the Eastern Mediterranean into several distinct provinces (Woodside, 1977); the Nile Cone, the Herodotus Basin, the Antalya Basin, the Finike Basin, the Eratosthenes Basin, the Çukurova Basin, the İskenderun Basin and the Levantine Basin. The greatest thickness is observed at the Nile Cone, the thinner sediments are found in the Levantine basin and on the Mediterranean Ridge (Figure 1.6, Woodside, 1977).

Also, several scientists have investigated the Plio-Quaternary sediments more detailed in different areas. İşler et al. (2005) examined the Miocene to recent kinematic evolution of the Antalya Basin. They mapped the thickness distribution of the Plio-Quaternary sediments in the Antalya Basin (Figure 1.7).

16
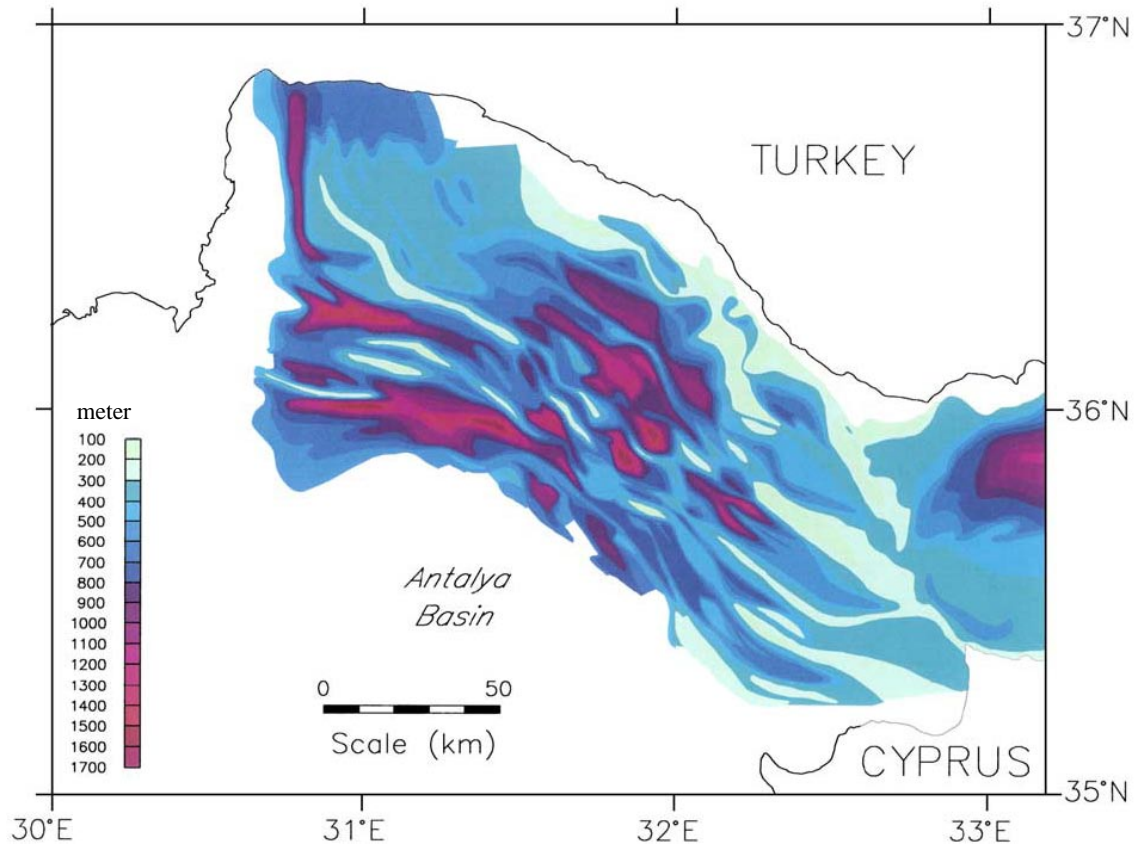
Figure 1.7. Isopach map of the Plio-Quaternary sediments of the Antalya Basin (after İşler et al., 2005).

The Çukurova Basin is formed by an E–W trending deeper outer Çukurova Basin in the west and a NE–SW trending shallower inner Çukurova Basin in the northeast (Aksu et al., 2005c; Figure 1.8). The thickness of the Plio-Quaternary sediments is maximum along the central axes of both the Inner and Outer Çukurova basins, and sharply thins toward the Girne Range and the southwestern Turkish coast (Aksu et al., 2005b). In the inner Çukurova basin, Plio-Quaternary deposits are characterized by a prograding wedge of deltaic sediments, which reaches its maximum thickness of ~ 2500 ms immediately seaward of the present-day mouths of Seyhan and Tarsus Rivers.

The Plio–Quaternary sediments in the Iskenderun Basin form a thick, relatively undisturbed wedge which thickens both to the southwest and northwest (Figure 1.8, Aksu et al., 2005c, Burton-Ferguson et al., 2005). The maximum thickness of about 1150 m occurs in the southwestern edge of the basin (Aksu et al., 2005c).

In the Latakia Basin area, Calon et al. (2005b) described the Plio-Quaternary sediments as a N-dipping and N-thickening wedge with a maximum thickness of ~1100 ms.

Vidal et al., (2000a) interpreted the M reflector, the top of Messinian evaporites, on seismic profiles taken in Levantine Basin. They correlate only the upper 400-600 m of deposits with the Plio-Quaternary sediments.
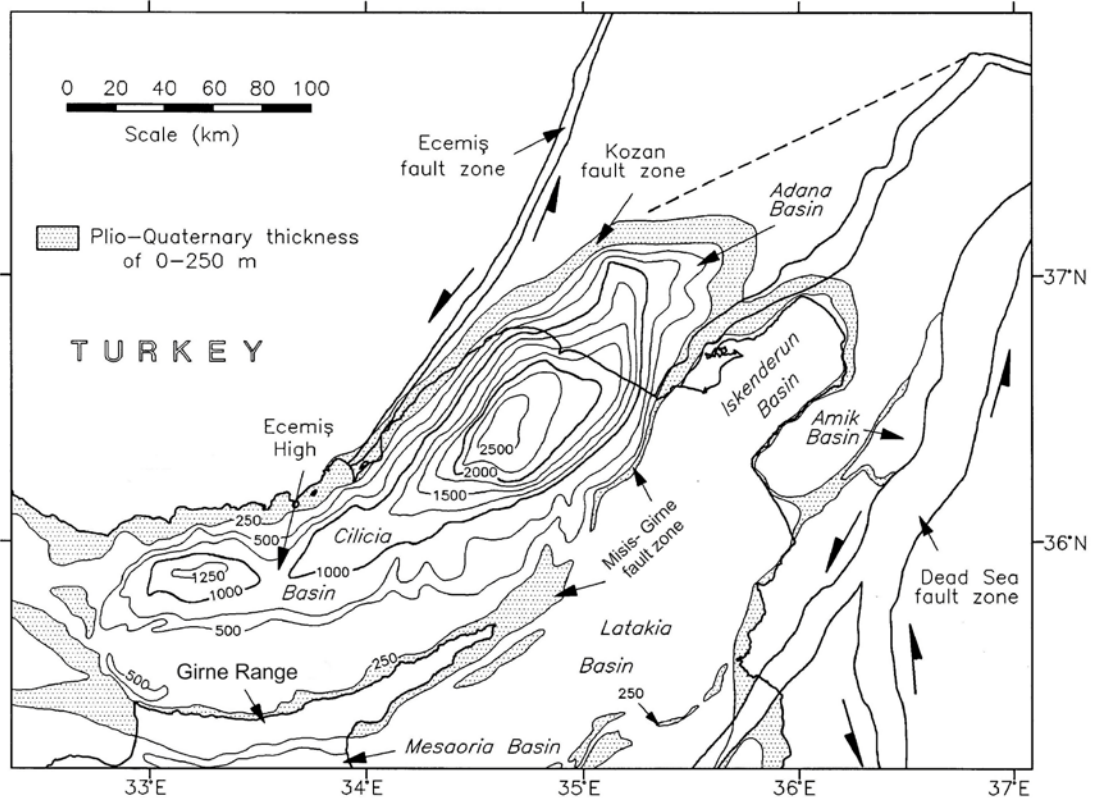
Figure 1.8 Plio-Quaternary sediments thickness map in the Adana-Çukurova basin (after Aksu et al., 2005c).

Evaporites

Evaporite deposition in Mediterranean was the result of the Messinian salinity crisis that is one of the greatest evaporitic events of Earth's history. At the end of the Miocene, about 5.96 million years ago (Krijgsman et al., 1999), the connections between the Mediterranean and Atlantic were interrupted (Hsü et al., 1978). During Messinian salinity crisis (i.e. 640 kyr; Krijgsman et al., 1999), thick evaporites (up to >2 km) were deposited on the seafloor of whole Mediterranean. The re-establishment of the connections between the Mediterranean and Atlantic at

the beginning of Pliocene terminated the Messian salinity crisis and led to restoring of normal marine conditions in the Mediterranean basin (Hsü et al., 1978).

The Messinian evaporites have high internal velocity (~4000 m/s) that prevents well seismic data acquisition. The general distribution of the evaporites in Mediterranean was given as a sketch map in the Plio-Quaternary deposits published by IOC in 1993 (Figure 1.9).
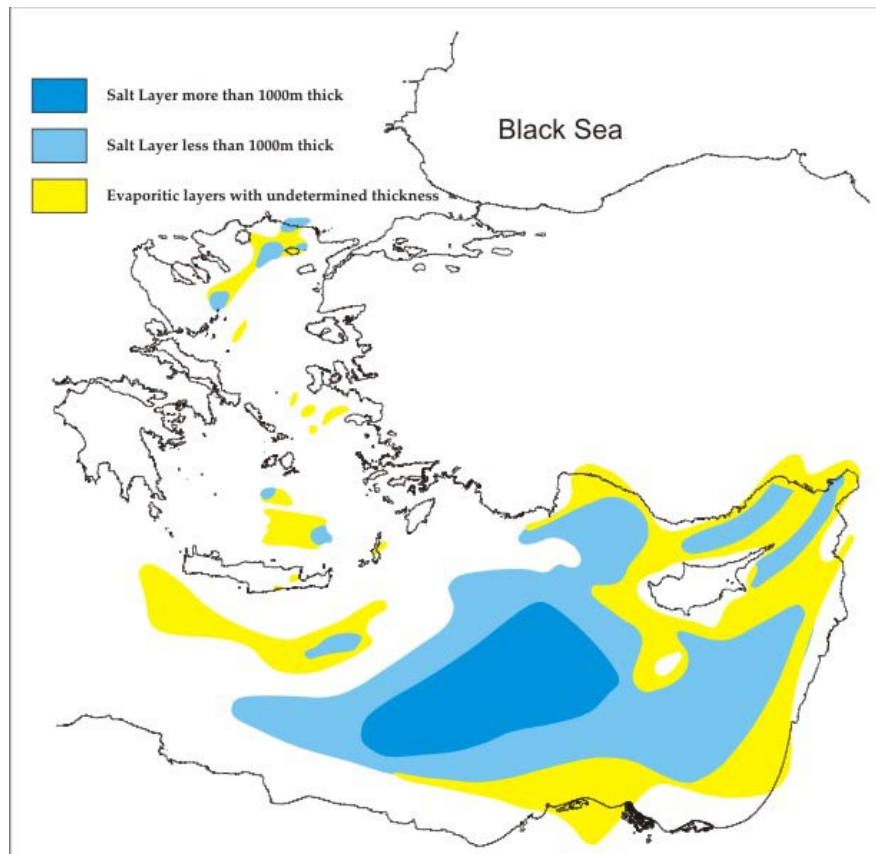
Figure 1.9 Evaporites distribution in the eastern Mediterranean Sea (modified from the sketch map in IBCM-PQ, 1993).

İşler et al. (2005) presented that the evaporites occur exclusively across the floor of the Antalya Basin in water depths greater than ~1800–1900 m. These evaporites show large variations in thickness ranging from <100 ms to >1200 ms in Antalya Basin (İşler et al., 2005).

In the Çukurova Basin, the maximum thickness of the evaporites is about of 500 ms (Aksu et al., 2005b). They defined that evaporites are absent along the shelf-slope transition of the southern Turkish margin.

Aksu et al. (2005c) suggested that Messinian evaporites are largely absent in the Iskenderun Basin. They infer that the absence of evaporites demonstrates that the basin was an erosive paleohigh stage in the Messinian.

In Latakia Basin, the Messinian evaporites are missing or very thin over the central axis of the Girne fold/thrust belt as well as the Larnaka Ridge (Calon et al., 2005a). However, in the basin, the evaporites have 600–750 ms thickness (Hall et al., 2005a).

Vidal et al. (2000a) suggest that the evaporatic layer has an average thickness of 1400 m in the Levantine Basin. This layer terminates abruptly against the deformation front at the southern slope of the Hecateaus Rise (Vidal et al., 2000a).

Pre-Messinian sediments

Pre-Messinian sediments underlay the M-reflector and the Messinian evaporites. Although the ages and thicknesses of the sediments that deposited prior the Messian, it is assumed in this study that they are parts of a single layer, the pre-Messian sediment layer. This is because that the evaporatic layer with high internal velocity prevents to investigate the properties of the pre-Messian sediments as expected.

1.4   The purpose of this study

Geophysical methods have been used for more than a century to better figure out the earth, especially to find the natural resources, such as mines and petroleum. However, because of the high cost of the geophysical explorations, only a small percent of the earth surface could be deeply investigated.

Gravity method, which investigates the lateral density variations in the earth crust, is used widely both on the land and at sea for the exploration of the natural resources. However, especially in a sea survey, there are many difficulties; firstly, the high cost of the sea surveys, secondly, the need of extra corrections (tidal effects, moving platform effects, etc) of data to have a precise measurement, and finally, the restriction of the measurements only on the ship track that cause the limited spatial resolution.

Nowadays, with the improvements in space technology, the satellites are used for the geophysical investigations. The altimetry data, the measure of the sea surface

height obtained by active radar satellites, are converted to gravity anomaly data. This gravity data, unlike ship data, provide complete coverage of whole the wet areas on the earth. However, the accuracy of the satellite derived data is doubtful. It should be compared and possibly calibrated with in situ data.

The Eastern Mediterranean with the Black Sea has very complex geological history as mentioned before. For now, a lot of studies that used direct method, such as seismic method, have been made to test the hypothesis about the evolution of this area. These studies enlighten the Pliocene-Quaternary structure of Eastern Mediterranean. However the deeper structure of this area is still in shadow. This is mostly the result of the existence of Messinian evaporites that prevent the well seismic data acquisition.

The purpose of this thesis is the investigation of the crustal structure of the eastern Mediterranean and Black Sea basins using satellite altimetry and ship-borne gravity data. Specifically, this includes: 1) development of the crustal models of both basins, 2) better understanding the tectonic setting and geodynamic processes controlling the evolution of the basins, and 3) mapping of the sedimentary strata and basement rocks in the region. More specifically, this work attempts to develop 2D and 3D gravity modeling programme, using ArcGIS and Matlab softwares, for evaluating crustal structure from satellite altimetry and ship –track derived gravity data and tries to determine the error range of the satellite-derived gravity data for future studies of this kind.

Our current knowledge about the deeper structures of the eastern Mediterranean and Black Sea basins comes largely from several marine seismic and ship-borne gravity surveys. Despite the paramount importance of gravity measurements in crustal structure studies, the ship-borne gravity data coverage is scarce compared to the basin sizes. This, and the complexity of the geology, as well as well the interaction of tectonic effects have become the main restricting factors in better understanding the crustal structure of the basins. In this study, ship-borne gravity data are supported by satellite-derived gravity data.

2 Material and methods

In this study, the forward gravity modeling method with ship-borne gravity data and satellite derived gravity data is used. Firstly, the theory behind the gravity and modeling method will be summarized. Then, the actual material, ship and satellite data used in this study will be presented.

2.1 Theoretical background

The theoretical background that is summarised from Dobrin (1981), Blakely (1995), Turcotte and Schubert (2002), is given under headings related to the topic studied. Firstly, some definitions behind the gravity method such as gravitational acceleration, gravitational potential, potential energy and the earth gravity will be explained. Secondly, the necessary corrections of the gravity measurements will be summarized under the gravity anomalies heading. Following this, the theory of the gravity modeling and finally the satellite gravity method will be described.

2.1.1 Gravity method

The gravity method involves measuring the acceleration due to the earth's gravitational field. The gravity method works when buried objects have different masses, which are caused by the object having a different density than the surrounding material. It is of proven success in studies of exploration and reservoir, as well as in studies of crustal structure. In particular, integrated analysis of gravity and seismic data provide information on the thickness of Earth's crust.

The theory of the gravitational prospecting is based on Newton's law of gravitation. According to Newton (1642 – 1727), each particle of matter in the universe attracts all others with a force directly proportional to its mass and inversely proportional to the square of its distance of separation. Consider masses m_1 and m_2 separated by a distance r. In terms of equations, Newton's law for gravitational force between the two masses is:

$$F = -\gamma \frac{m_1 m_2}{r^2}$$

where γ, known as the universal gravitational constant, depends on the system of units employed. The minus sign arises because the force is always attractive. In the centimeter-gram-second (cgs) system, the value of γ is $6.670 \times 10^{-11} Nm^2kg^{-2}$. This value for γ implies that the gravitational force between two 1 kg objects separated by 1 m is 6.67 x 10^{-11} N.

Gravitational acceleration

The acceleration of a mass m_2 due to the attraction of a mass m_1 a distance r away can be obtained by dividing the attracting force F by the mass m_2. In particular, if m_1 is the mass of the earth, M_e, the acceleration of the mass m_2 at the surface of the earth is

$$a = \frac{F}{m_2} = -\gamma \frac{m_{earth}}{r^2_{earth}}$$

where r_{earth} is the radius of the earth.

The acceleration, being the force acting on a unit mass, is the conventional quantity used to measure the gravitational field acting at any point. All masses located at the same position in the field are subject to same gravitational acceleration. In the cgs system, the dimension of acceleration is *cm/s²*.

The numerical value at the earth's surface is about 980 cm/s². In honour of Galileo, the unit of acceleration of gravity, 1 cm/s², is called the *gal*. In gravity prospecting, the milligal (*mGal*, 1/1000 gal) is used because gravity differences over the earth's surface are very small ($\leq 10^{-5}$ gal).

Gravitational potential

Gravitational fields are conservative, that is to say, the work done moving a mass in a gravitational field is independent of the path traversed and depends only on the end points.

The gravitational potential (v) at a point in the gravitational field is defined as the work done in taking a unit mass from that point to infinity against the force of gravitational attraction. From this definition:

$$v = -\gamma m_1 \int_{\infty}^{r} \frac{1}{r^2} dr = \gamma \frac{m_1}{r}$$

Gravitational potential energy

The work obtained in bringing a body from infinity to a point in the gravitational field is called the gravitational potential energy of the body at that point. It is represented by

$$u = -\gamma \frac{m_2 m_1}{r}$$

The gravitational potential energy at infinity is assumed to be zero.

Gravity of the Earth

The force exerted on a body at the Earth's surface has two main sources; the gravitational attraction of the earth and the centrifugal acceleration due to its rotation. The gravity field is the sum of both components.

Since the earth is not a perfect homogenous sphere, the acceleration of gravity, g, is not constant over the earth's surface. It is now known that the magnitude of gravity on the earth's surface depends on the five superimposed factors, in order of their impact on gravity: latitude, elevation, density variations in the subsurface, topography of the surrounding terrain, and earth tides.

The shape of the earth, as determined by geodetic measurements and satellite tracking, is spheroidal, bulging at the equator and flattening at the poles, such that the difference equatorial and polar radii, divided by the former, is 1/297. This ratio is known as the polar flattening. As a result of the difference between the equatorial and polar radii of the earth, gravity at the poles exceeds gravity at the equator by 5186 mGal.

There are two reference surfaces, the reference spheroid (ellipsoid) and geoid, which are used as a basis of gravity measurements. The reference spheroid is a mathematical figure that is related to the mean sea level surface with excess land masses removed and ocean deeps filled. Thus it is an equipotential surface, that is, a surface on which the value of the gravitational potential is the same. From the international gravity formula, whose constants are based upon the mean Earth

ellipsoid adopted by the World Geodetic System 1984 (WGS84), the theoretical or normal gravity value g_C at any point on this spheroid is given by:

$$g_0 = 9.7803267714 \cdot \frac{1 + 0.00193185138639 \cdot \sin^2 \lambda}{\sqrt{1 - 0.00669437999013 \cdot \sin^2 \lambda}}$$

where λ = latitude.

Geoid is the actual equipotential surface that coincides with the average sea level without the effects of ocean currents, weather and tides. On land the geoid can be thought of as the level of water in an imaginary canal connected at each end with an ocean.

The reference spheroid assumes there is no undulation in the earth's surface. However, the shape of the geoid is dominated by broad undulations. The geoid undulations range worldwide from -107 m to 85 m relative to WGS84 ellipsoid (Li and Götze, 2001).

2.1.2 Gravity anomalies

The observed gravity or measured gravity value on the earth surface is the summation of the theoretical gravity, the normal gravitational attraction of a hypothetical earth containing no lateral density inhomogeneties, and the effects of crustal and upper mantle density variations and various others. The following sum shows the components of the observed/measured gravity:

observed gravity = attraction of the reference ellipsoid

+ effect of elevation above sea level

+ effect of "normal" mass above sea level

+time-dependent variations

+effect of moving platform

+effect of masses that support topographic loads

+effect of crust and upper mantle density variations.

The first five effects are caused by known sources and they can be removed from the measured data. To the geophysicist, the most important unknown source is the effect of crustal and upper mantle density variations. Unfortunately, this quantity

is a relatively minor part of the observed gravity (less than 0.01 percent of observed gravity).

A sequence of gravity corrections are applied to the original gravity reading and results in various named gravity anomalies.

Free-air correction:

The International Gravity Formula estimates the changes with latitude on the ellipsoid surface of theoretical gravity. The free-air correction accounts for the change of theoretical gravity due to stations being located above or below the reference ellipsoid. Since the gravity varies inversely with the square of distance, it is necessary to correct for changes in elevation between observation point and reference ellipsoid. This correction takes no account of the material between the observation point and the sea level and it can be calculated from the following formula:

$$g_{free-air} = -0.3086 \cdot 10^{-5} h$$

where h = height above sea-level.

As the negative sign implies, the free-air correction is added to the observed gravity value when the observation point is above mean sea level and subtracted when below it. Thus the free-air anomaly:

$$\Delta g_{free-air} = g_{observed} - g_{free-air} - g_{theoritical}$$

As the geoid corresponds to sea-level, it is not necessary to correct the free-air effect for the shipboard measurements.

Tidal correction:

The earth tides caused by the sun and moon result in periodic "time-dependent" variations in the Earth's gravity field. For removing the tidal effect caused by the sun and the moon, tidal correction can be applied to observed gravity values. Since the tidal effects never exceed 0, 3 mGal, it can be neglected. However it should be accounted for when high precision surveys are conducted.

Eötvös correction:

Due to centrifugal force caused by the Earth's rotation, gravitational attraction of the earth changes for an observer in motion. This motion-related effect,

called the Eötvös effect, must be accounted for gravity measurements performed on moving platforms, such as ships or aircraft. The Eötvös correction is given by

$$g_{e\ddot{o}tv\ddot{o}s} = 7.503v \cdot \cos\lambda \sin\alpha + 0.004154v^2$$

where v is the speed in knots, α is heading with respect to the north and λ is latitude. Eötvös correction is regarded as a limiting factor in the accurate measurements gravity field provided by moving platforms.

Bouguer correction:

The Bouguer correction account for the effect of a mass that may exists between the level of observation and sea level, which are ignored in both free-air correction and theoretical gravity/normal gravity formula. The simple Bouguer correction assumes an infinite horizontal slab of rock of uniform density whose thickness, is the elevation difference between the observation point and the sea level. The gravitational attraction of an infinite slab is given by

$$g_{slab} = 2\pi\gamma\rho h$$

where h is the thickness of the slab. Using a typical value of the crustal density of 2670 kg/m^3, the simple Bouguer correction becomes:

$$g_{simple-bouguer} = 0.1119 \times 10^{-5} \cdot h$$

where h is height above sea level. Therefore, the simple Bouguer anomaly is given by

$$\Delta g_{simple-bouguer} = g_{observed} - g_{free-air} - g_{simplebouguer} - g_{theoritical}$$

For gravity measurements over water, the Bouguer correction amounts to replacing the water (density = 1000 kg/m^3) with a slab of density 2670 kg/m^3 and thickness equal to bathymetric depth. The Bouguer anomaly is the difference between the measured value at the point of observation and the theoretical value calculated for that elevation or water depth and the appropriate density of the earth's materials. Bouguer anomaly equals the free air anomaly if marine gravity surveys are carried out at sea level. However, most scientists do not prefer to use Bouguer anomaly at sea because that masks the effects of subsurface density variations.

Terrain Correction

In areas of very flat relief, the simple Bouguer correction is usually all that is required. However, in areas of irregular topography, accurate gravity measurements require the use of the complete Bouguer correction, which consists of the simple Bouguer correction and the terrain correction. Namely, terrain correction accounts for variations in the observed gravitational acceleration caused by variations in topography near the observation point.

Isostatic Correction

The system or principle by which topography is compensated by variations of the crust called isostasy. According to concept of isostasy, the Earth was in hydrostatic equilibrium at depth, requiring topography to be compensated either by lateral variations in crustal thickness (Airy's hypothesis) or crustal density (Pratt's hypothesis). Isostatic corrections are intended to remove the effect of masses in the deep crust or mantle that isostatically compensate for topographic loads at the surface. Calculation of isostatic effects can be made on the basis of either principle.

Residual – regional separation

While the general objective of the gravity method is to obtain information about the earth's subsurface, it is in essence aiming at two objectives: (i) it helps to determine the lateral location of any gravity variations; (ii) it provides the detailed analysis in order to quantify the nature (depth, geometry, density) of the subsurface feature causing the gravity variations. To determine the secondary topic, it is usually necessary to separate the anomaly of interest (residual) from the remaining background anomaly (regional). Then the residual gravity anomaly is modeled to determine the depth, density and geometry of the anomaly's source. In interpreting gravity data in engineering and environmental applications, there are many techniques that can be used to accomplish the regional-residual anomaly separation (Dobrin, 1981; Telford et al., 1990).

2.1.3 Gravity modeling

Although there are several methods for interpreting the gravity data, the main techniques of interpretation of gravity field data can be divided into three categories: forward method; inverse method; and data enhancement and display (Figure 2.1;
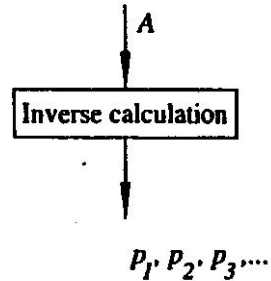
Blakely, 1995). In this study the forward modeling method is used, which is explained in the next section.

Forward modeling

In forward modeling method, firstly a mass distribution model is formed, and then the gravity anomaly of this model is calculated.

The model is constructed based on previous geophysical data. The gravity response of the model is compared with the observed gravity data whether they are coincident. If not coincident, the model has to be changed and the new gravity response calculated. This procedure is repeated until they match. The parameterization of the model has to be adjusted to the information content of the geological and geophysical data such as boreholes, drilling, seismic, and magnetic. Since the solution is non-unique –ambiguous, forward modeling is a favorite word of geophysicists.

FORWARD METHOD

Guess at initial
model parameters

$P_1, P_2, P_3, \cdots$

Calculate model
anomaly

A_o

Compare model anomaly
with observed anomaly

A

Do they
match?

No

Adjust model
parameters

New
$P_1, P_2, P_3, \cdots$

Yes

Stop

INVERSE METHOD

A

Inverse calculation

$P_1, P_2, P_3, \cdots$

ENHANCEMENT
AND DISPLAY

A

Transform anomaly
into enhanced anomaly

A'

Display
anomaly

Figure 2.1 Three categories of techniques used in interpretation of gravity field data
(after Blakely, 1995).

Before the use of computers, gravity anomalies were interpreted using characteristics curves calculated from simple geometries/models (Nettleton, 1942). Talwani et al. (1959) have developed an algorithm for computing gravity anomalies produced by 2D bodies of polygonal cross-section (Figure 2.2). This resulted in the use of computers for gravity modeling. The 2D sources were later modified by Rasmussen and Pedersen (1979), and Cady (1980).

30
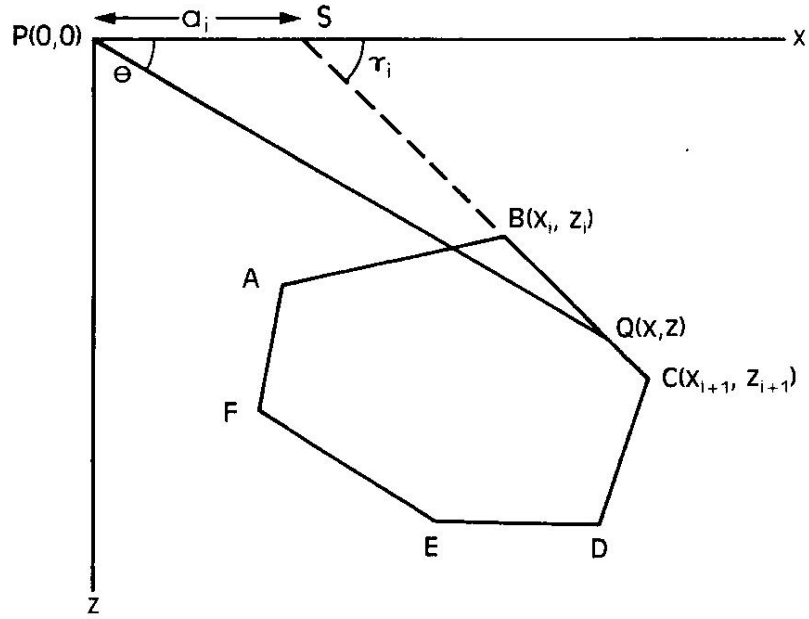
Figure 2.2. Geometry of a 2D polygon (Talwani et al. 1959).

The gravitational attraction of the polygon at the point P can be calculated by

$$\Delta g = 2\gamma\rho \sum_{i=1}^{6} \left\{ \frac{x_i z_{i+1} - z_i x_{i+1}}{\left(x_{i+1} - x_i\right)^2 + \left(z_{i+1} - z_i\right)^2} \right\} \cdot \left\{ \left(x_{i+1} - x_i\right)\left(\theta_i - \theta_{i+1}\right) + \left(z_{i+1} - z_i\right)\ln\left(\frac{r_{i+1}}{r_i}\right) \right\}$$

where $r_i = (x_i^2 + z_i^2)^{1/2}$.

Three-dimensional density distributions were initially modeled by Talwani and Ewing (1960) using horizontal polygonal laminas that approximate the shape of the body. Plouff (1976) derived the formula to calculate the 3-D gravity anomalies of a prism with arbitrary dimensions (Figure 2.3). This is an extremely challenging technique it gives accurate results in the calculating the gravity anomalies of any arbitrary shaped 3-D model. As the gravity field above a single grid node is influenced by all masses in the surrounding of the observation point, the local gravity field becomes a stack of contributions from all surrounding bodies, which are rectangular shaped prisms on an equal-spaced grid. The accuracy of this approximation can be improved by decreasing the widths of the prisms.
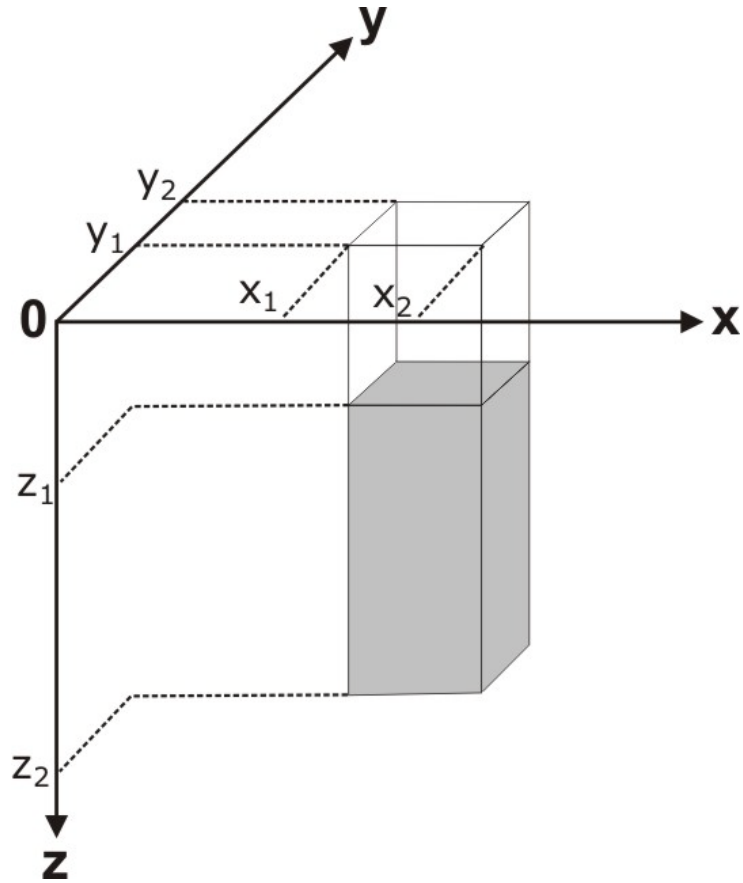
Figure 2.3. The gravity anomaly of a prism (modified from Plouff, 1976).

The gravitational attraction of a prism is calculated by the equation given below (Plouf, 1976).

$$\Delta g = G \cdot \Delta\rho \sum_{i=1}^{2} \sum_{j=1}^{2} \sum_{k=1}^{2} \mu_{ijk} \cdot \left[z_k \arctan\frac{x_i y_j}{z_k R_{ijk}} - x_i \cdot \log(R_{ijk} + y_j) - y_j \log(R_{ijk} + x_i) \right]$$

where $R_{ijk} = \sqrt{x_i^2 + y_j^2 + z_k^2}$ and $\mu_{ijk} = (-1)^i (-1)^j (-1)^k$

2.1.4 Satellite gravity method

The shape of the sea surface is controlled by the Earth's gravitational field. Ridges and trenches on the ocean bottom, as well as mass variations below the bottom cause changes in sea surface elevation. These changes range in amplitude from a few centimeters to some hundreds of meters. And they persist after sea height variations caused by winds and currents have been averaged out over time. The

undulations of the sea surface "marine geoid" are measured by the satellites carrying onboard altimeter instruments.

The Skylab spacecraft, launched in 1973, provided the first opportunity for satellite based radar altimetry. It was basically a research mission for which data was obtained for the designing of future altimeters. Over the time span since the Skylab, technological developments have transformed satellite radar altimetry from a technique by which major geoid features with order 10 m amplitude could be resolved to one where resolution of dynamic ocean signals as small as a few cm is possible. The history of missions of satellite altimetry is shown in Table 2.1.

Table 2.1. Satellite altimeters mission history. GEOS: Geodynamics Experimental Ocean Satellite, SEASAT: SEA SATellite, GEOSAT: GEOdetic SATellite, ERS: European Earth Remote sensing Satellite, TOPEX: TOPographic EXperiment, NASA: National Aeronautics and Space Administration, JPL: Jet Propulsion Laboratory, ESA: European Space Agency, CNES: Centre National d'Études Spatiales (French Space Agency)

Satellite	GEOS-3	SEASAT	GEOSAT	ERS-1	T/P	ERS-2
Operated by	NASA	NASA/JPL	US-NAVY	ESA	CNES/ NASA	ESA
Launch (month/year)	04/1975	06/1978	03/1985	07/1991	09/1992	04/1995
Acquisition until…	12/1978	10/1978	09/1989	03/1996	now	now
Mission duration (month)	42	3,5	54	57	168+…	137+…
Inclination (°)	115	108	108	98,54	66,04	98,54
Frequency (GHz)	13,9	13,5	13,5	13,5	13,6 5,3	13,5
Mean Height (km)	840	800	800	780	1330	780
Precision (cm)	25	5	4	3	2	3

Satellite altimetry

Altimetry is a technique for measuring height. Satellite altimetry measures the round-trip time of a radar signal between the satellite and the ocean surface. The principle of radar altimetry is shown in Figure 2.4 (Sandwell and

Smith,1997).According to this, if the altitude of the satellite above the reference ellipsoid is known then the height of the geoid with respect to the reference ellipsoid, N, is given by

$$N = h - \Delta h_s = H_1 - H_2 - \Delta h_s$$

To obtain the most accurate value, the corrections applied to satellite altimeter measurements include the instrument, atmospheric refraction, air-sea interface, and external geophysical corrections. Since these corrections are out of the scope of the present study they are not explained here.

In practice, altimeter data, collected by different satellites over many years, are combined to achieve a high data density and to average out sea surface disturbing factors such as waves, winds, tides, and currents.
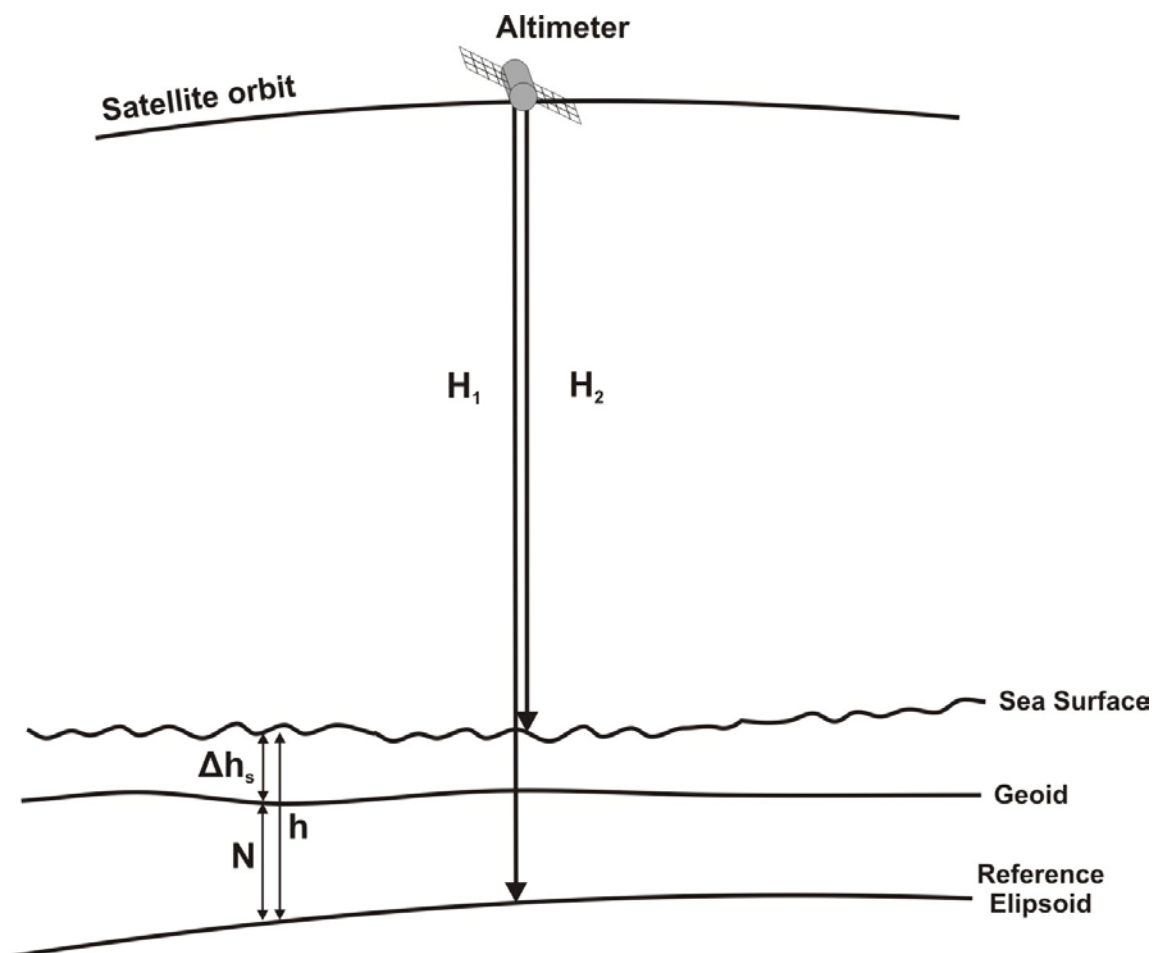
Figure 2.4 Satellite altimetry method (modifed from Sandwell and Smith, 1997).

Gravity from satellite altimeter data

The geoid, actual equipotential surface coincides with the average sea level (ignoring tides and other dynamical effects in oceans). The geoid heights over the oceans can be converted to the gravity anomalies data for geological and geophysical applications. Moreover, after the conversion, the satellite-derived gravity measurements can be compared and combined with gravity anomaly measurements made by ships. The algorithms of the conversion are based on laws of physics, geometry and statistics.

Several conversion techniques were developed during the recent decades to construct global marine gravity field from satellite altimeters. The following two global marine free air gravity maps, Figures 2.5 and 2.6, have been presented by Andersen and Knudsen (1995), and Sandwell and Smith (1995) who used different conversion methods.
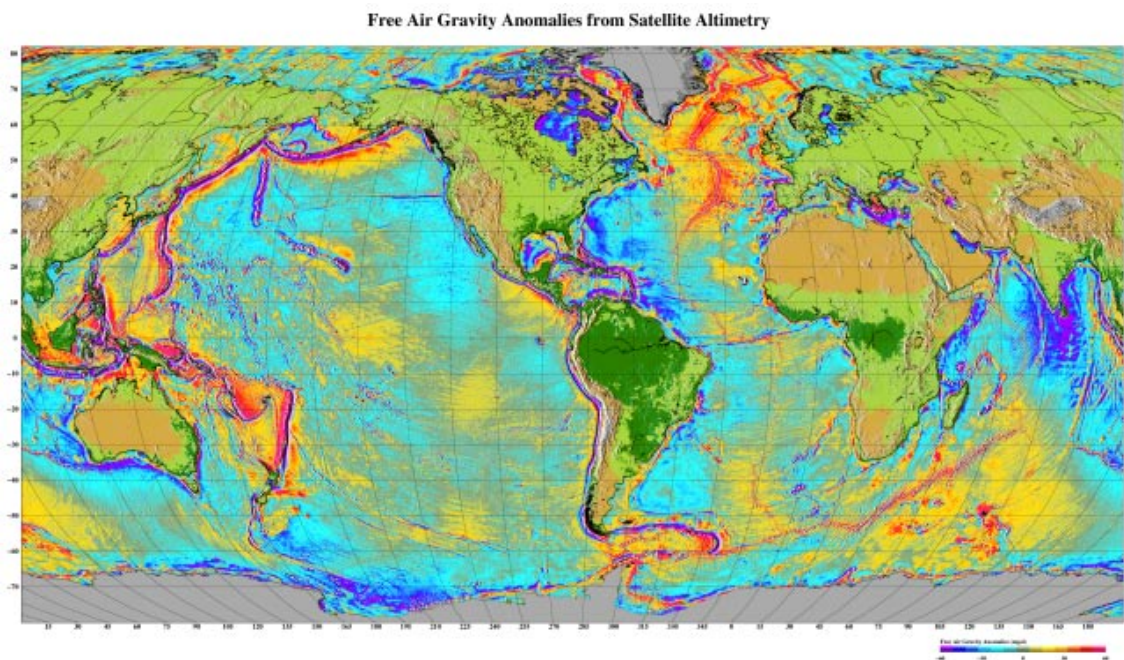
Figure 2.5 Free-Air Anomaly map (KMS2002 version of Andersen and and Knudsen, 1995).
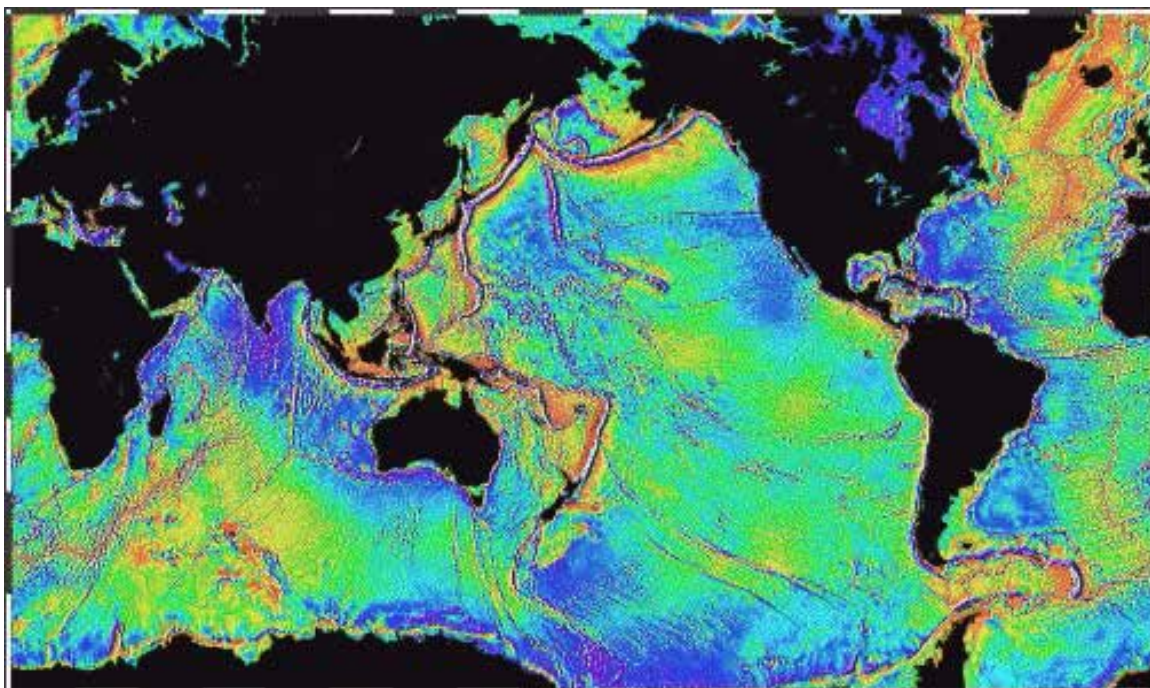
Figure 2.6 Free Air Anomaly map (15.1 version of Sandwell and Smith, 1995).

Gravity data directly derived from geoid data are designated "free-air" gravity data. Free-air gravity data can be compensated for the influence of the sea floor topography, its associated isostatic effects and land topography. Following such compensation, the derived Bouguer Gravity field is computed.

2.2 Data

In this study, ship and satellite data that are in public use were evaluated. In the first two headings the origin of the ship borne and satellite derived gravity data will be explained. Then, the sources of data necessary to construct the crust model will be presented.

2.2.1 Shipborne gravity data

Shipborne gravity data were obtained from National Geophysical Data Center (NGDC)'s database. These data were collected during the 1960s, 1970s and 1980s by various institutions, and are in public use now (Figure 2.7, Table 2.2).
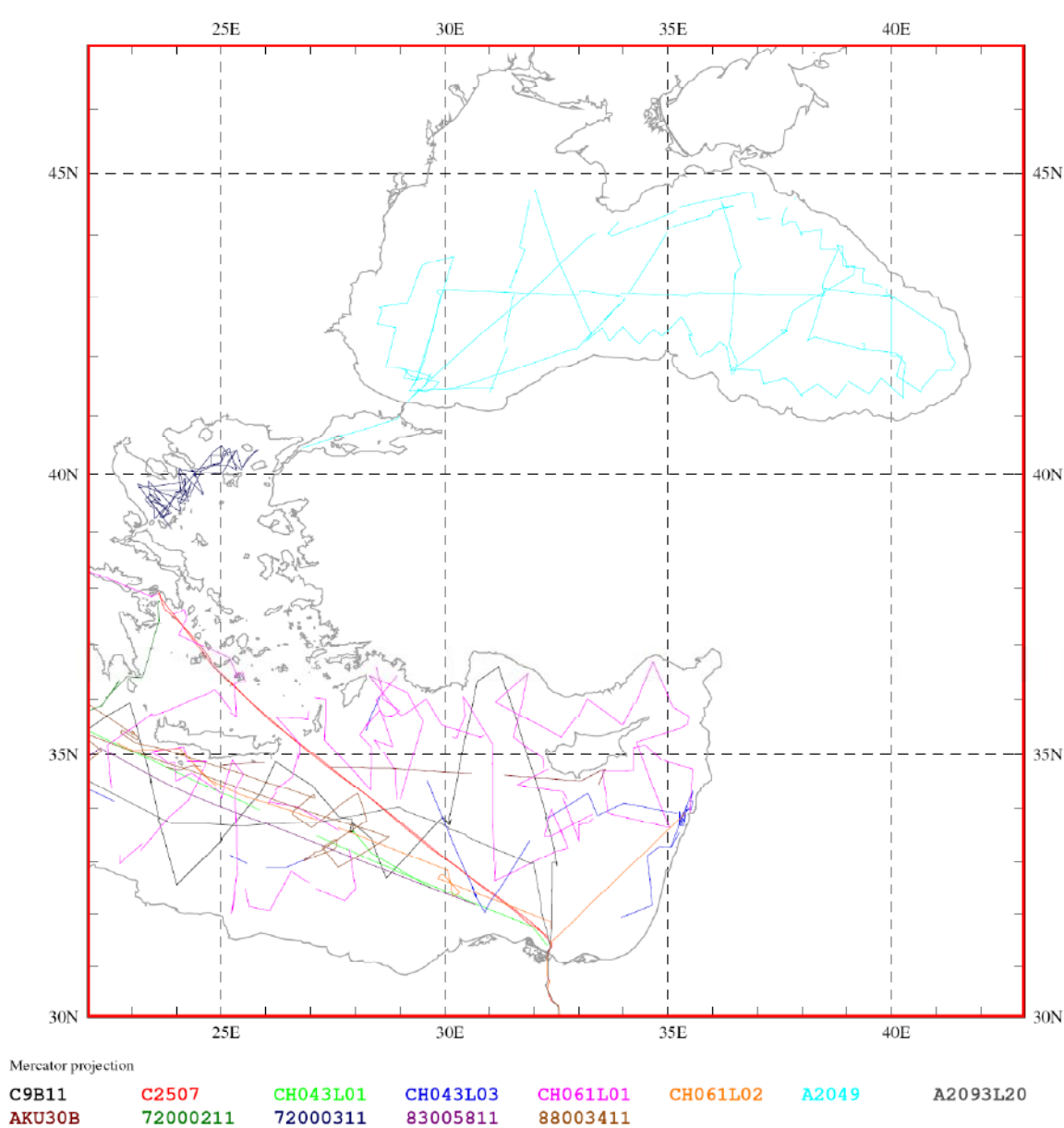
Figure 2.7. Ship borne gravity data. Colored lines indicate the surveys, see Table 2.2.

Table 2.2. The sources of the ship borne gravity data

Survey Id	Ngdc Id	Institution	Platform Name	Date	Country
C9B11	1010030	LDEO	CONRAD	1965	USA
C2507	1010242	LDEO	CONRAD	1984	USA
CH043L01	2010019	WOODS HOLE O.I.	CHAIN	1964	USA
CH043L03	2010021	WOODS HOLE O.I.	CHAIN	1964	USA
CH061L01	2010026	WOODS HOLE O.I.	CHAIN	1966	USA
CH061L02	2010027	WOODS HOLE O.I.	CHAIN	1966	USA
A2049	2020020	WOODS HOLE O.I.	ATLANTIS II	1969	USA
A2093L20	2020085	WOODS HOLE O.I.	ATLANTIS II	1977	USA
AKU30B	29050009	IPE-MOSCOW	AK KURCHATOV	1979	RUSSIA
72000211	67010023	B.N.D.O. / C.N.E.X.O.	JEAN CHARCOT	1972	FRANCE
72000311	67010024	B.N.D.O. / C.N.E.X.O.	JEAN CHARCOT	1972	FRANCE
83005811	67010126	IFREMER	JEAN CHARCOT	1983	FRANCE
88003411	67010194	IFREMER	JEAN CHARCOT	1988	FRANCE

2.2.2   Satellite derived gravity data

Gravity data derived from satellite altimetry were obtained from Sandwell and Smith (1997) database at Scripps Institution of Oceanography.

The gravity data set is in public use and it can be obtained for the whole earth surface or for a specific region (http://topex.ucsd.edu/marine_grav/mar_grav.html). It can be downloaded as either an ASCII file or IMG format. The resolution of data is 1 minutes (~1.85 km). It is not suitable for high resolution gravity survey, however for the wide regional researches as in this study, the resolution is well enough.

This global gravity anomaly data have been updated several times with new altimetry data to improve the accuracy. In this study the v15.1 dataset was used.

2.2.3   Model data

The data used for the model are given in the following sub-headings; topographic data, bathymetric data, Plio-Quaternary sediment thickness data and seismic data.

Topographic data - GTOPO30

To construct the upper part of the crust model, the GTOPO30 land elevation data were used. GTOPO30 is a global Digital Elevation Model (DEM) for land

topography. It has a horizontal grid spacing of 30 arc seconds (~1 km). GTOPO30 was derived from several raster and vector sources of topographic information.

GTOPO30 is freely available electronically through an Internet anonymous File Transfer Protocol (FTP) account at the EROS Data Center (ftp://edcftp.cr.usgs.gov/pub/data/gtopo30/global).

GTOPO30 has been divided into 33 smaller pieces to facilitate electronic distribution (Figure 2.8). In this study, only two pieces (E020N40 and E020N90) that covers the Eastern Mediterranean and Black Sea were used.
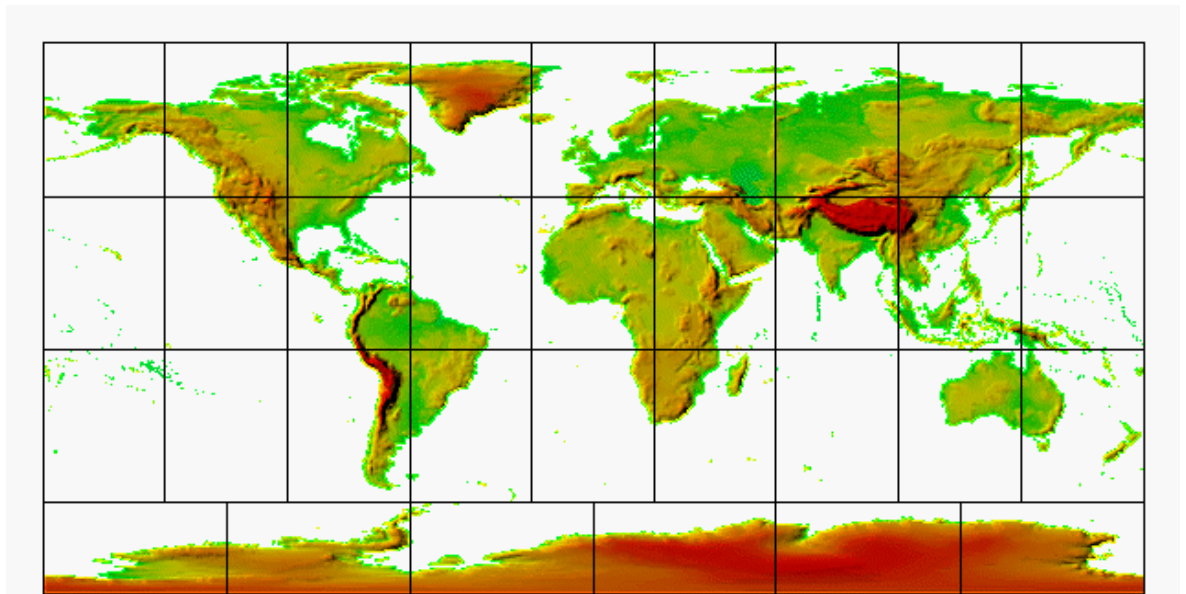
Figure 2.8. GTOPO30 – Topographic data map (GTOPO30, 1996).

Bathymetric data – GEBCO

To determine the topography of the upper-wet areas of the model, the GEBCO digital bathymetry data were used (IOC, IHO and BODC, 2003).

The General Bathymetric Chart of the Oceans (GEBCO) is a project of the Intergovernmental Oceanographic Commission (IOC) of UNESCO and of the International Hydrographic Organization (IHO). Its goal is to provide the most authoritative, publicly-available bathymetry for the world's oceans.

The GEBCO project produces global ocean floor bathymetry data sets based upon echo-sounding data collected by ships and compiled by experienced

geoscientists. Interpretation is helped by the use of directional fabric shown by satellite-derived gravity information.

The Centenary Edition of the GEBCO Digital Atlas, the latest release, was published on CDROM in April 2003. It includes a global one minute interval grid and a global set of digital bathymetric contours and coastlines (Figure 2.9).
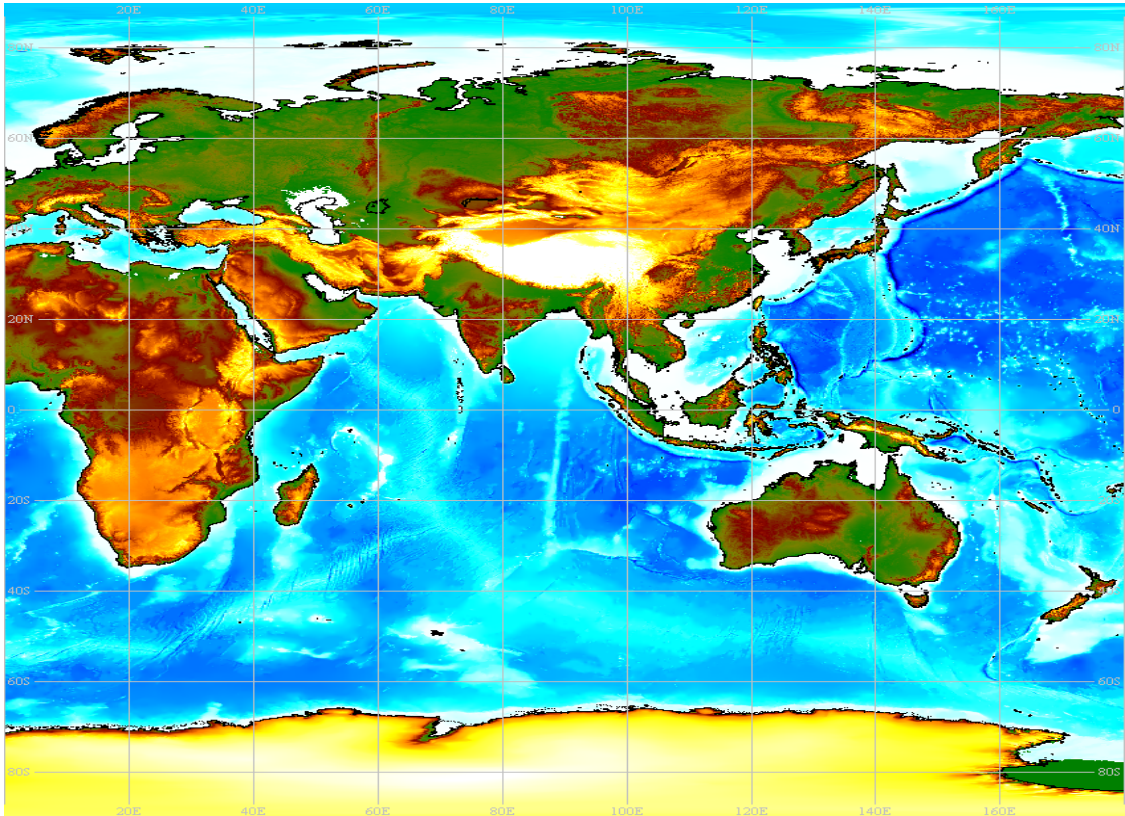
Figure 2.9. The GEBCO 1 min gridded earth elevation map (IOC, IHO and BODC, 2003).

This latest release also incorporates land elevations derived from the Global Land One-km Base Elevation (GLOBE) project data set, however they weren't used in the present study.

Plio-Quaternary Sediment thickness data

For the initial thickness of the Plio-Quaternary sediments and Messinian evaporites of the model, the IOC Plio-Quaternary Sediments thickness maps were used (Figures 1.6 and 1.9). It consists of 10 sheets at 1:1,000,000 scale that cover the whole Mediterranean. In this study, four sheets that contain the Eastern Mediterranean, Aegean Sea and Black Sea were used.

The IOC Plio-Quaternary sediment thickness map was published by the Charts Division of the Head Department of Navigation and Oceanography in Russia under the authority of the Intergovernmental Oceanographic Commission (IOC) of UNESCO. The primary data derive from numerous marine seismic surveys of the depth to the top of the Messinian salt layer, together with land compilations. Contours are in increments of 0.2 sec two-way travel time. The bathymetry is from 200 m contours of the original IBCM with supplemental 20 m, 50 m, and 100 m contours at sea.

There exist only hard-copy version of IOC Plio-Quaternary Sediments thickness maps, and no digital version unfortunately. However, in this study, the scanned version at high resolution of these maps were digitised using the ArcScan extension of the ArcGIS software. The main advantage of this software is to capability of georeferencing of the scanned maps on a digital map that is already projected.

Seismic data

To control the accuracy of the crust model, seismic data where available were used. Primarily seismic data source for this study is the "Geophysical Data Report of the Eastern Mediterranean Sea" published by Cambridge University. It consists of the data collected during the cruises of the RRS Shackleton in 1972 and 1974.

The interpreted and published data from several surveys are also used in the present study (Vidal et al., 2000a; Vidal et al., 2000b; Aksu et al., 2005b).

3 Results

In this study, the crustal structures of the Eastern Mediterranean and Black Sea based on ship borne data and satellite gravity data were carried out. In order to carry out the above mentioned task, the subjects were examined in three consecutive steps. First step is the comparison of the satellite derived gravity data values with those gravity data measured along the ship tracks to verify the data quality. Then, the gravity anomalies related to subsurface structures are interpreted by new generated free-air anomaly and Bouguer anomaly maps. Finally, a three dimensional model of the crust is constructed to analyze the thickness and density variations of subsurface structures of two basins.

3.1 Satellite gravity data versus ship borne gravity data

In order to verify the applicability of the satellite altimeter derived gravity data, the comparison of the data with ship borne gravity data is very important. Two versions of Sandwell's satellite data, v11 and v15, and ship data are used in the comparison. The origin of the data is explained in Material and Method section of this study.

The ship tracks used in the comparison exercise and the residuals of ship and satellite data are shown in Figures 3.1, 3.2 and 3.3 for the Black Sea, and in Figures 3.5, 3.6 and 3.7 for the Eastern Mediterranean, respectively. Additionaly, bathymetric and morphologic maps of the Black Sea and Mediterranean Sea with the locations of profiles are presented in Figures 3.4 and 3.8, respectively. Although the Agean and Marmara seas are out of the content of this study, the two ship tracks available in the region are presented in Figure 3.9 and discussed in detail for the purpose of general evaluation of the satellite gravity data in the Turkish Seas. Residuals of ship and satellite data are also shown in Figure 3.10.

3.1.1 Black Sea

In Figures 3.1 and 3.2, six profiles, taken along ship tracks in the Black Sea, were analyzed to compare ship-borne free-air anomaly data with two satellite derived free-air anomaly data. The bathymetry and location of the profiles are shown in the Figure 3.4.

In general, all data displayed similar trends probably depending on sub bottom features. Except SW-NE trending profile in the central Black Sea (Figure 3.2c), the ship borne data have higher anomaly values than satellite data.

In the profile BS_01 parallel to the long axis of the Black Sea that extends from west to east (Figure 3.1a) free-air anomalies have a correlation with the sea floor only at the beginning of the line. The residuals between ship and satellite data vary between ±25 mGal (Figure 3.3a).

In the deeper parts of the profiles BS_02 and BS_03, from the western Black Sea (Figure 3.1b, 3.1c), the satellite derived free-air anomalies have lower values than the ship data. In the profile for BS_02, the residual changes from 10 mGal to 35 mGal (Figure 3.3b). However, towards to coast (Figure 3.1c) where the shoaling has led to the steep slope on the sea floor (Figure 3.4), the ship-borne gravity anomalies decrease whereas the satellite derived gravity anomalies increase. Thus the positive residual of the profile BS_03 decreases to ~-60 mGal (Figure 3.3c).

In the eastern part of the Black Sea, as in the western part the curves' trends of both ship and satellite data curves are similar (Figure 3.2a, 3.2b). In the profile BS_04, the difference between ship and satellite data were calculated as ±40 mGal (Figure 3.3d). The abrupt change in the residual occurs where the sea floor rises suddenly (Figures 3.4, 3.3d). The residuals between ship and satellite data on the profile BS_05 varies from -20 to 30 mGal, except for the residual of -40 mGal near the coast (Figure 3.3e).

At the beginning of the diagonal profile BS_06 in the central Black Sea where the depth values are missing (Figure 3.2c), the residual is about -120 mGal, however, in offshore the residual becomes zero (Figure 3.3f).
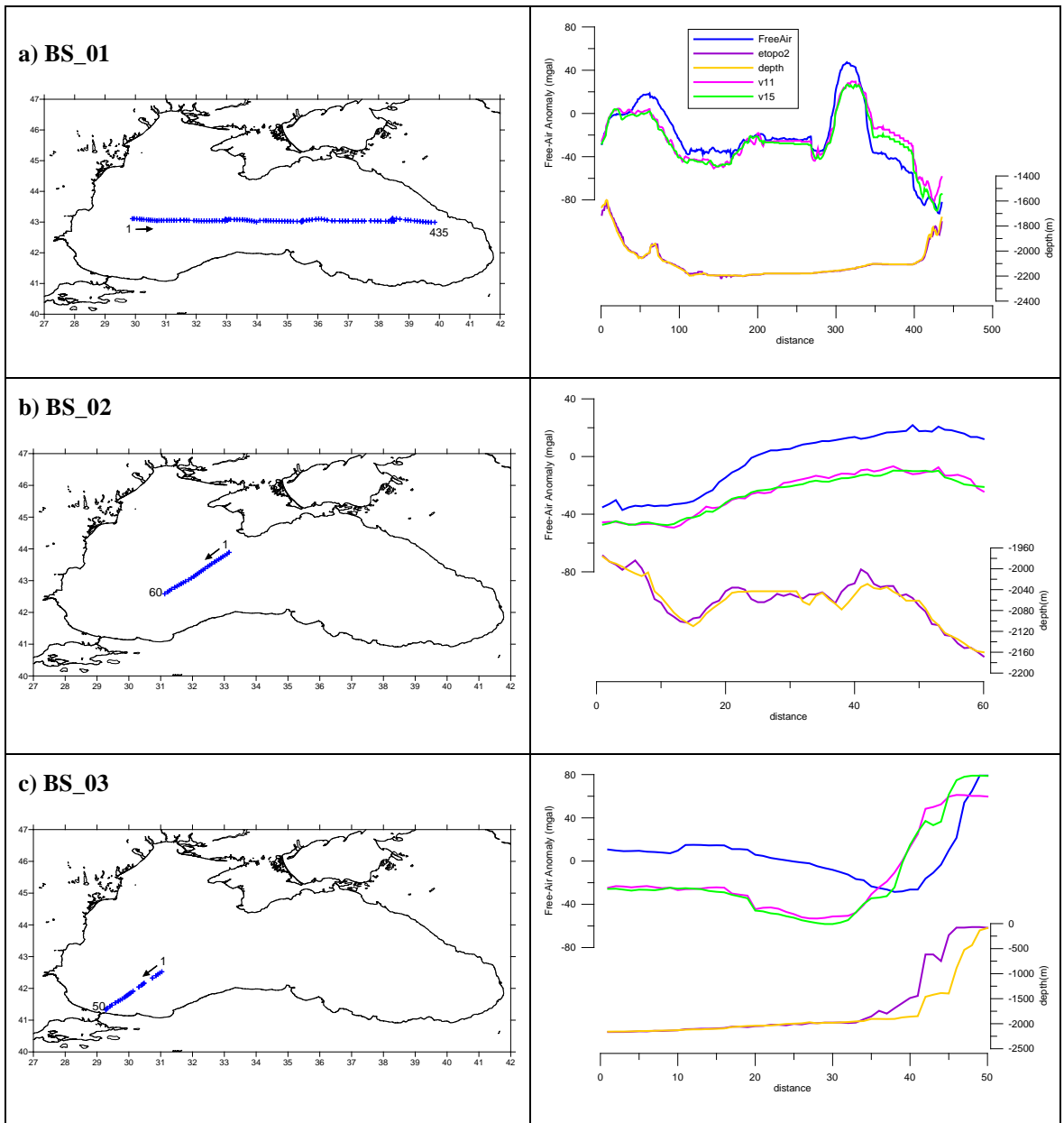
Figure 3.1 Shipborne data versus Satellite data for the Black Sea.
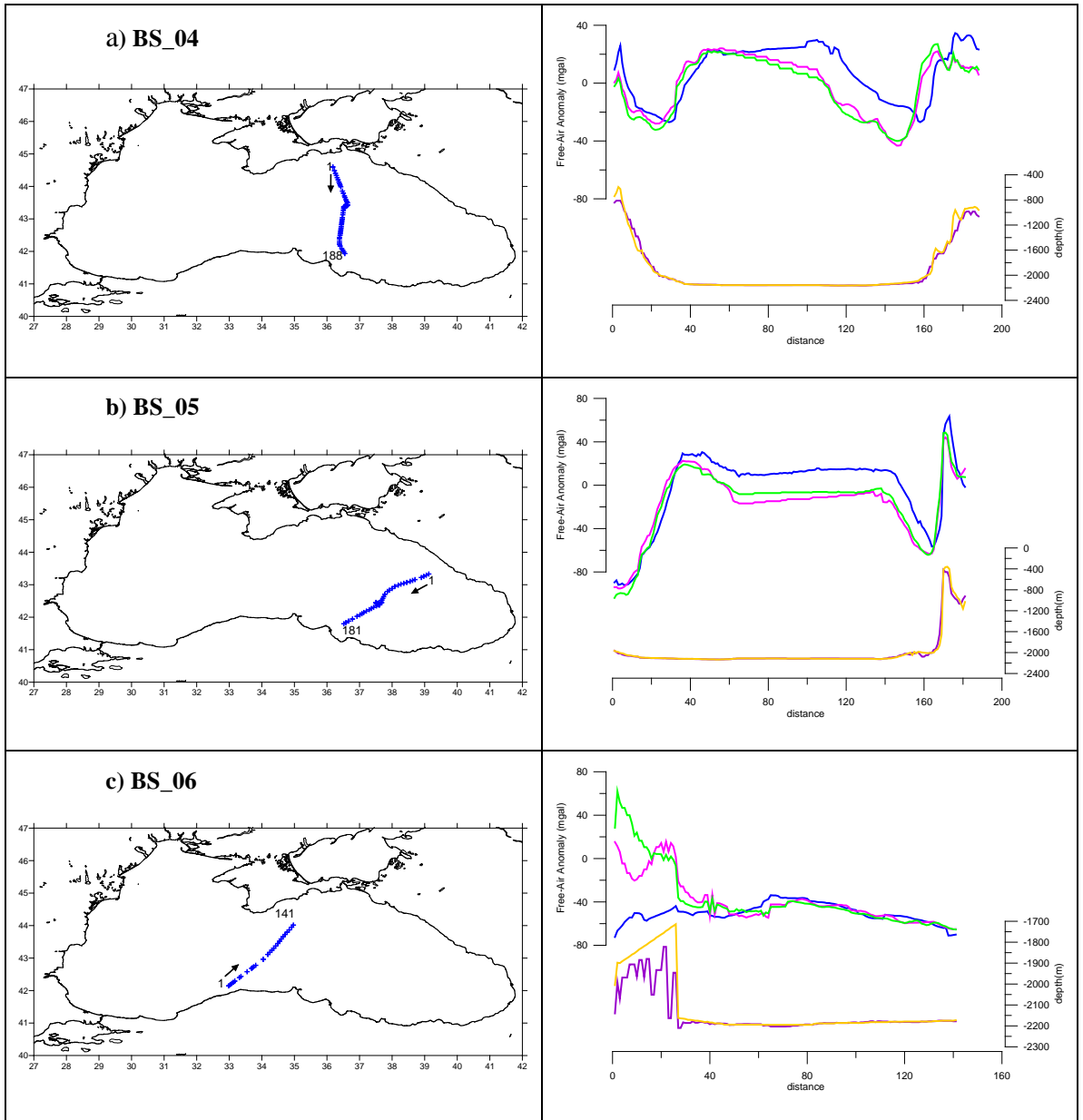
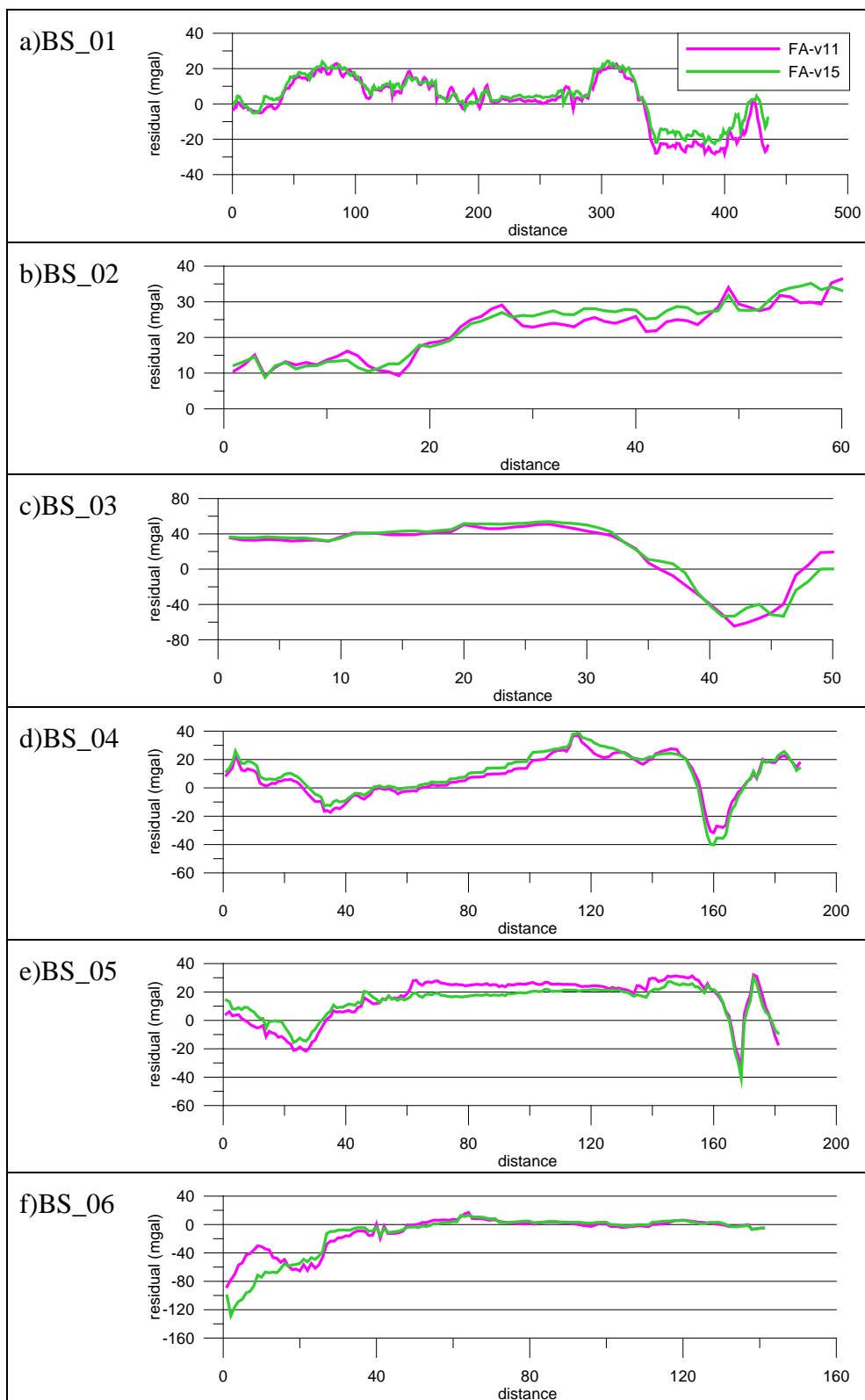Figure 3.2 Shipborne data versus Satellite data for the Black Sea.

Figure 3.3 Residuals of ship versus satellite data in the Black Sea.
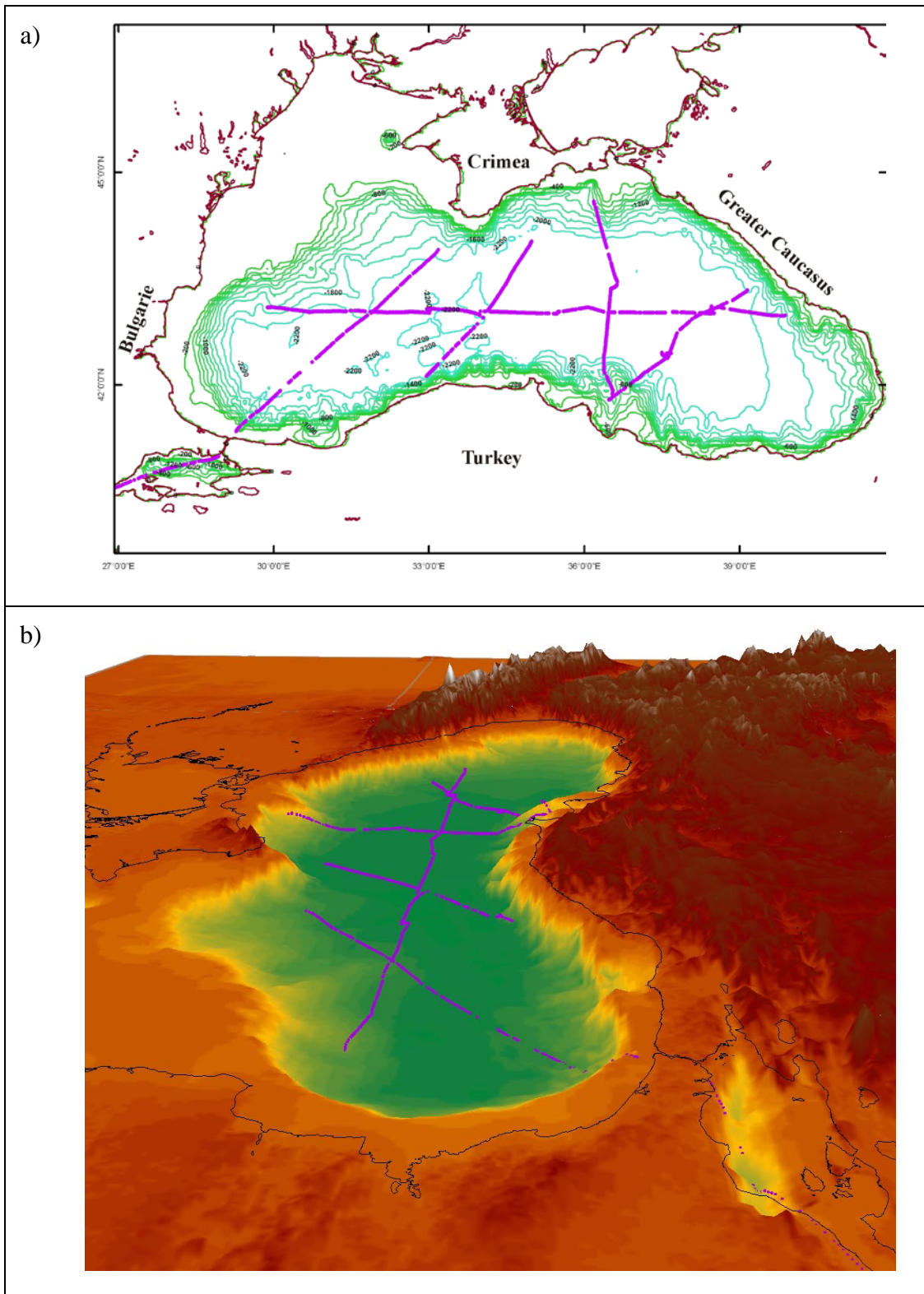
Figure 3.4. Bathymetric map (a) and morphological map (b) of the Black Sea with the location of profiles.

3.1.2   Eastern Mediterranean

In the Eastern Mediterranean, free-air anomaly data calculated from in situ measurements and satellite derived gravity data were analyzed along six profiles (Figure 3.5, 3.6). The residuals between ship and satellite data, and the location of the profiles and bathymetry of the Eastern Mediterranean are presented in Figures 3.7 and 3.8, respectively.

As in the Black Sea, the general trend of the curves on both the ship and satellite data are similar. However the differences between satellite data and ship data in Eastern Mediterranean are higher than those found in the Black Sea. Generally, the measured gravity data have greater values than the satellite data.

In the profile EM_01 (Figure 3.5a), the maximum residual between ship and satellite data appears to be -60 mGal (Figure 3.7a) and is caused by the Eratosthenes seamount. The remaining part of the profile shows a variation of about ±20 mGal.

Because of the rough sea-floor morphology at the beginning of the profile EM_02 (Figure 3.5b), from the Antalya Basin to the Anaximander Mountains (Figure 3.8), the residual is up to 100 mGal (Figure 3.7b). Over the Anaximander Mountains that rises up 1000 m from the adjacent sea floor, the residual is about -45 mGal (Figure 3.7b).

The profile EM_03 (Figure 3.5c) starts from the Finike Basin, and extends towards to Herodotus Basin passing over the Anaximander Mountains (Figure 3.8). The residual over the Anaximander Mountains is about 40 mGal whereas the Herodotus basin is characterized by ±20 mGal.

The profile EM_04 consists of several sub-profiles located in relatively shallow areas of the Eastern Mediterranean. In the Antalya basin (Figure 3.6a; zone1), the residual is up to 50 mGal (Figure 3.7d). In zone 2, towards to Anamur-Koruçam zone (Figure 3.8), the residual reaches to its maximum value of -150 mGal, in the all profiles. In Çukurova Basin (Figure 3.6a; zones 3-6) the residuals range between ±50 mGal. The other sub profiles (Figure 3.6a, zone 7 and 8) situated in Latakia Basin and Levantine Basin, satellite data have low values than ship data. The maximum residual seems to be 75 mGal (Figure 3.7d).

The profile EM_05 (Figure 3.6b) over the smooth sea bottom extending from Levant Margin to the Nile Cone (Figure 3.8) shows the maximum residual deviation of ±30 mGal (Figure 3.7e).

In the Figure 3.6c, the profile EM_06 starts from the Pliny-Strabo trenches and extends to Nile Cone (Figure 3.8). At this profile, the residual changes -20 mGal to 80 mGals over the Pliny-Strabo trenches and Mediterranean Ridge (Figure 3.7f). After that, the residual between ship and satellite data remain constant around 20 mGal crossing over the Herodotus Basin (Figure 3.7f).
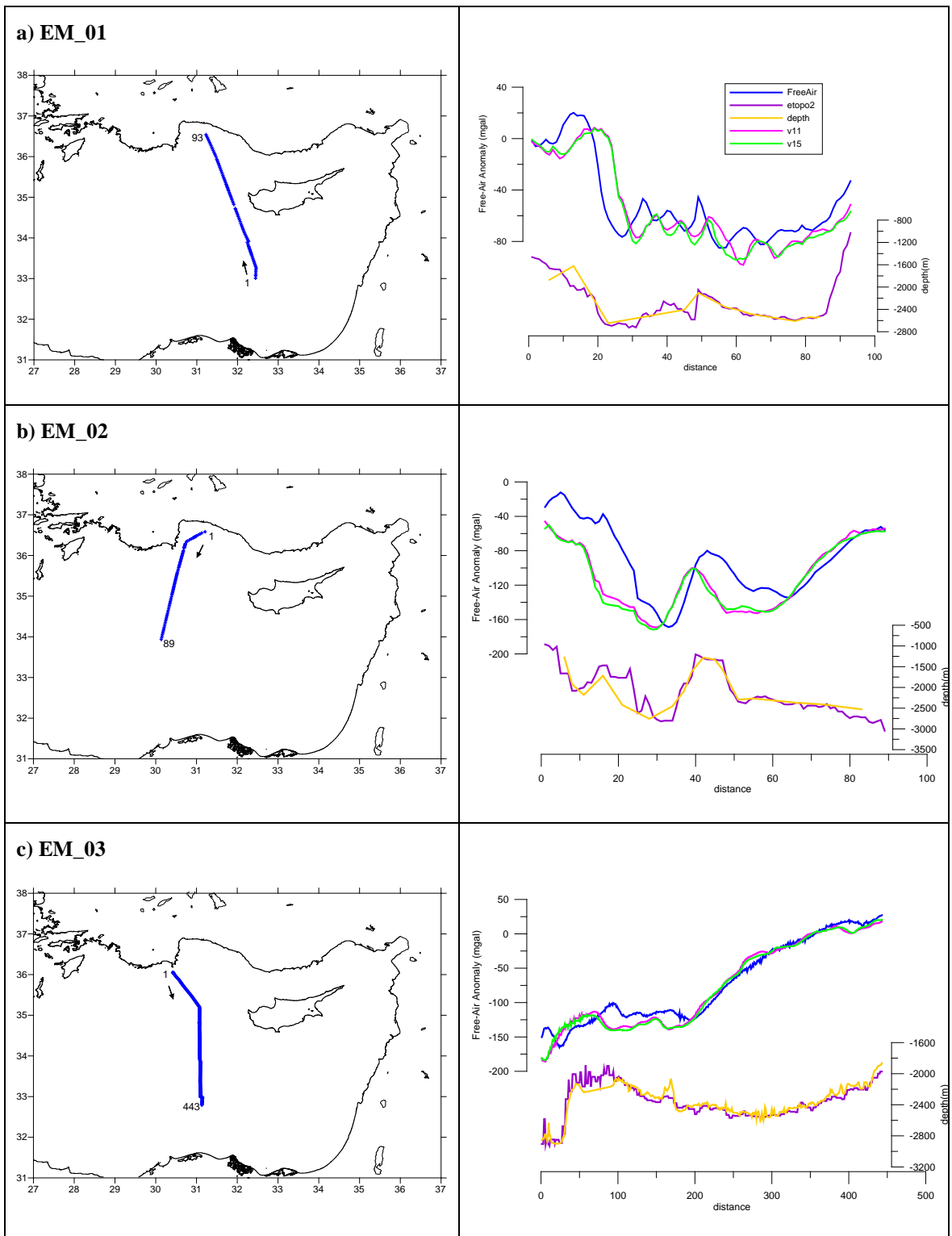
Figure 3.5. Shipborne data versus Satellite data for the Eastern Mediterranean.
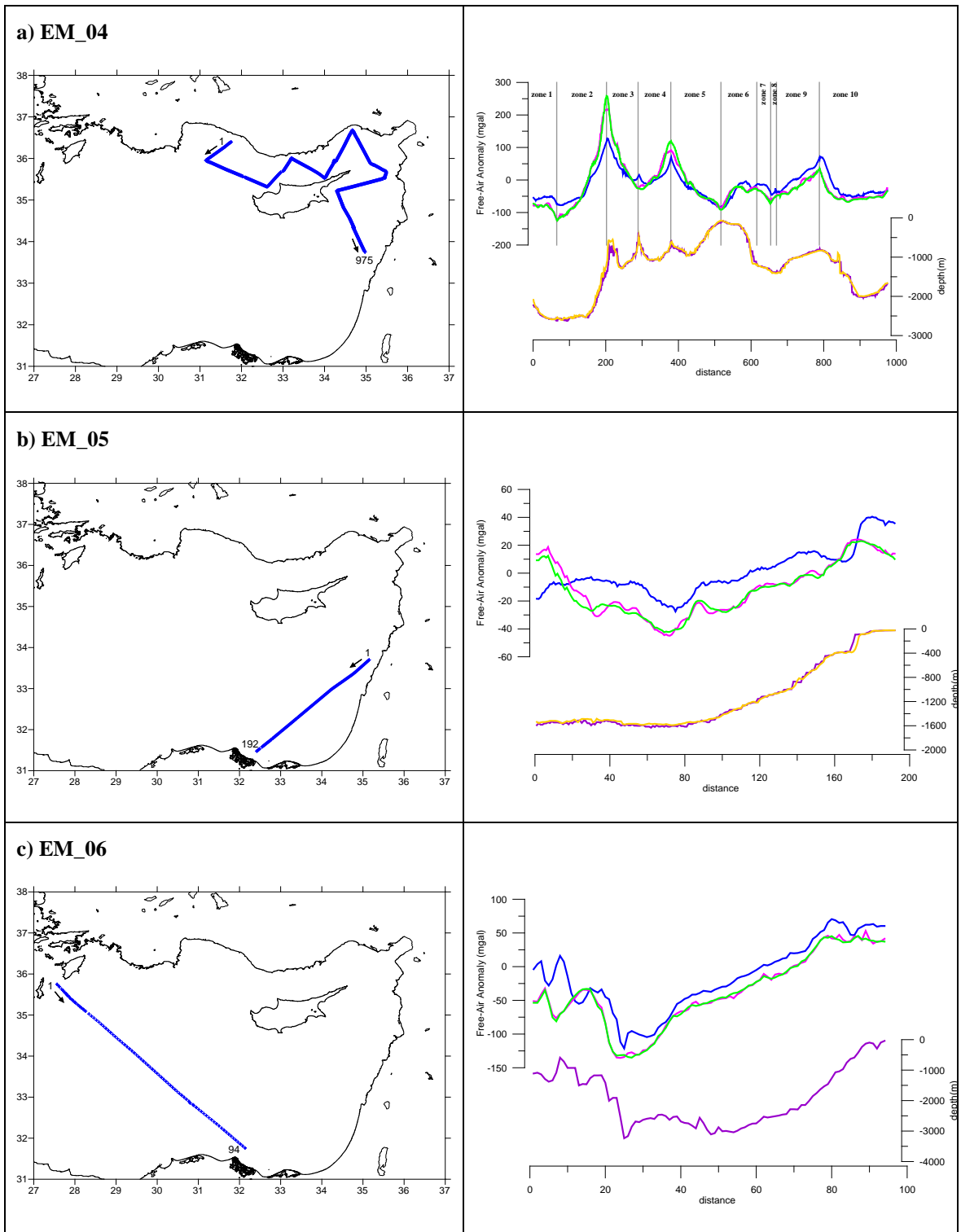
Figure 3.6. Shipborne data versus Satellite data for the Eastern Mediterranean.
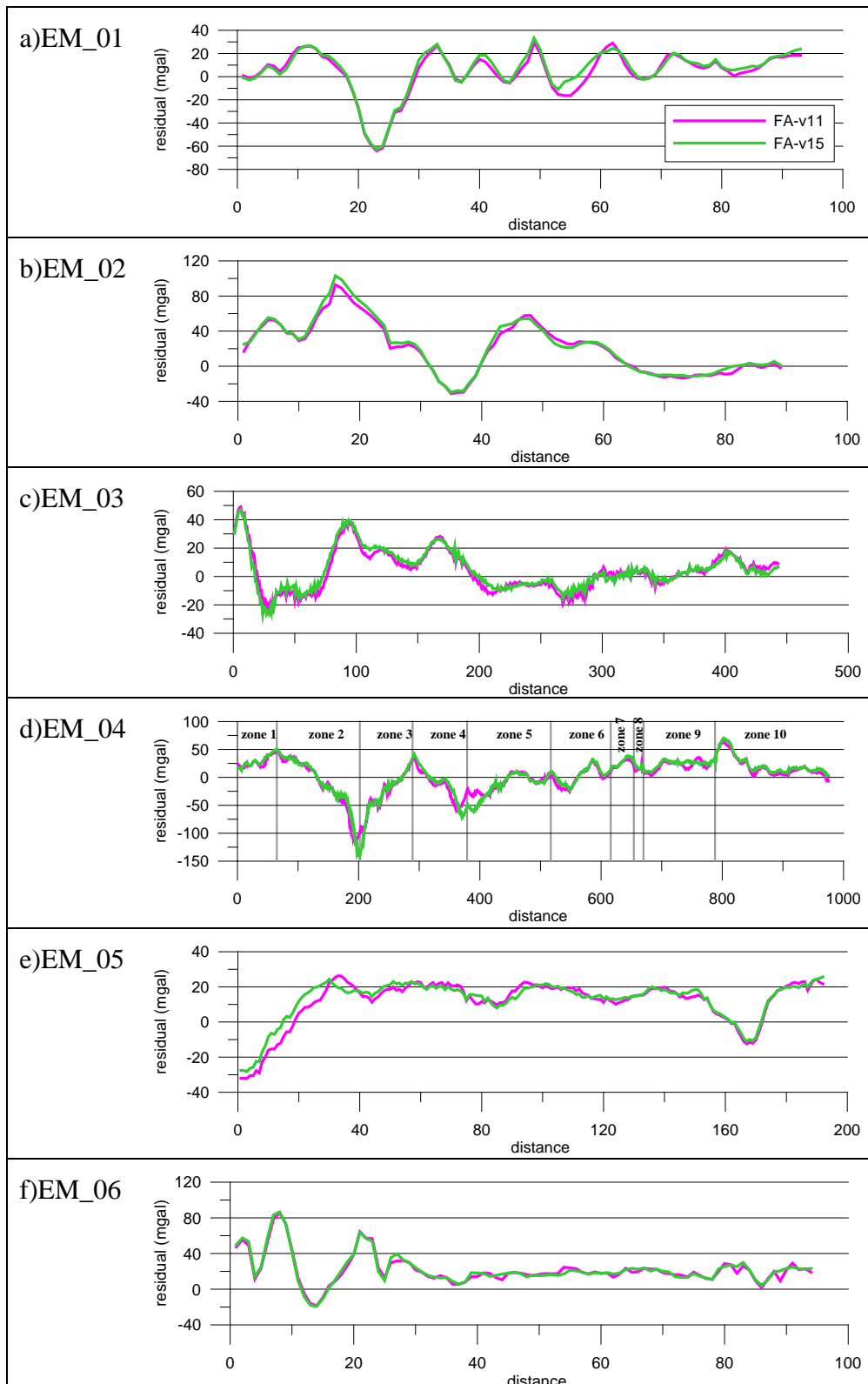
Figure 3.7. Residuals of ship versus satellite data in Eastern Mediterranean.
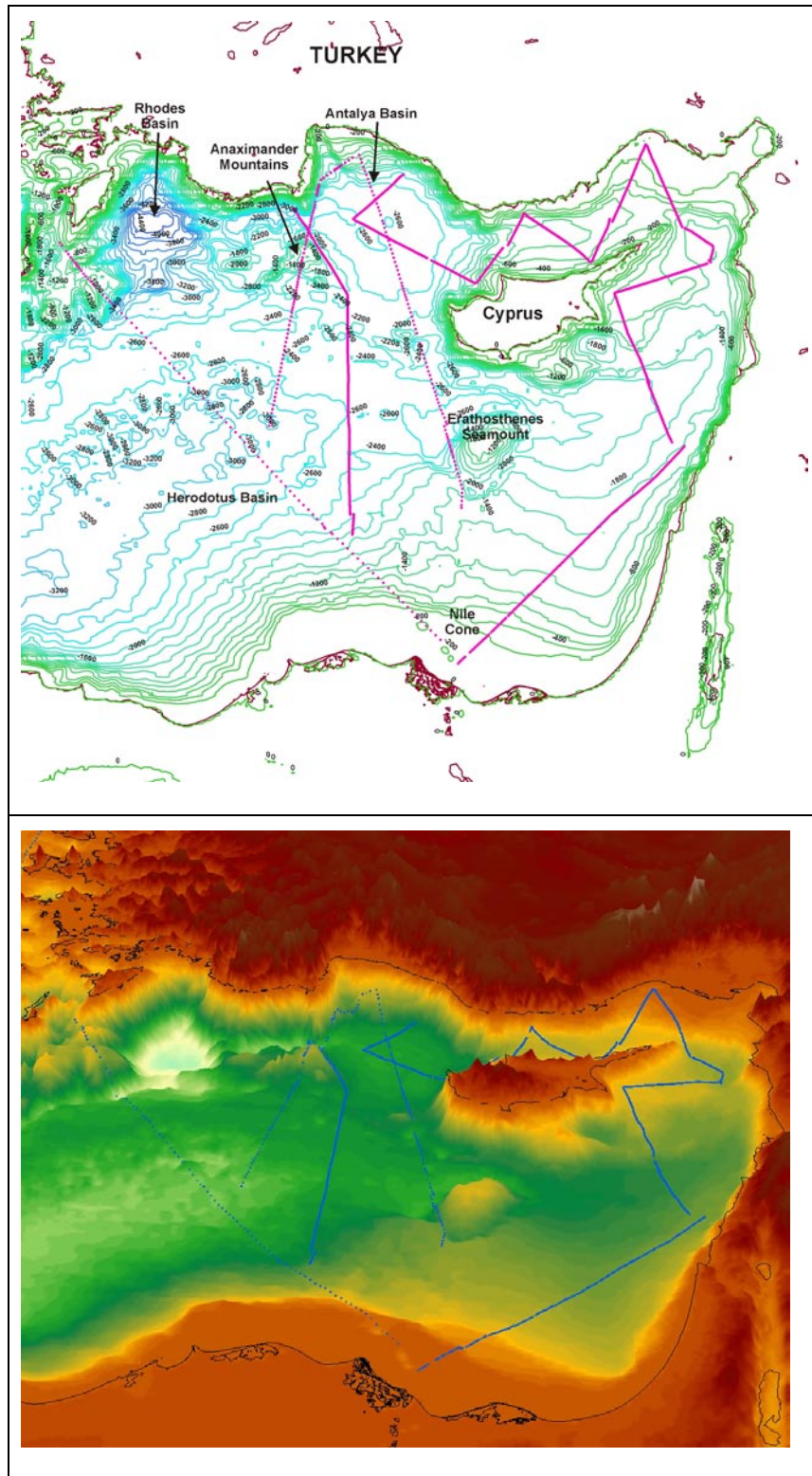
Figure 3.8. Bathymetric map (a) and morphological map (b) of the
Mediterranean Sea with the locations of profiles.

3.1.3 Aegean and Marmara Seas

Two profiles, one in the Aegean Sea and another in the Marmara Sea were analyzed for a general evaluation of satellite gravity data in Turkish seas (Figure 3.9).

As it can be seen from the etopo2 curve in Figure 3.9a, the Aegean Sea has a relatively shallow depth and rough topography. Despite the uneven topography, the residual between satellite and ship data range between -40 and 60 mGal (Figure 3.10a).
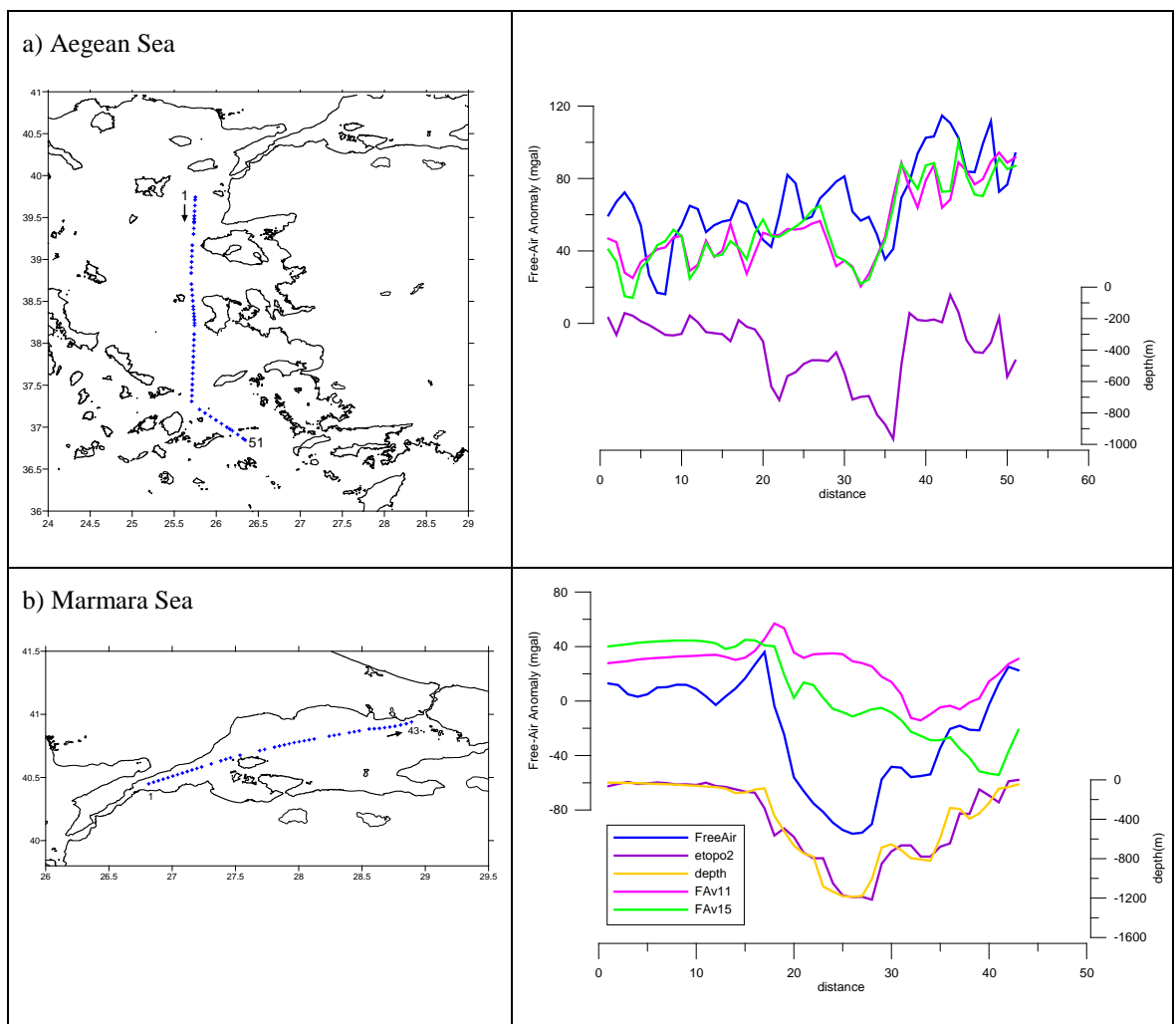
Figure 3.9. Shipborne data versus Satellite data for the Aegean Sea and Marmara Sea.
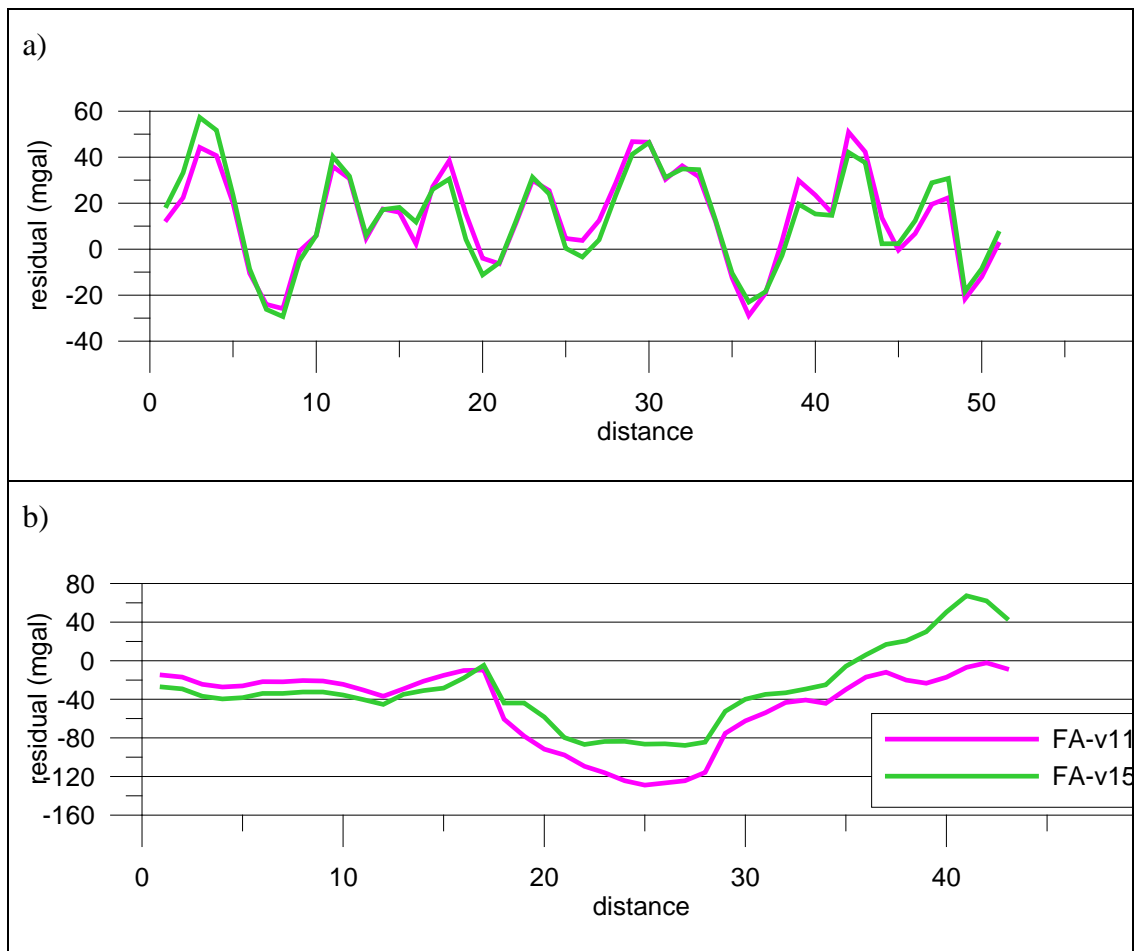
Figure 3.10 Residuals of ship versus satellite gravity data in the Aegean Sea (a) and Marmara Sea (b).

In the Aegean Sea the general trend of the anomalies are similar. However, in the profile from the Marmara Sea (Figure 3.9b), the ship data shows significantly low values compared with the satellite values. The residual varies between -130 and 60 mGal (Figure 3.10b).

3.2 Gravity anomaly maps

The new generated gravity maps are presented in this section. The free-air and Simple Bouguer gravity anomaly maps were interpreted in terms of potential field of the earth for the Black Sea and Eastern Mediterranean, respectively.

The free-air maps are composed of the satellite derived gravity anomalies. The Simple Bouguer anomaly maps are generated from the free-air maps using etopo2 and GEBCO elevation data.

3.2.1 Black Sea

Free-Air Anomalies

The free-air anomaly map for the Black Sea is presented as a relief map in Figure 3.11a, and as a contour map in Figure 3.11b.

The weak negative free-air anomalies are dominant in the Black Sea (Figure 3.11a). Additionally, there exist some local isolated negative anomaly lows. For example, off the Bulgarian coast, a relatively small area has negative anomalies lower than -80 mGal. In the Sorokin trough, a gravity low of up to -100 mGal that limited by the coastline occurs. Off the north-eastern coast of Black Sea a long-narrow negative zone exists with a maximum magnitude of -108 mGal.

Positive free-air anomalies are generally limited by the continental shelf of the Black Sea (Figure 3.11a, b). The large north-western shelf has free-air anomalies up to 60 mGal.

Over the mountains that surround the Black Sea, free-air anomalies are strongly positive. Their magnitudes reach 100 mGal over mountains along the Turkey coast, and 180 mGal over the Greater Caucacus Mountains and the southern Crimea. The remaining coastal plain around Black Sea has positive values ranging between 0 and 60 mGal.
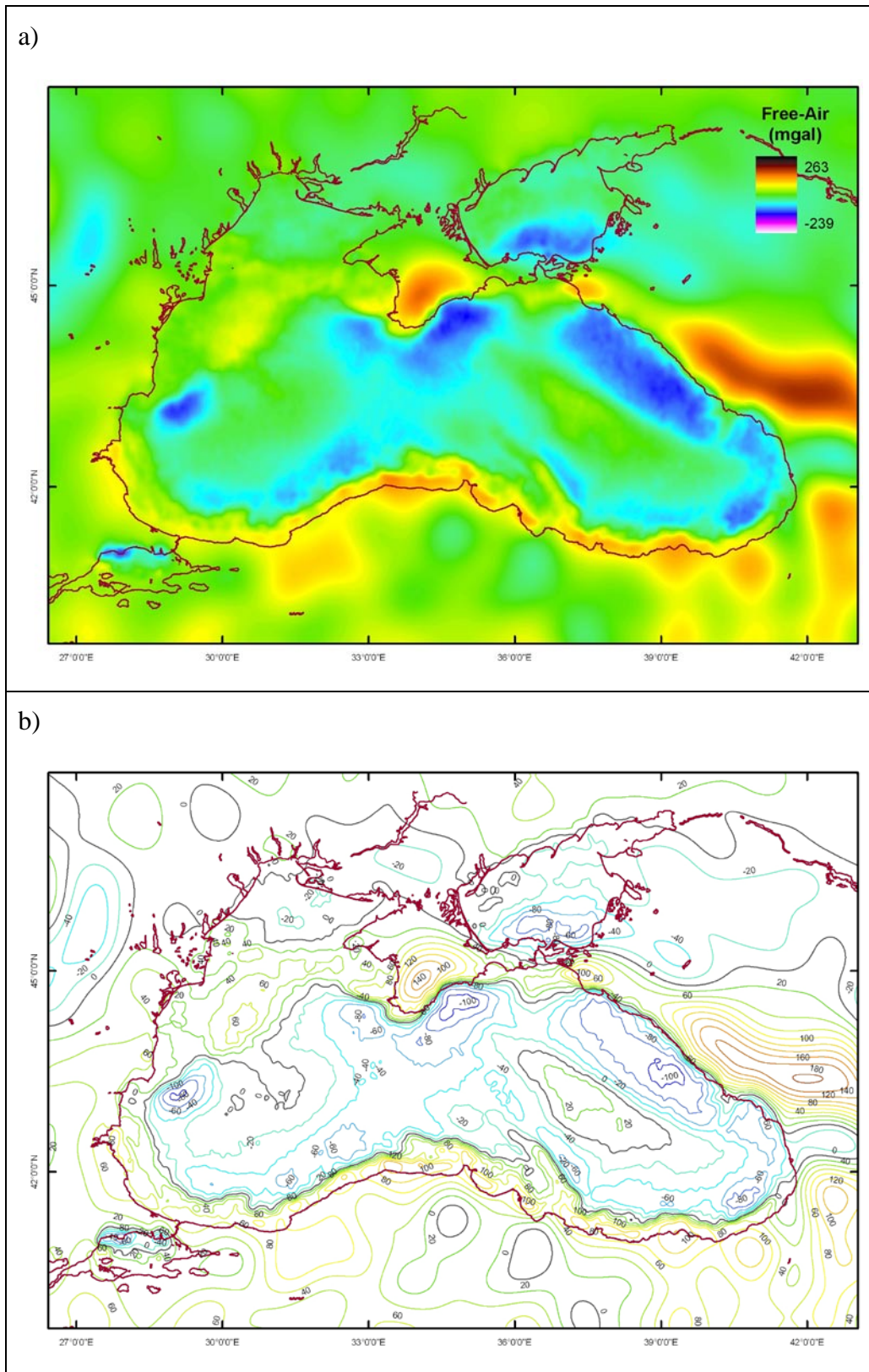
Figure 3.11 Free Air anomaly maps of the Black Sea. a) relief map b) contour map
(20 mGal interval). Values were derived from satellite altimetry data (Sandwell and
Smith, 1997).

A large gradient of the free-air anomalies occurs in Crimea area between land and offshore. The anomalies range from 140 mGal on land to less than -100 mGal at sea (Figure 3.11).

Both the eastern and western basins of the Black Sea are characterized by weak positive anomalies (Figure 3.11a, b).

Two small gravity lows exist in Marmara Sea, along the northern shelf. The free air anomaly decrease as low as -60 mGal.

Bouguer Anomalies

The simple Bouguer anomaly map for the Black Sea is presented as a relief map in Figure 3.12a, and as a contour map in Figure 3.12b.

Generally the Bouguer anomalies conform to the Black Sea topography. Despite a few local negative zones, water area is dominated by positive anomalies. The strong positive anomalies occur at the center of the Black Sea basin (Figure 3.12a). Both eastern basin and western basin have high Bouguer anomalies of up to 160 mGal and 140 mGal, respectively.

In most of the Black Sea zero contours follow the coastline. In the Turkey, the Simple Bouguer anomalies increase eastward from -60 mGal to -220 mGal, possibly due to topographic rise.
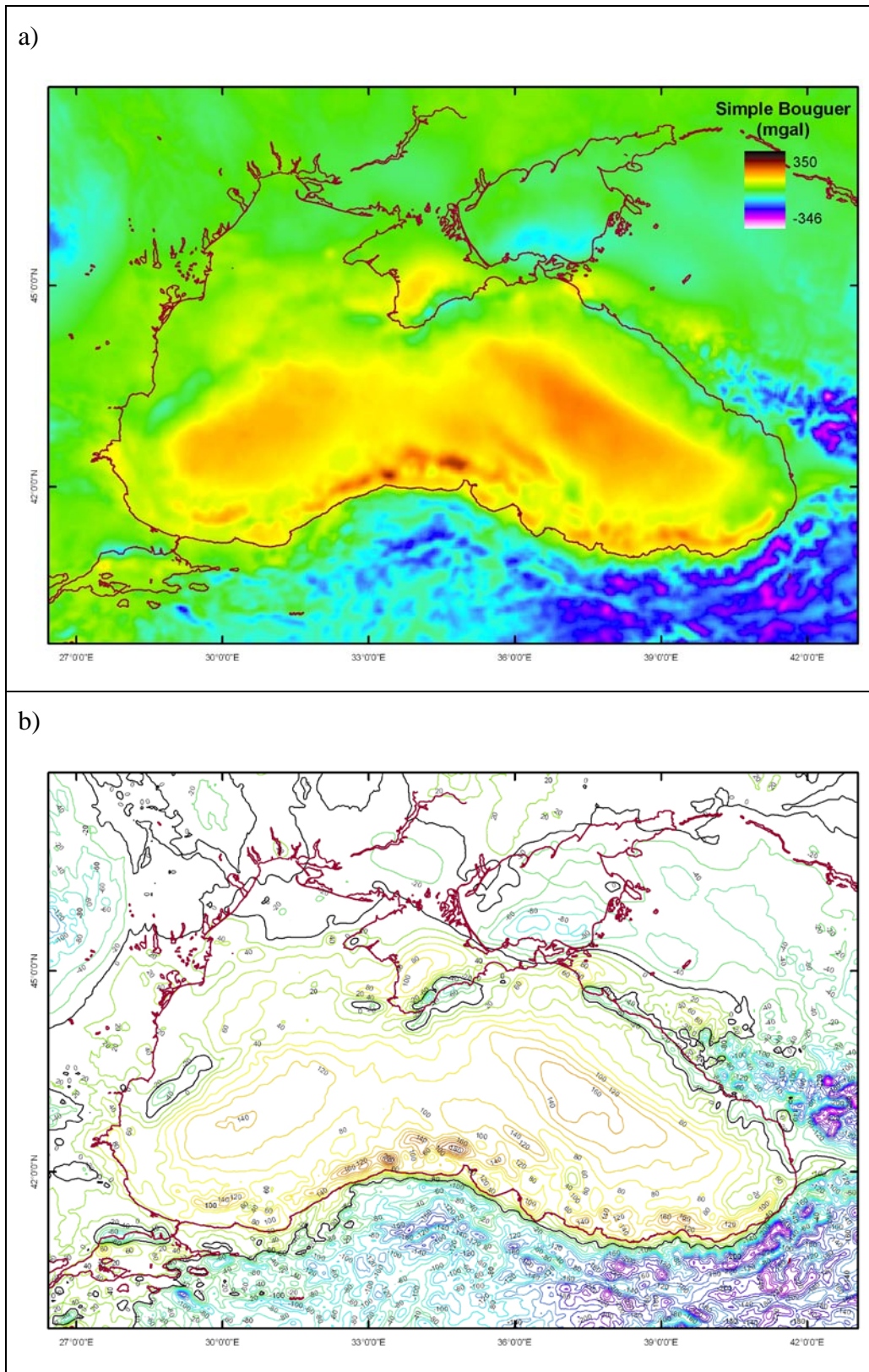
Figure 3.12 Simple Bouguer anomaly map of the Black Sea. a) relief map b) contour map (20 mGal interval).

3.2.2   Eastern Mediterranean

Free-Air Anomalies

The Free-Air Anomaly map for the Eastern Mediterranean is presented as a relief map in Figure 3.13a, and as a contour map in Figure 3.13b.

The Eastern Mediterranean is characterized by mainly negative free-air anomalies offshore and positive free-air anomalies on land (Figure 3.13a, b).

The maximum negative free-air value of -240 mGal locates in the Rhodes abyssal plain, whereas the maximum positive free-air anomaly value of 263 mGal occurs on the Cyprus Island (Figure 3.13b).

The zone between Rhodes, Turkey and Cyprus is dominated by high negative values (< -100 mGal). In this zone, a discontinuity occurs over the Anaximander Seamounts where the anomalies rise up to about -30 mGal. This negative zone extends between Cyprus and Erathostenes Seamount with free-air anomalies of less than -100 mGal and continues through Latakia basin (Figure 3.13).

The Herodotus abyssal plain and the southern Levantine basin have relatively less negative free-air anomalies (> -100 mGal). Some positive free-air anomalies over the marine areas are observed on Erathostenes Seamount that rises over 1000 m above the sea floor and on Nile delta. The anomaly values reach to 50 mGal on the Erathosthenes Seamount and to 80 mGal on the Nile Delta (Figure 3.13b).

In Eastern Mediterranean, the free air anomaly values changes very rapidly in short distance. Between Turkey and Rhodes, free-air anomaly first decreases from 120 mGal to about -240 mGals and then increases again to 80 mGals (Figure 3.13). One similar large gradient was observed between Cyprus and Eratosthenes seamount, the anomalies range from 263 mGal to less than -100 mGal (Figure 3.13).

The Levantine Basin's coastline has a positive belt of free-air anomalies with the magnitude of about 40 mGal. The island of Cyprus is dominated by significantly large positive anomalies up to 260 mGal.
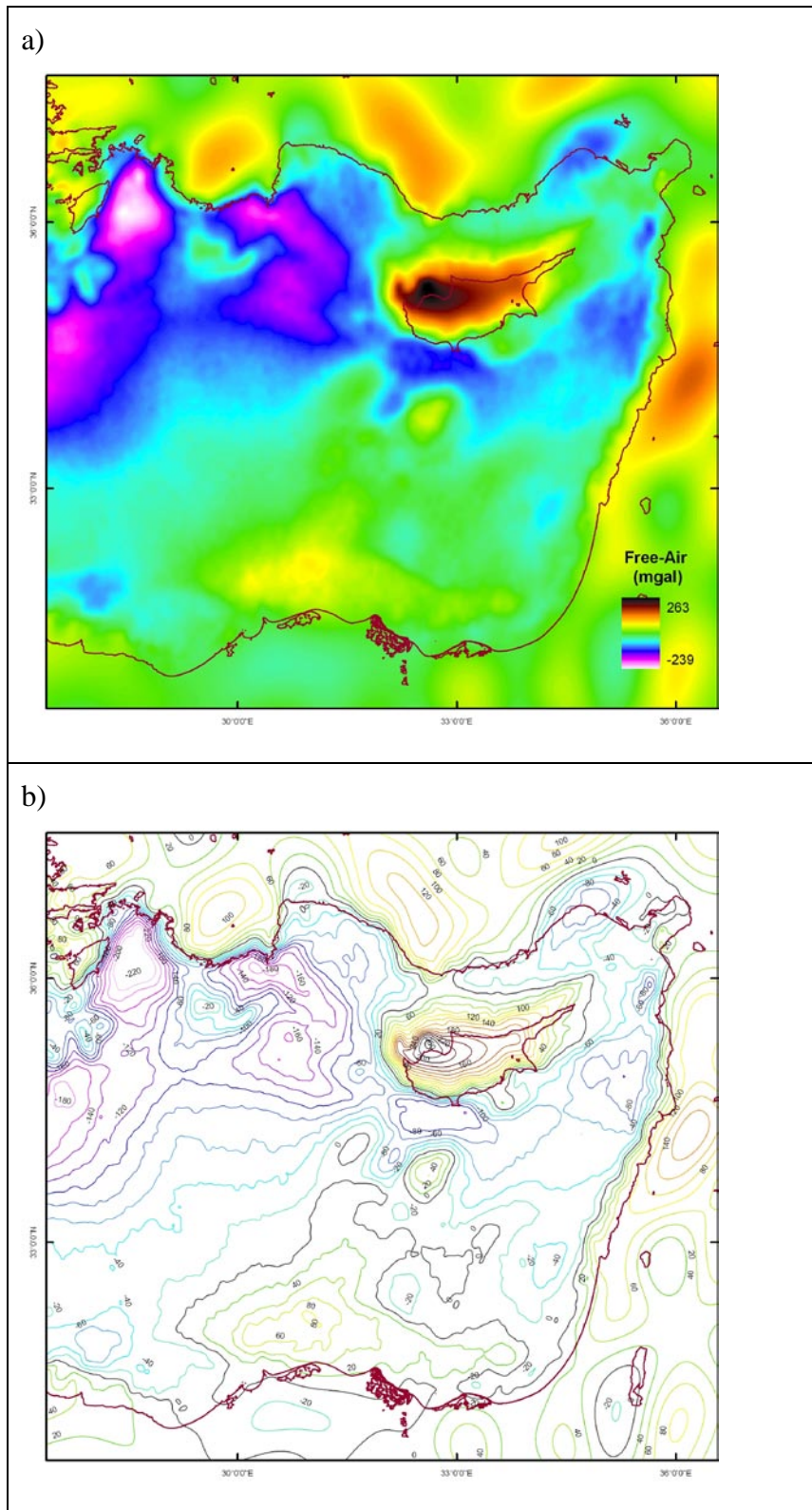
Figure 3.13 Free-air anomaly map of the Eastern Mediterranean. a) relief map b) contour map (20 mGal interval).

Bouguer Anomalies

The simple Bouguer Anomaly map that generated from satellite altimetry derived gravity data is presented in Figure 3.14.

As it would be expected, in the simple Bouguer anomaly map (Figure 3.14) the land areas have negative and water-covered areas have positive anomalies generally with some exceptions. From Syria to North Africa, a long and narrow belt along the coast has positive anomalies (Figure 3.14). In the northern part of the Eastern Mediterranean, negative anomaly zone follows the Anatolian coastline; however in the Mersin Bay it follows the shelf break (Figure 3.14).

A large area from Herodotus basin to Levantine basin is dominated by the positive anomalies up to 180 mGal (Figure 3.14b). In the northern foot of the Eratosthenes Seamount, they anomaly reach 200 mGal where the depth is about 3000 meter (Figure 3.14b).

The maximum positive Bouguer anomaly values occur off the northwestern Cyprus. The anomalies reach more than 350 mGal (Figure 3.14b) and continue eastward with decreasing along the Misis-Girne range. Westward, the anomaly values decrease suddenly from 330 mGal to 80 mGal within the distance of 40 km (Figure 3.14). Toward to Antalya Bay, the Northern Cyrus anomaly decreases with a smooth gradient to 60 mGal. The shelf of the bay has negative values.

Mersin Bay appears as the extension of the Taurus Mountains negative zone where the maximum negative Bouguer anomalies with a magnitude of about -280 mGal (Figure 3.14).

Three negative gravity lows are followed between positive anomalies (Figure 3.14a). One is placed over the Anaximander Mountains and has a maximum negative anomaly of -40 mGal. Another one is observed over the Rhodes trough with a magnitude of -130 mGal. The last one appears between Cyprus and Eratosthenes seamount. Despite the adjacency to the maximum positive anomaly, it has a negative anomaly of -100 mGal.
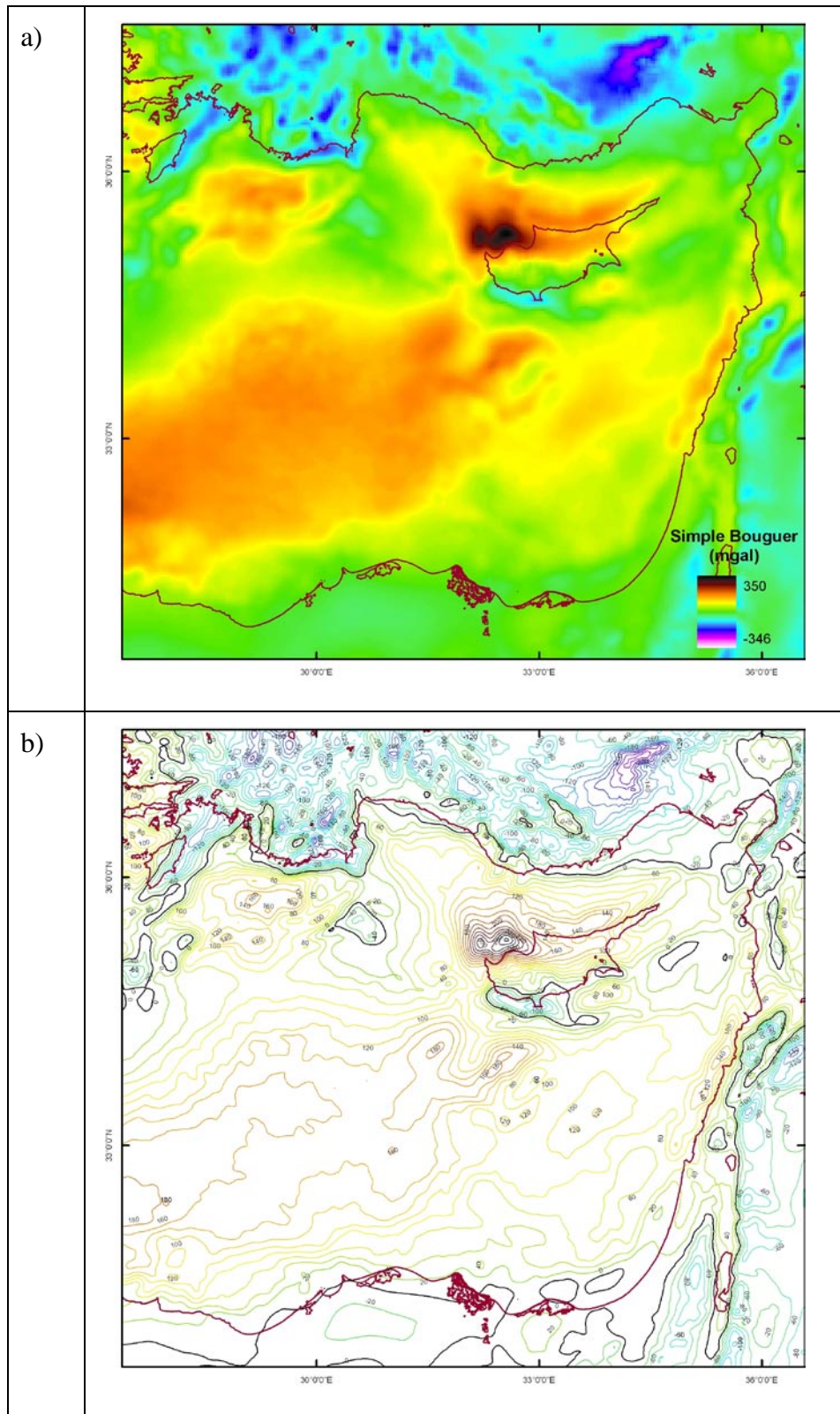
Figure 3.14 Simple Bouguer anomaly map of the Eastern Mediterranean. a) relief
map b) contour map (20 mGal interval).

3.2.3   Free-air map versus simple Bouguer map

Free-air gravity anomalies and Bouguer gravity anomalies have been used for a long time to interpret the subsurface of the earth.

The free-air anomalies are preferred for modeling density structure of the full crust, from the topography to the Moho. They are generally used for the construction of the offshore gravity anomaly maps. Free-air gravity anomalies useful for regional studies in offshore areas can be generated directly from the satellite altimetry data. Free-air anomaly is comparable to the Bouguer anomaly over continents since the measurements are corrected to the sea level.

The simple Bouguer correction represents the effect of a uniform slab having a thickness equal to the station elevation and a given density, typically 2670 kg/m3 (Hinze, 2003). Simple Bouguer anomalies have all primary elevation effects removed and therefore are popular for the construction of gravity anomaly maps on land (Nabighian et al., 2005). If a Bouguer anomaly is required for oceanic graviy measurements, it must be calculated by replacing the seawater with rocks of average crustal density. However, the bouguer anomaly at sea is less useful than on land, because Bouguer anomalies are strongly positive over the sea, thus the Bouguer correction completely masks the effects of subsurface density variations. To prevent this, today most geophysicists use Free-air anomaly at sea but use Bouguer anomaly on land (Figure 3.15; Ayala et al., 2003. Starostenko et al., 2004).

We can use gravity measurements to determine whether an area is in isostatic equilibrum. If a region is in isostatic equilibrum, there should be no gravity anomaly and hence no excess or lack of mass above the compensation depth.
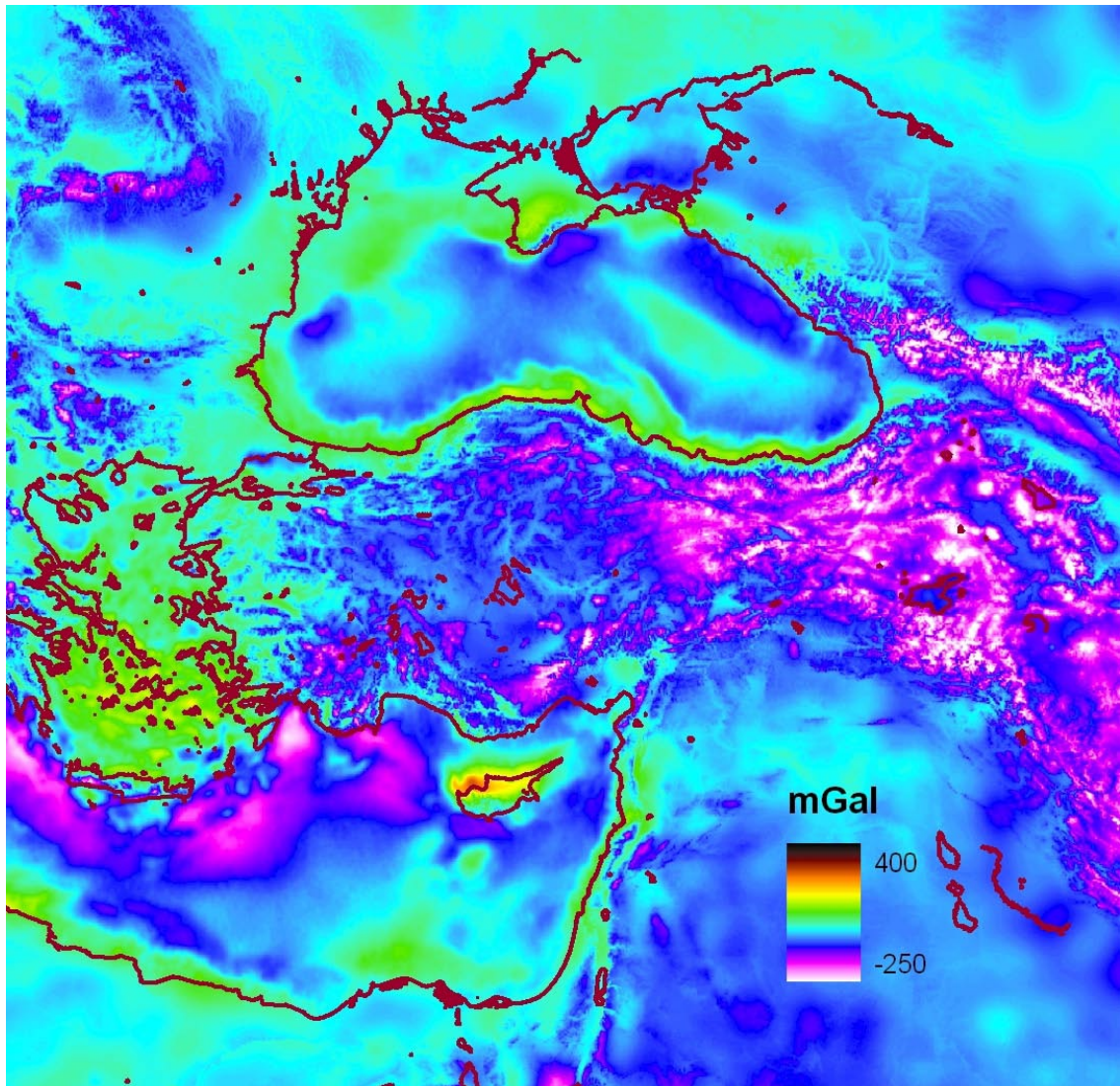
Figure 3.15. Map showing free-air anomalies at sea and Bouguer anomalies on land.

3.3 Gravity Modeling

In this section, calculated gravity responses of the crust models are presented for Black Sea and Eastern Mediterranean, respectively. The models consist of layers with varying thicknesses and densities. The initials values of the thickness and densities of the layers were obtained from previous studies. The thickness and density values were changed until the best fit was obtained.

Model layers thicknesses were compiled from published data and then interpolated in 5 x 5 km grids. The grids are also the horizontal dimensions of the prisms which are used in gravity calculation (Figure 3.16). The vertical dimension of

the prisms was chosen 200 meters (Figure 3.16). Therefore, a model layer consists of several prisms corresponding thickness value of the layer.
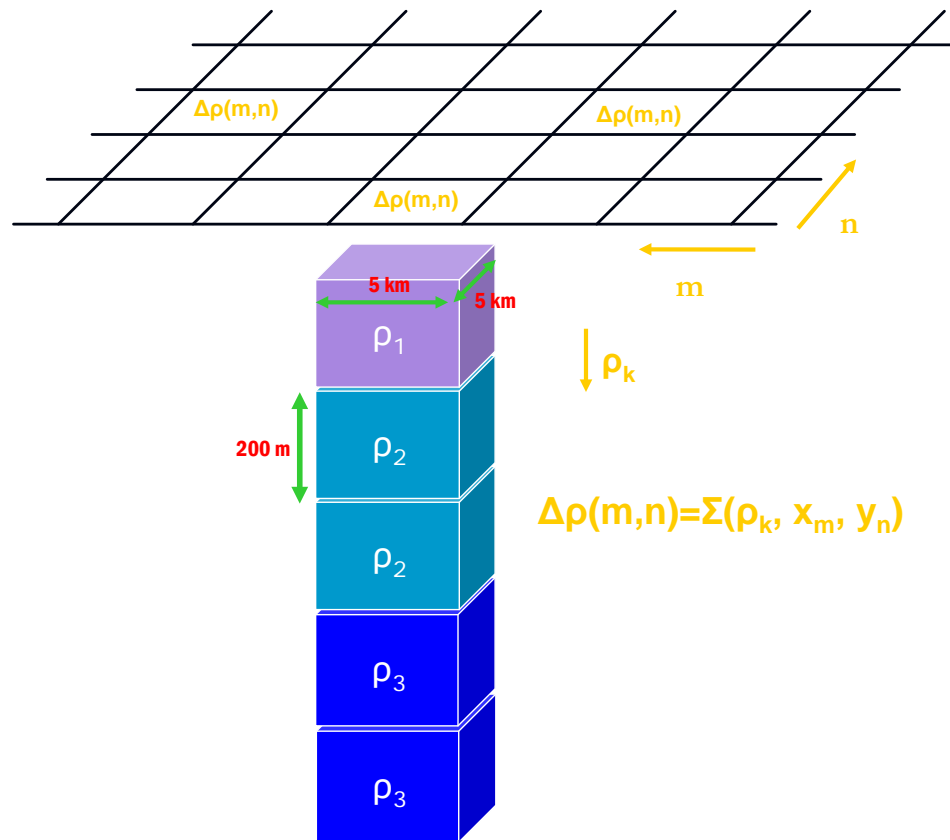
Figure 3.16 Prism method used in the modeling.

Each prism was assigned a density contrast value depending on model layer. The density co" ntrasts of the model layers used in the gravity modeling were calculated according to the reference density of the upper mantle of 3.3 g/cm^3 (Yegorova and Starostenko, 1999; Yegorova and Starostenko, 2002; Starostenko et al., 2004). The densities of the subsurface layers were derived by internal velocities of the layers calculated from seismic refraction data (Yegorova and Starostenko, 1999; Yegorova and Starostenko, 2002; Starostenko et al., 2004).

In this study, the crust model is formed by 3 layers between the sea surface and Moho depth; water layer, sediments and the crystalline basement. The thickness of the water level was compiled from the etopo2 bathymetric dataset. As the density of sea water is 1.03 g/cm^3, the density contrast that will be assigned to the prisms is equal to -2.27 g/cm^3.

The initial thickness values of the sediment layer were obtained from seismic reflection data. Previous studies showed that the sediment densities vary between 2.0 g/cm^3 and 2.65 g/cm^3. The density of the crystalline crust ranges vertically from 2.65 to 3.1 g/cm^3. In this study, because of the computing difficulties, an average density for each layer was used in the gravity modeling. Average density of 2.35 g/cm^3 is used in computation for the sediment layer. For the crystalline crust, an average density value of 2.9 g/cm^3 is used. As a results of the gravity modeling, the gravity effect of each model layers; sea-water, sediments and crust, were obtained.

Firstly, the gravity effects of sea water and sediment layer were computed separately. After that, the total gravity effect of both layers was calculated. Because of the extreme anomalies that caused mainly the lower density of sea water, it is necessary to normalize the results (Yegorova and Starostenko, 1999; Yegorova and Starostenko, 2002; Starostenko et al., 2004). For this, a value of 790 mGal that is the average gravity effect of the model for the crust of the stable East European Platform was added to the total effect.

It is assumed that the residual gravity effect obtained from subtracting the normalized effect from the observed gravity anomaly arises from the crystalline crust.

3.3.1 Black Sea

A gravity model of the crust of the Black Sea was constructed based on previous geologic and geophysical data. The thickness and the gravity effect of water layer are presented in Figure 3.17 and Figure 3.18.
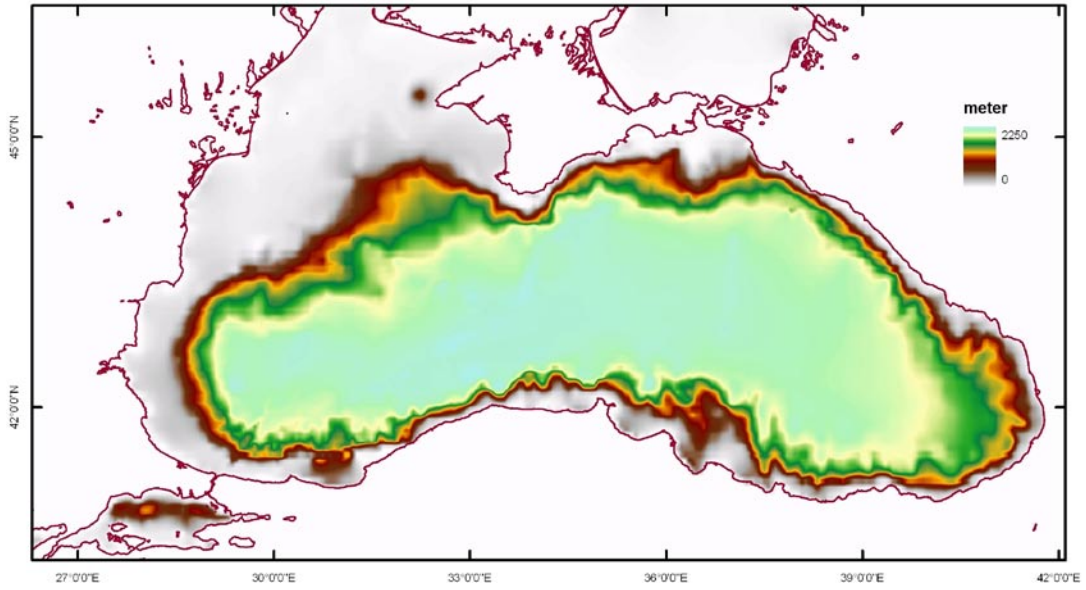
Figure 3.17 Sea water thickness used in gravity modeling of the Black Sea crust.
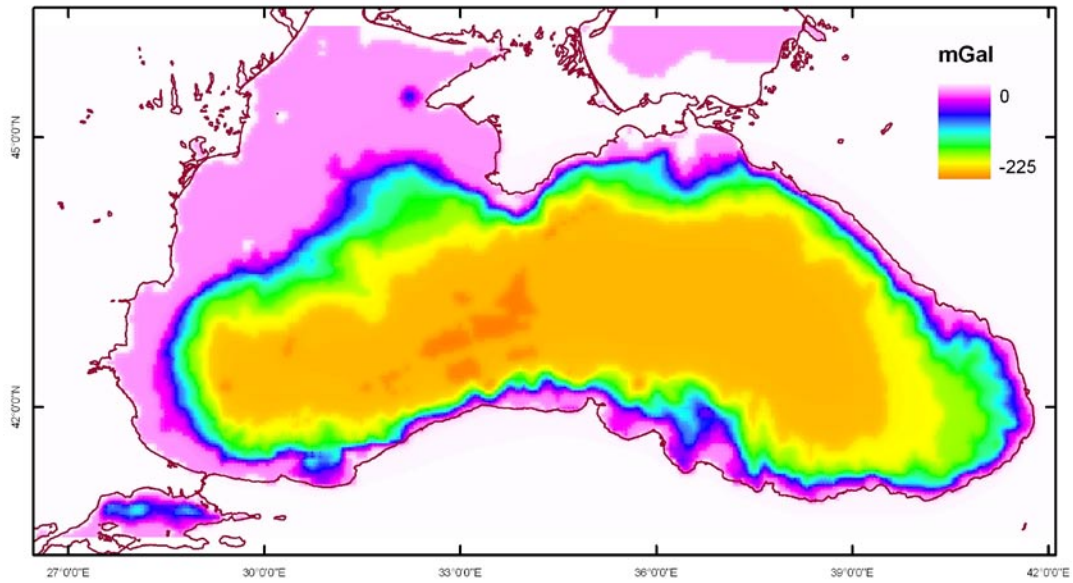
Figure 3.18 Gravity effect of the water layer (density of the seawater was taken to be 1.04 g/cm^3).

The major surface of the Black Sea has a depth of greater than 2000 meters where the maximum depth is around 2200 meters (Figure 3.17). Accordingly, the maximum gravity effect value of -225 mGal occurs in western Black Sea basin (Figure 3.18). Except for the northwestern shelf where the depths are less than 200 m, entire Black Sea has high gravity effects.

Seismic studies carried out that the maximum sediment deposition in the Black Sea exists in the basins of the eastern and western Black Sea (Figure 3.19). The oldest sediments had been deposited during Triassic time (208-245 years ago) in western basin (Finetti et al., 1988). On the other hand, in the eastern Black Sea basin, the oldest sedimentation was in Jurassic time (144-208 years ago) (Finetti et al., 1988). Consequently, the western basin is filled up more than 13 km of sediments, whereas the eastern Black Sea basin contains up to 12 km thickness of sediments. On the Mid Black Sea High, the ridge that separate two basins, relatively low sediment deposition occurs.

Based on the mentioned previous data, a sediment layer model is constructed and presented in Figure 3.19. The gravity effect of this constructed sediment layer is calculated and mapped (Figure 3.20).

As would be expected, the greatest gravity effects occur at the centers of basins where the sediment accumulation are highest (Figure 3.20). This maximum gravity effects is -488 mGal in western Black Sea basin and -406 mGal in eastern Black Sea basin. Over the Mid Black Sea High, a gravity effect of about -160 mGal is observed. The high gravity effects in the basins reduce quickly to -8 mGal towards the Anatolian and Caucasus coasts of the Black Sea (Figure 3.20).
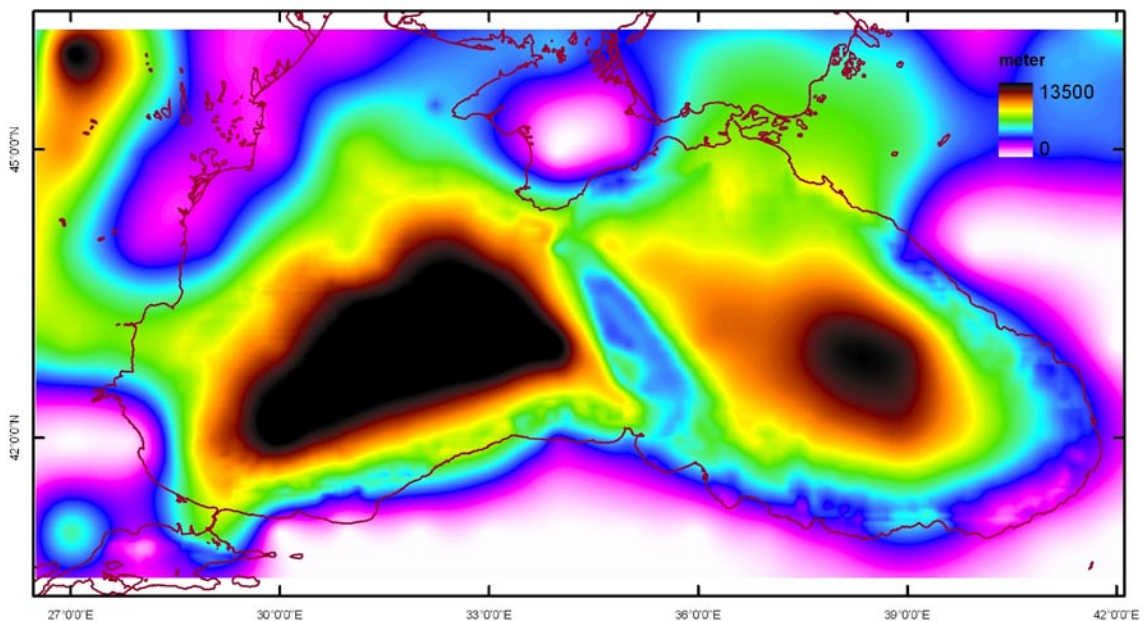
Figure 3.19 Sediment distribution in the Black Sea.
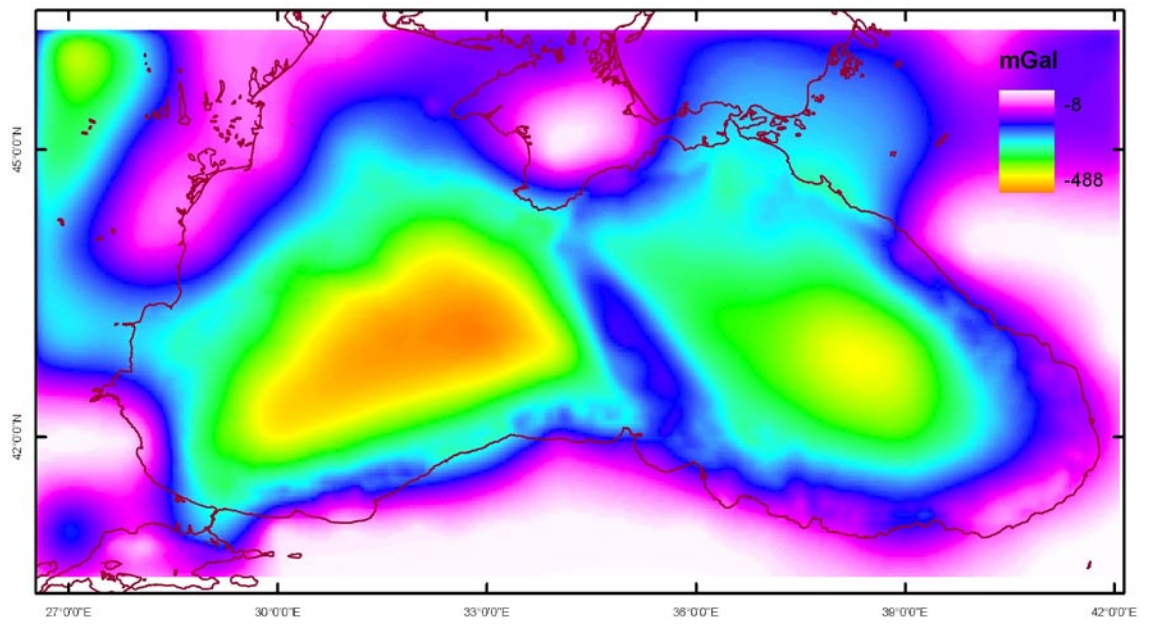
Figure 3.20 Gravity effect of the sediment layer (density of the sediment layer was taken to be 2.35 g/cm^3).

Figure 3.21 Combined gravity effect of water and sediments.

Figure 3.22 The residual gravity effect by the crust after removing the other effects from the observed gravity.

The total gravity effect of the water and sedimentary layer is presented in Figure 3.21. As would be expected the greatest gravity effects occur at the center of the basins where the water depth and the sediment accumulation are highest.

The residual gravity anomaly due to crust is presented in Figure 3.22. It has been obtained by removing the total gravity effect of water and sediments, and the mantle gravity effects from the observed gravity data. The gravity effect of the mantle was obtained from Belousov et al. (1988). The average gravity effect of the mantle is about 80 mGal (Belousov et al., 1988).

According to the calculated gravity effect of the crust (Figure 3.22), eastern and western Black Sea basins have minimum gravity effects; about -150 mGal in the western Black Sea basin, and about -190 mGal in the eastern basin. Between two basins, over the Mid Black Sea High, a gravity effect of -450 mGal is observed. The gravity effect of the crust increases towards to land, and reaches more than -700 mGal.

As the assumed density for the crust is constant ($2.85 g/cm^3$), the main component of the gravity effect variations is thickness. Based on the residual gravity effect, crystalline crust thicknesses were calculated and mapped in Figure 3.23. The

thinnest crystalline crust exists in the western Black Sea basin with a thickness of about 5 km. The crust of the eastern Black Sea basin however, has a minimum thickness of about 15 km. The Mid Black Sea High has an average crust thickness of about 20 km.

The main results of the gravity modeling are the crust structure and the Moho depth beneath the Black Sea. Moho discontinuity in the Black Sea is mapped in Figure 3.24. The Moho depth is closest to the surface in western Black Sea basin. Here, the Moho exists 19 km below the sea surface. In the eastern Black Sea the Moho is relatively deeper. It lies at about 23-28 km below the present day sea surface. Along the circumference of these two Black Sea sub basins the Moho is marked by 30 km. Moho depth deepens toward the land.
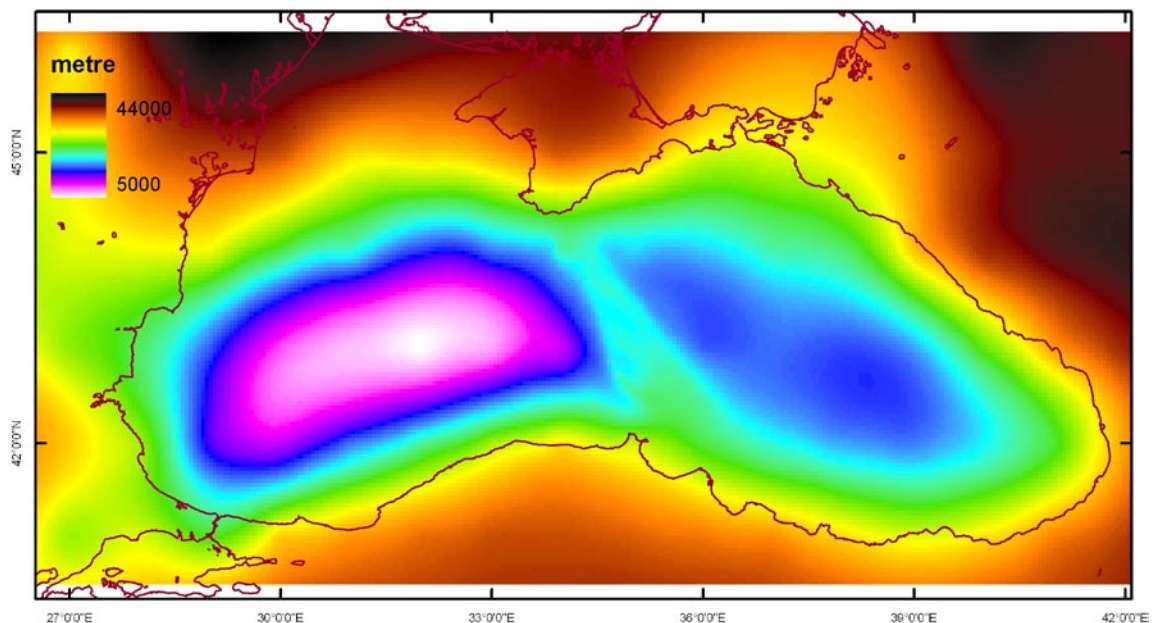
Figure 3.23 The crystaline crust thickness distribution of the Black Sea.
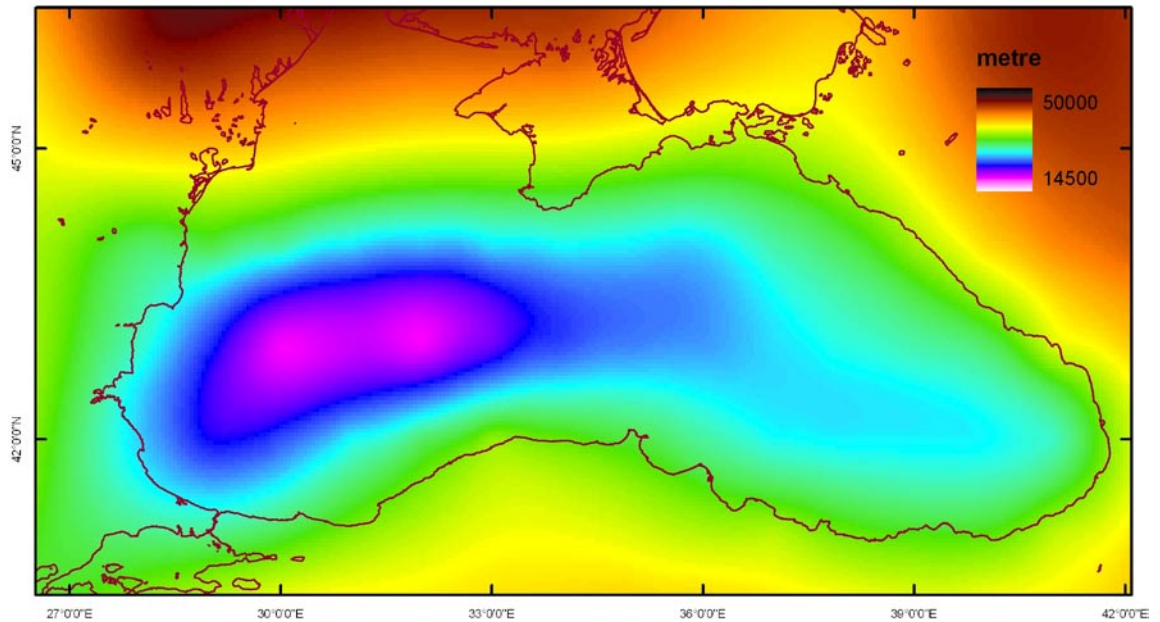
Figure 3.24 Moho depths of the Black Sea.

3.3.2   Eastern Mediterranean

A gravity model of the crust of the Eastern Mediterranean was constructed based on previous geologic and geophysical data.

The thickness of the sea water is presented in the Figure 3.25 and the gravity effect of water layer of the Eastern Mediterranean is presented in Figure 3.26.

The water layer has the maximum thickness in Rhodes trough with more than 4500m (Figure 3.25). As the gravity effect is related directly with the bathymetry, the maximum gravity effects (-410 mGal) occurs in the deepest region of the study area, Rhodes trough (Figure 3.26). The gravity effects decrease to -140 mGal and -100 mGal over the Anaximander and Eratosthenes seamounts, respectively, where the thickness is relatively lower than the adjacent areas (Figure 3.25).

The sea water over the Nile Cone and Çukurova-İskenderun-Latakia basins produces relatively low gravity effects (Figure 3.26).
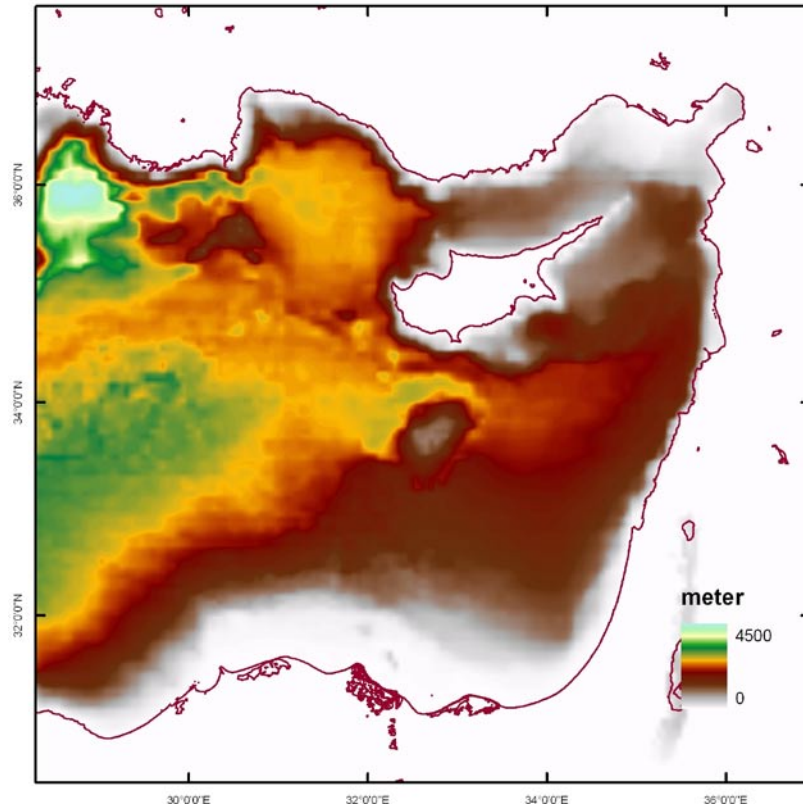
Figure 3.25 Sea water thickness of the Eastern Mediterranean.
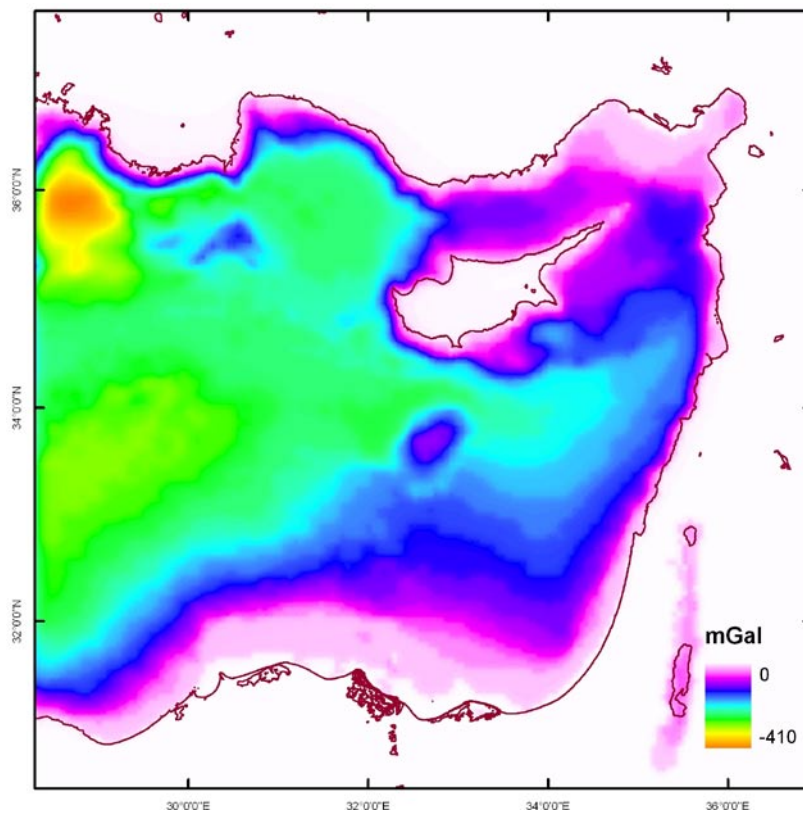
Figure 3.26 Gravity effect of the water layer (density of the seawater was taken to be 1.04 g/cm^3).

As it can be seen in the Figure 3.27, the sediment deposition reaches the maximum thickness off the Nile River mouth (15 km). Levantine Basin is filled with sediments transported by Nile River. Toward the Herodotus Basin the thickness of sediments diminishes to 9-10 km. Over the Eratosthenes seamount only about 5 km of sediment accumulation were observed. Some local, relatively thick sediment deposition can be followed in Çukurova, Adana and Antalya basins. The calculated gravity effect of the Eastern Mediterranean sediment layer is shown in Figure 3.28. The Levantine Basin, Nile Cone and Herodotus Basin are characterized by high gravity effect. The maximum gravity effect occurs off the Nile Cone with a magnitude of -605 mGal (Figure 3.28). The surroundings of Cyprus Island and along the Anatolian coast, a relatively low gravity effect are followed. Local gravity highs are observed over the Antalya, Adana and Çukurova basins; -180 mGal, -210 mGal and -240 mGal, respectively.
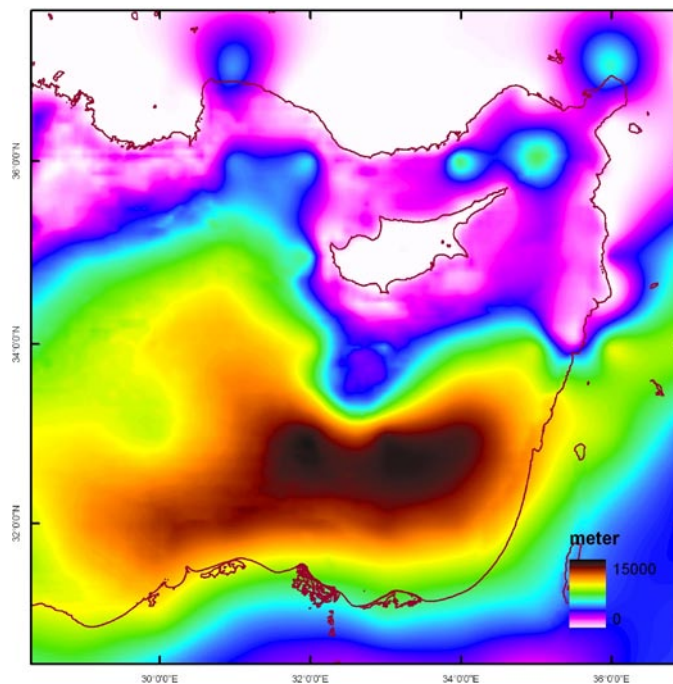
Figure 3.27 Sediment distribution in the Eastern Mediterranean.
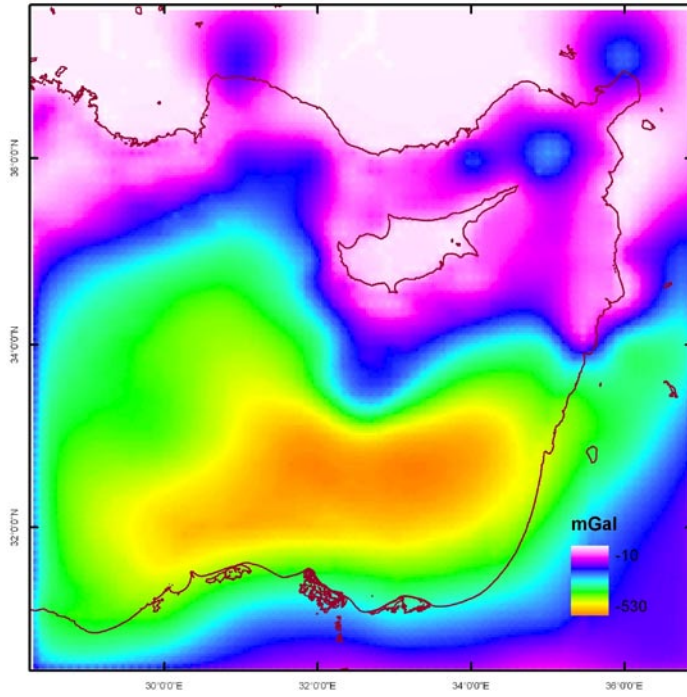
Figure 3.28 Gravity effect of the sediment layer (density of the sediment layer was taken to be 2.35 g/cm^3).
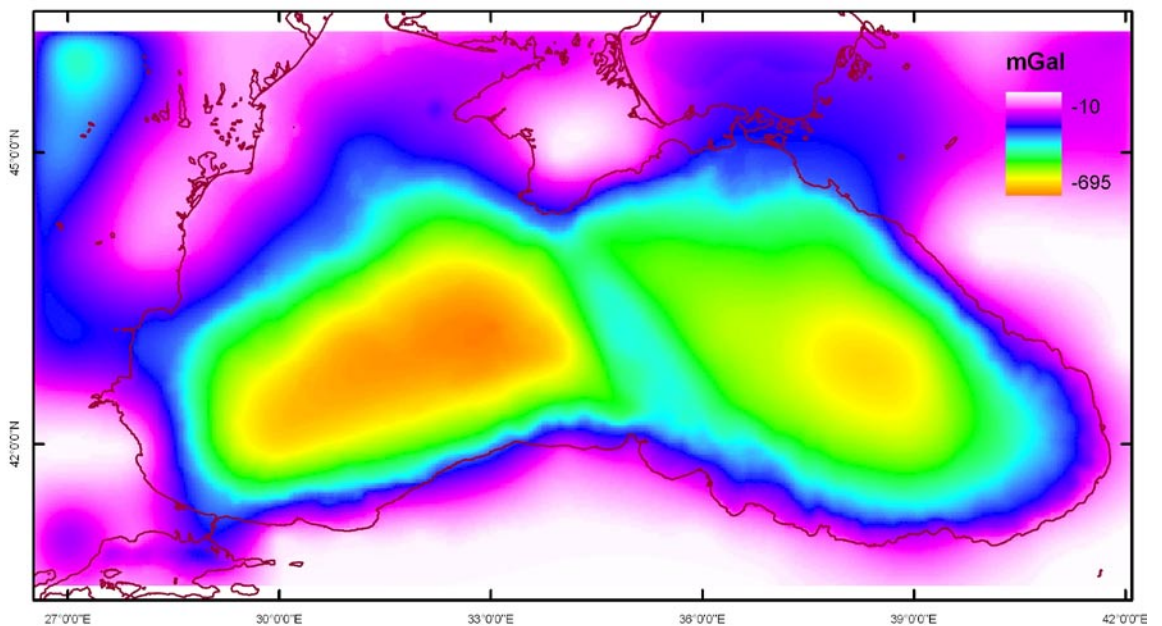

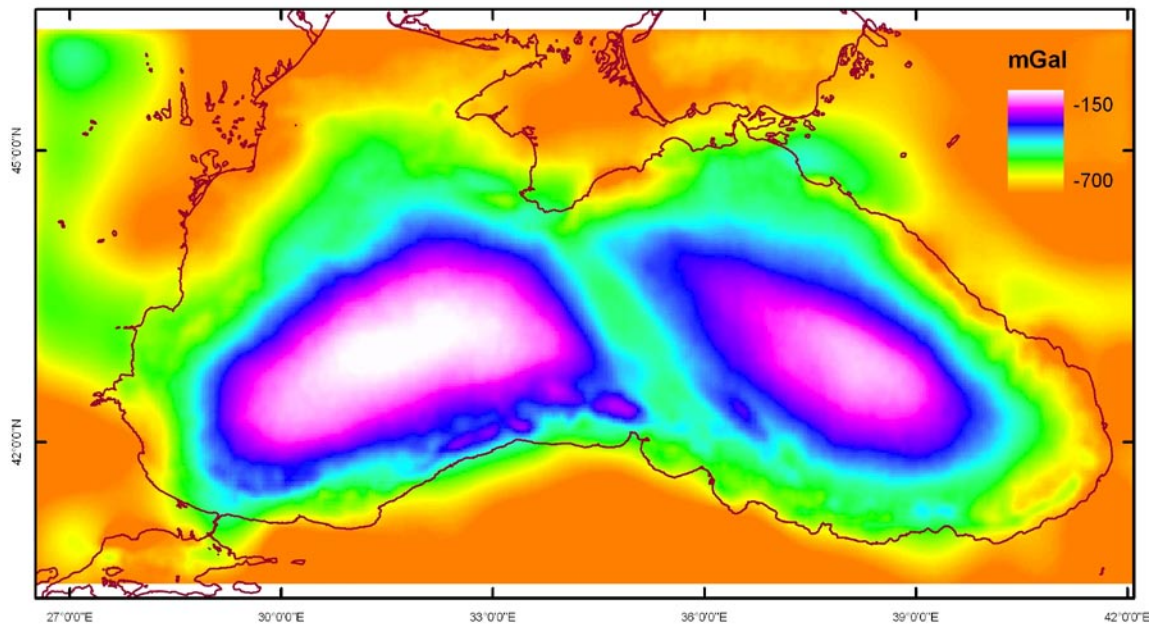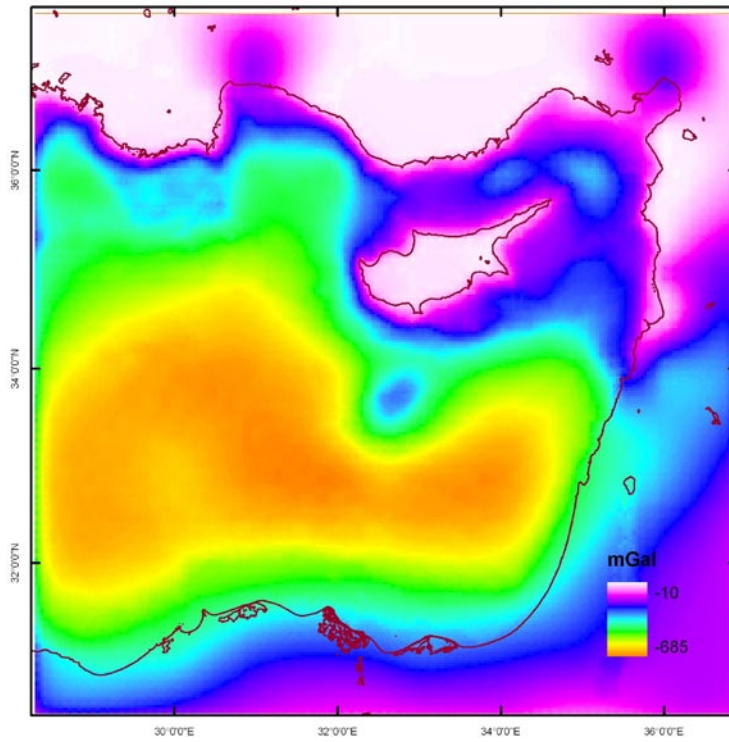Figure 3.29 Combined gravity effects of water and sediments.
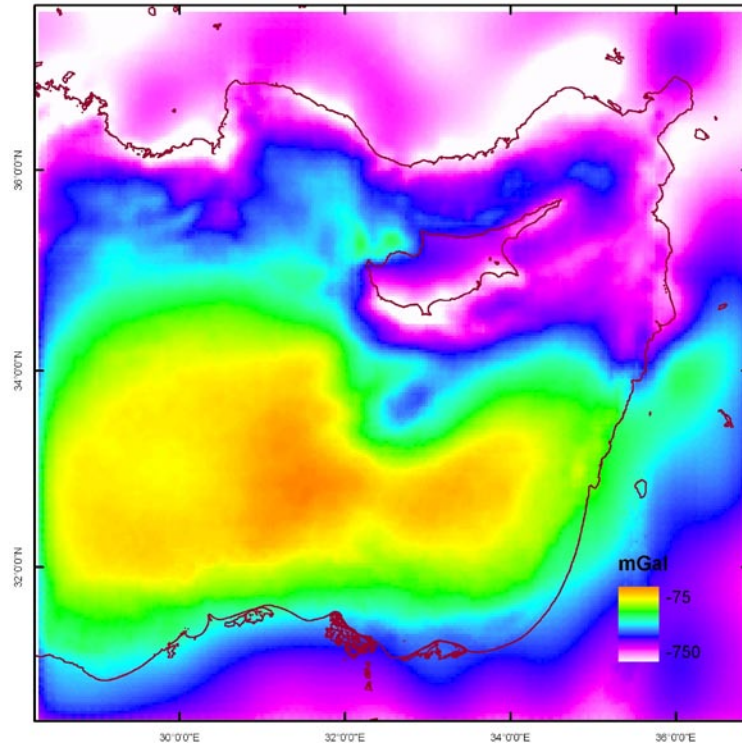
Figure 3.30 The residual gravity effect by the crust after removing the other effects from the observed gravity.

Both water and sediment layers produce large gravity effects (Figure 3.26 and 3.28). The combined gravity effect of these two layers is presented in Figure 3.29. The Herodotus Basin and Levantine Basin are characterized by the higher gravity effects in the study area. Eratosthenes seamount and Anaximander Mountains separated from adjacent areas by low sediment deposits. The northwestern corner of the study area that includes Çukurova, İskenderun, Cyprus basins and Cyprus Island, has the lowest gravity effect. Comparing the other basins, this area is defined as shallow water depth.

To obtain the residual gravity anomaly, the combined gravity effect of the water and sediment layers were removed from the observed gravity anomalies. However, unlike the Black Sea, there is no reference for the gravity effect of the mantle. As the one of main objective is to define the crystalline crust thickness, it is accepted that the gravity effect of the mantle is accepted to be -80 mGal, as in Black Sea. The resulted residual gravity anomaly is presented in Figure 3.30. A zone that surrounds the Herodotus and Levantine basins is seen in Figure 3.30 with low gravity effects.

The density of crystalline crust was assigned as 2.85 g/cm^3. Thus, the thickness of the crystalline crust is the primary factor of the gravity effect. A crystalline crust thickness model was calculated and presented in Figure 3.31. The thickness of the crystalline crust under the Herodotus and Levantine basins oscillates between 9 km and 12 km. In the south and southeastern part of the study area, the crust thickens toward the land. Under the Cyprus Island, the crust has an averaged thickness of 23 km. Toward the Turkey; the crust thickens smoothly and reaches 35 km. Between Cyprus and Syria, an elongated zone is marked by a relatively thin crust of about 20 km. The crust under the Eratosthenes Seamount has a thickness of 20 km.

From the constructed and calculated subsurface layers, the distribution of Moho depth is calculated and mapped in Figure 3.32. The Moho depth is characterized by slowly changing relief. It rises beneath the Cyprus and Herodotus basins to 22 km. Apart from Antalya and Rhodes basins, the Moho depth varies between 22 km and 30 km over the sea. It thickens toward to land.
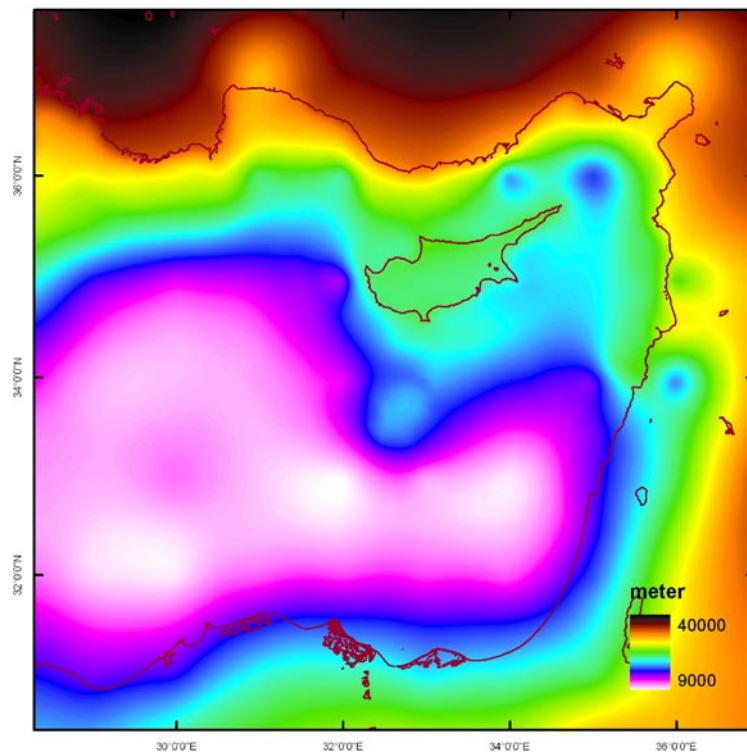
Figure 3.31 The crystaline crust thickness distribution of the Eastern Mediterranean.
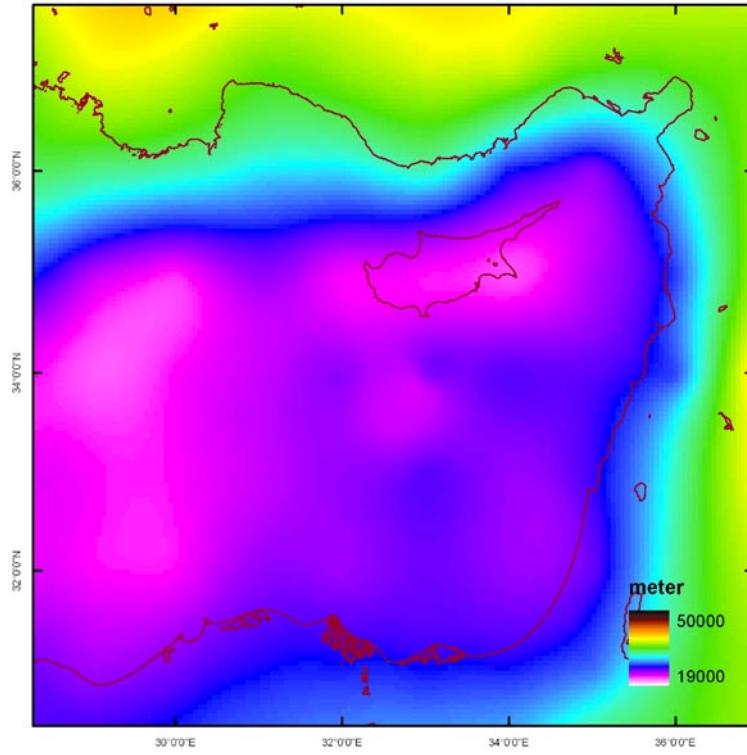
Figure 3.32 Moho depths of the Eastern Mediterranean.

4   Discussion

Since the main objective of this thesis is to investigate the gravity anomalies and crust structure of the Eastern Mediterranean and Black Sea using satellite altimeter derived gravity data, firstly it is necessary to discuss the satellite altimetry method and the applicability to the gravity surveys. Then, the gravity anomalies that are calculated from the satellite derived gravity data will be interpreted. Finally, the results of the gravity modeling of the crust will be presented.

4.1   Satellite altimetry method

The height of sea surface is accepted as zero in many scientific applications. However, because of the potential field of the earth, the height varies from place to place. The satellite altimetry method is aimed to determine the sea surface topography. After the elimination of the dynamic effects, the remainder presents the real sea surface topography.

Satellite gravity data are derived from altimetry data. Different dataset were created by different scientist groups from different countries by using different methods and techniques. All these datasets are being updated in time with re-tracking of the new satellite data to improve the precision.

Although many disadvantages occur, the advantages of the satellite derived data are significant. One of the advantages is the spatial resolution and coverage. Satellite completes its orbit around the Earth in a few days or less. As the earth is constantly rotating, satellites cover the whole earth surface very short time comparing ship surveys.

Because of the noise that effects the satellite measurement such as atmospheric gases, atmospheric particles, computation errors, the obtained data should be confirmed. This can be done by comparing the satellite data with in situ measurement data. Several comparisons have been made for different regions of the world, i.e., Australia by Featherstone (2003), Aden Gulf by Maia (2006).

In this study, satellite derived gravity data are extracted along the available ship tracks to compare with ship borne data. The statistics of the residuals between ship and satellite data are presented in Table 4.1 for the Black Sea and in Table 4.2 for the Eastern Mediterranean.

Tables 4.1 and 4.2 show that the marine data and satellite gravity data do not match at with each other. The residual between them reaches in some profiles (BS_06, EM_04) up to 140 mGal. These abnormal differences usually happen in the shallow water and steeply sloping sea floor areas (Figures 3.2c, 3.6a).

In abyssal areas, where the sea floor is morphologically flat with a gentle slope, the values of the ship and satellite data tend to come to close each other (Figure3.1b, 3.5c, and 3.6b) and the standard deviations decrease (Table 4.1, 4.2).

Table 4.1 Minimum and maximum gravity anomaly values and standard deviations of residuals between ship borne and two versions of satellite gravity data, in Black Sea.

	v11			v15		
	min	max	std	min	max	std
BS_01	-28,3	22,8	14,08	-22,5	24,4	11,95
BS_02	9,2	36,4	7,23	8,8	35,2	7,8
BS_03	-64,6	50,9	34,27	-53,3	54	34,67
BS_04	-31,6	36,9	14,29	-40,3	39,1	15,67
BS_05	-34,5	32,1	15,24	-40,6	29,9	11,46
BS_06	-87,5	17,1	22,33	-128,5	13	30,51

Table 4.2 Minimum and maximum gravity anomaly values and standard deviations of residuals between ship borne and two versions of satellite gravity data, in Eastern Mediterraean.

	v11			v15		
	min	max	std	min	max	std
EM_01	-64	29,4	19,01	-62,8	33,3	18,73
EM_02	-31,3	92,8	29,25	-29,9	103	30,67
EM_03	-23,4	49	13,99	-26,7	47,1	13,81
EM_04	-114,1	64,6	29,89	-140,6	69,8	32,28
EM_05	-32,1	26,4	12,84	-28,1	25,7	11,21
EM_06	-18,5	85,6	17,22	-19,2	86,6	17,72

In summary, there are significant differences exist between marine gravity data and satellite data even they are sometimes coincided sometimes. These large differences occur usually in the coastal zone because of the difficulties in the altimeter data correction (Featherstone, 2003).

Another reason for the difference between marine and satellite data is the quality of the ship data used in this study which were collected in 1970s and 1980s. Accuracy of the measurements at that time can be low compared to the recent measurements. New marine gravity data that include precise navigation and corrections should be used for the comparison to check the real quality (suitability) of the satellite gravity data. Sandwell and Smith (1997) has used new marine gravity data to check his dataset. He compared his satellite dataset with R/V Condrad and R/V Ewing marine gravity data. He concluded that the rms differences are less than 4 mGal (Sandwell and Smith, 1997).

The general opinion about satellite altimeter data is that despite its advantages such as coverage and spatial resolution, it has not been considered for fine scale surveys (Featherstone 2003; Maia 2006).

4.2   Gravity anomalies of the Black Sea and E.Mediterranean

The sea floor morphologies of Black Sea and Eastern Mediterranean (Figures 3.4, 3.8) are different. Black Sea is a semi-enclosed basin consisting of shelf, basin slope, basin apron, and abyssal plain (Figure 3.4). The central part of the Black Sea is flat, smooth surface. On the contrary, the Eastern Mediterranean has various undersea features such as seamounts, trenches (Figure 3.8). The sea floor shape affects the gravity anomalies in both seas; however the complex morphology of the Eastern Mediterranean sea-floor features appears as one of the primary factors of the anomalies in gravity.

In the Black Sea, especially the sea-floor shape effects on the gravity anomalies are best in the coastal regions (Figure 3.1, 3.2). Over the abyssal plain, large variations in the gravity exist despite the flat surface (Figure 3.1a). Probably the source of this anomaly comes from the sub-sea floor structures, in the crust of the Black Sea.

Despite some local gravity minima and maxima, the free-air gravity in the Black Sea has weak anomalies ranging between -40 and 40 mGal (Figure 3.11b). The positive weak anomalies occur especially in the centers of eastern and western basins. The negative weak anomalies follow the Mid Black Sea High crossing the Black Sea (Figure 3.11a, b).

The strongest positive simple Bouguer gravity anomalies in the Black Sea exist over the eastern and western basins. From the seismic studies, it is well known that both basins are filled by large sediment deposition (Robinson et al., 1995; Robinson et al., 1996; Spadini et al., 1996; Rangin et al., 2002; Nikishin et al., 2003).

In the Eastern Mediterranean, however, especially over the trenches and the ridges, the gravity anomalies reflect the morphological variations on the sea floor. For instance, Anaximander Mountains, Eratosthenes seamount and Nile Cone have relatively low gravity relative to the adjacent areas.

It is believed that negative zone between Rhodes, Turkey and Cyprus corresponds to Mediterranean ridge. Mediterranean Ridge is the plate boundary between African and Eurasian Plates. According to seismic researches, Mediterranean Ridge is considered as a subduction zone (Finetti and Morelli, 1973). Both the anomaly and the topographic rise disappear off the Cyprus. Anaximander Mountains show a relative gravity high in this negative zone. It was suggested that the Anaximander Mountains form the offshore continuation of the structural units exposed onshore in southwest Turkey (Woodside and Dumont, 1997; tenVeen et al., 2004).

Eratosthenes Seamount is a topographic high that is considered to be a continental fragment (Ben-Avraham et al., 2002). Based on seismic studies Ben-Avraham et al., (2002) suggests that Eratosthenes Seamount has a thinned continental crust. It is generally agreed that the Eratosthenes seamount is now in the process of collision with the Cyprus active margin forming a part of regional Africa-Eurasia plate boundary (Robertson, 1998b).

A free-air anomaly high occurs just offshore from Egypt over the Nile Cone. The source of this positive anomaly is probably due to the load of the deltaic sediments from Nile River. Tibor et al. (1992) explained that large volumes of clay and silt have been transported from Nile River since the Pliocene.

The source of the gravity high in Cyprus is possibly from the oceanic ophiolites that are well documented (Robertson, 1998a). This anomaly is bounded to the south by a chain of gravity lows, probably corresponding to the trench of the subduction zone.

4.3   Gravity modeling

The direct methods to investigate the subsurface of the earth are not so efficient financially. Only very small portions of the earth can be examined in detail, with seismic method and/or borehole logs. Also, seismic methods don't provide sufficient penetration to investigate the deep structure such as lower crust and Moho depth. On the other hand, some indirect methods such as gravity modeling are needed to present the subsurface features even in large areas.

In this study, some assumptions were made before the gravity modeling. Firstly, although many authors considered that both Black Sea and Eastern Mediterranean are out of isostatic equilibrium (Woodside and Bowin, 1970; Spadini et al., 1996; Ben-Avraham et al., 2002), it is considered that the crust is in isostatic equilibrium. Secondly, the upper mantle density is accepted to be constant (3.3 g/cm^3), however, small variations are possible. When the variation happens, the constructed gravity model may be different from what it should be in real. And finally, a value of -790 mGal is accepted to normalize the values.

The relation of gravity model and result is not unique. Two or more different gravity models can produce the same gravity effects. So, the constructed model has to be concordant as possible as with priori geologic and geophysical data.

The gravity effect of a model depends on the density, the thickness and the distance between the model and observation point. Based on previous data, firstly the gravity effects of the water and sediment layers were calculated with a constant density. So, the gravity effect values depend on mainly the thickness and the distance. When compared the thickness maps and gravity effects maps, the similar trend can be followed, thick layer produce more gravity attraction than a thin layer.

The gravity modeling of the crustal structure of the Black Sea and the Eastern Mediterranean is intented to reveal the distribution of the crust thickness and the Moho depth. The Moho, the boundary between crust and mantle, is the main seismic discontinuity in the continental lithosphere. The Moho depth is important to understand the regional geodynamic evolution and processes.

Black Sea consists of two sub basins that are filled by thick sediment deposits. Eastern Black Sea basin has a maximum sediment thickness of 12 km and western Black Sea basin 13 km. The sediment accumulation is well presented by

seismic reflection studies by Finetti et al. (1988). They showed that the basins are composed of parallel, flat and undistorted sediment sequences. The thickness of the crystalline crust lying beneath the sediments varies in the Black Sea basin. In the eastern Black Sea basin the crust is thicker than the western basin.

The character of the crust that underlies the western Black Sea basin is accepted oceanic to suboceanic (Tugolesov et al., 1985 cf. Starostenko et al., 2004; Finetti et al., 1988; Nikishin et al., 2003). The crust of 4-5 km in thickness in this study supports the oceanic type (Figure 4.1). In the eastern Black Sea basin, Nikishin et al. (2003) mentioned a thinned continental crust. On the other hand Verzhbitsky et al. (2002) claimed that the eastern basin consists of 4 km of continental and 6 km of oceanic crust based on heat-flow data. In this study, as an average density is used for the crust, it is believed that the eastern basin has a continental crust 15 km in thickness (Figure 4.1).

According to the Moho depth map, the Moho discontinuity rises from a depth of 36 km in Turkey to 19 km in western Black Sea basin and then falls again to 45 km in Russia. In the eastern Black Sea basin the Moho rises to about 25 km. The Moho depth values (Figure 3.24) over the land are more certain than those at sea. This arises from the absence of the sediments in land areas. It was used in this study an average density for the sediments, but the sediment deposits in the Black Sea consists of at least five different stratigraphic units with different densities. However, the distribution of the Moho depth in this study agrees generally with the previous works of Balavadze and Mindeli (1965) and Starostenko et al. (2004).

The values of sediment thickness, crust thickness, Moho depths and crust types of the Black Sea suggested by previous investigations are compared with results of this study in Table 4.3.

Table 4.3. Comparison of previous studies in Black Sea with the results of this study. Note the results of this study are the minimum values obtaine at that site.

Black Sea					
Western Basin	Verzhbitsky et al., 2002	Spadini et al., 1996	Nikishin et al., 2003	Starostenko et al., 2004	This study
Sediment Thickness	12 km	13 km	3-19 km	14 km	13 km
Crust Thickness	-	~5 km	~6 km	~3 km	5 km
Moho Depth	-	20 km	25 km	19 km	19 km
Crust Type	oceanic	oceanic	oceanic	oceanic	oceanic?
Eastern Basin					
Sediment Thickness	13 km	11 km	2-12 km	10 km	12 km
Crust Thickness	10 km	~12 km	8 km	~10 km	15 km
Moho Depth	-	25 km	25 km	22 km	23 km
Crust Type	thinned continental	non oceanic	continental	continental	continental?

Eastern Mediterranean is a morphologically complex area. Because of the existence of the plate boundary between African Plate and Anatolian Microplate, the properties of the crust vary significantly. Despite a lot of studies carried out to investigate the crust structure since 1970s, there is still no consensus. The main factors of the uncertainty are that the large thickness of the crust, the evaporate series that partially prevent the seismic penetration and the crust property differences between African and Anatolian plates.

In this study, the crust thickness and Moho depth of the Eastern Mediterranean were investigated. The crust thickness of the Eastern Mediterranean is presented in Figure 3.31 and the Moho depth map in Figure 3.32. As obvious in Figure 3.31, the rapid change in thickness of the crust follows a route parallel to Anatolia, then turns southward, passes between Cyprus and Erathostenes Seamount and continues northeastward. This route is seem concordant to the plate boundary which is suggested by many authors (Biju-Duval et al., 1978; Nur and Ben-Avraham, 1978; Riad et al., 1981; Rotstein and Kafka, 1982; Rotstein and Ben-Avraham, 1985; Robertson et al., 1994, 1995; Anastasakis and Kelling, 1991; Ambraseys and Adams, 1993; Kempler and Garfunkel, 1994; Oral et al., 1995; Robertson, 1998a; Vidal et al., 2000b).

According to Ben-Avraham et al., (2002), Eratosthenes Seamount is a continental fragment. The greater crust thickness that separate Eratosthenes Seamount from adjacent areas (Figure 3.31) supports this theory. On the other hand, Ben-Avraham (1989) suggests that Eratosthenes Seamount was rifted from the African continental crust during younger rifting episodes. In this study, there is no evidence to support this idea.

It is possible to describe two types of crust in the Eastern Mediterranean. The crust under Herodotus and Levantine Basin is thinner than the northern portion of the study area. These two portions are separated with the plate boundary mentioned above. The thin crust under Levantine Basin is inferred to be oceanic (Ryan et al., 1973; Nur and Ben-Avraham, 1978; Makris et al., 1983; Makris and Stobbe, 1984; Makris et al., 1994; Ben-Avraham et al., 2002). On the contrary, Vidal et al. (2000a) concluded that sediment deposits in the Levantine basin are underlain by a possible thinned or transitional continental crust. The calculated thickness of the Levantine and Herodotus basin in this study supports the oceanic crust idea rather than continental crust. On the other hand, the plate boundary at the eastern part of the Cyprus Arc is interpreted as a typical transpressional feature (Woodside et al., 2002). For that, both portions of crust separated by plate boundary should be the same type.

According to the Figure 3.32, most of the Eastern Mediterranean has a Moho depth of less than 30 km. Beneath the land, the Moho depth descends to 40 km. Although Cyprus and the Eratosthenes Seamount are considered to have continental thick crust, the Moho rises to closest depth to the sea surface beneath these two structures. In contrast, the Moho deepens toward to the Levantine basin whose crust is described whether as an oceanic or as an continental, thin crust. This controversy arises from the sediment transportation from Nile River. Both Cyprus and Eratosthenes Seamount are poor in sediment deposition (Figure 3.27). Levantine Basin however, consists of a thick sediment accumulation. This loaded sediments weight causes the deepening of Moho.

The values of sediment thickness, crust thickness, Moho depths and crust types of the eastern Mediterranean Sea suggested by previous investigations are compared with results of this study in Table 4.4.

Table 4.4. Comparison of previous studies in eastern Mediterranean Sea with the results of this study. Note the results of this study are the minimum values obtaine at that site.

Eastern Mediterranean

Levantine Basin	Makris and Stobbe, 1984	Robertson, 1998	Vidal et al., 2000a	Ben-Avraham et al., 2002	This study
Sediment Thickness	16 km	12 km	10 km	10-14 km	15 km
Crust Thickness	-	-	-	9 km	9-10 km
Moho Depth	~32	-	-	20 km	25 km
Crust Type	oceanic	oceanic	thinned continental	oceanic	oceanic?
Eratosthenes Seamount					
Sediment Thickness	-	-	-	~4 km	5 km
Crust Thickness	-	25 km	-	~23 km	20 km
Moho Depth	~28 km	-	-	26-28 km	27
Crust Type	continental	continental	-	continental	Continental?

4.4   Overall Discussion

In the first section of the results, satellite altimetry derived gravity data and ship borne gravity data were compared. Six profiles in the Black Sea, six profiles in the Eastern Mediterranean, one profile in the Marmara Sea and one in the Aegean Sea along the ships track were analyzed. Both the satellite and ship data were drawn in the same graphs and the standard deviations of these data were computed.

It is considered that the satellite and ship data do not coincided well. The residuals between ship and satellite data show large variations. However, the data quality of the ship measurements used in this study is not so clear. It is important to consider the contribution of space technology to the geophysical researches. By now, the satellite altimeter derived gravity data has already given the general trend of the gravity anomalies in large study areas. Moreover, with new altimeter measurements, the satellite gravity dataset have been improved continuously. However today, ship data are still obligatory for a detailed small scale studies.

In the second section, the free-air anomalies and simple Bouguer anomalies in Black Sea and in Eastern Mediterranean were generated and interpreted. According to these satellite-based new gravity anomalies maps, Eastern Mediterranean is marked by mainly negative free-air anomalies. However in the Black Sea the negative gravity anomalies are weak. The sea floor morphology has significant effect on the gravity in Eastern Mediterranean Sea but no in the Black Sea. This difference is probably because of the different tectonic evolutions and settings.

Black Sea is characterized by gravity anomaly over the eastern and western Black Sea basins as expected. From the seismic researches, it is now clear that these two basins are filled by sediment deposits of more than 12 km in thickness. The sediment accumulation off the Nile River in the Eastern Mediterranean also produces significant gravity anomalies.

In the final section, three-dimensional gravity models of the Black Sea and Eastern Mediterranean were constructed to analyze the crustal structures. From the models it can be concluded that the Black Sea is composed of two sub basins; western and eastern basins and the thicknesses of the crust are 5 km and 15 km, respectively.

In the Eastern Mediterranean, two types of crust were interpreted. Levantine Herodotus basins have a thin crust lying under thick sediment deposits.

5   Conclusion

Although the gravity prospecting is expensive, it is still considerably cheaper than the seismic method. However, for a large study area, the gravity prospecting causes waste of time and money. Especially in the regional studies the satellite derived gravity data can provide valuable information to the scientists. The uses of the satellite data to produce the gravity values lead to people to improve the precision of data.

Moreover, it is important to derive geophysical and geodetic data from satellite measurement specifically for our country and vicinity. Some example already exist (Kılıçoğlu, 2005). Nevertheless, this can only be achieved by increasing the resolution.

Despite the high standard deviations in this study (Table 4.1, 4.2) the satellite derived gravity data are suitable for the gravity modeling. The spatial resolution of the satellite data is enough for the large scale studies of this kind.

From the satellite derived gravity data, new Free-air gravity anomaly map and Simple Bouguer anomaly map that generated from free-air data and GTOPO30 DEM data, were compiled for Black Sea and Eastern Mediterranean in this study. These maps are useful to interpret the general structure of the study areas.

The density of sea-water (1.03 g/cm^3) is replaced by 2.69 g/cm^3 to calculate Simple Bouguer anomalies. This results in strongly positive Bouguer anomalies over the sea and masking the effects of subsurface density variations. The preferred way is to use free-air anomalies at sea and Bouguer anomalies on land.

According to new compiled maps, sea floor topographic features don't affect Black Sea but affect the Eastern Mediterranean gravity field. The sediments filled in the Black Sea sub basins show weak free-air anomalies ranging between -40 and 40 mGal. The buried ridge in the Black Sea has negative weak free-air anomalies effect on the gravity field.

In the Eastern Mediterranean, the bathymetric features are coincided with the gravity anomalies. Over the Mediterranean Ridge, Anaximander Mountains and Eratosthenes Seamount are characterized by negative gravity lows. Over the Nile

Cone, the positive gravity anomalies are observed, most probably due to high sediment accumulation.

Gravity data require extensive processing to apply varied corrections. Also, resultant models are non-unique and generally require some knowledge of the subsurface geology or additional data from other methods. However, the gravity modeling is significant for the researches to study the earth's deep structure where it is very hard or impossible to get seismic information. Furthermore, three dimensional gravity modeling has the advantage to show the horizontal distribution of the results.

Large scale three dimensional density models for Black Sea and Eastern Mediterranean have been constructed. The model consists of three layers; water, sediments and the crust. The gravity effects of the two first layers were calculated. Then, based on the residual of observed minus the total of the first layers, the crust layer was constructed. Finally, the thickness of the crust and the depth of Moho discontinuity were determined.

According to the constructed models and calculated gravity effects, the crustal structures of the Black Sea and Eastern Mediterranean were carried out. In the western Black Sea basin, the thickness of the crystalline crust is about 5 km whereas in the eastern Black Sea basin is about 15 km. The Moho rises from about 30 km, along the shoreline to 19 km in the western Black Sea.

In the Eastern Mediterranean Sea, it is believed that two type of crust exist. The crust beneath the Levantine and Herodotus basins is characterized by thin and possibly oceanic crust. The northern part of the study area, Cyprus and Eratosthenes seamount are marked by thick continental crust. The rapid change in the crust thickness over the sea possibly presents the plate boundary.

REFERENCES

Aksu, A.E., Uluğ, A., Piper, D.J.W., Konuk, T., Turgut, S., 1992a. Quaternary sedimentary history of Adana, Cilicia and Iskenderun Basins, northeast Mediterranean Sea. Mar. Geol. 104, 55– 71.

Aksu, A.E., Calon, T.J., Piper, D.J.W, Turgut, S., Izdar, E.K., 1992b. Architecture of late orogenic basins in the eastern Mediterranean Sea. Tectonophysics 210, 191– 213.

Aksu, A.E., Hall, J., Yaltırak, C., 2005a. Editorial: Miocene to recent tectonic evolution of the eastern Mediterranean: new pieces of the old Mediterranean puzzle. Mar. Geol. 221, 1-13.

Aksu, A.E., Calon, T.J., Hall, J., Mansfield, S., Yaşar, D., 2005b. The Cilicia-Adana Basin complex, eastern Mediterranean: Neogene evolution of an active fore-arc basin in an obliquely convergent margin. Mar. Geol. 221, 211–259.

Aksu, A.E., Calon, T.J., Hall, J., Yaşar, D., 2005c. Origin and evolution of the neogene iskenderun basin, Northeastern Mediterranean Sea. Mar. Geol. 221, 135–151.

Ambraseys N.N., Adams R.D., 1993. Seismicity of the Cyprus region, Terra Nova 5, 88–94.

Anastasakis, G., Kelling, G., 1991. Tectonic connection of the Hellenic and Cyprus Arcs and related geotectonic elements. Mar. Geol. 97, 261– 277.

Andersen, O.B., and Knudsen, P.,1995. Global gravity field from the ERS-1 geodetic mission. Earth Observation Quarterly, No. 47, 1-5.

Ayala, C., Torne, M., Pous, J., 2003. The lithosphere-asthenosphere boundary in the western Mediterranean from 3D joint gravity and geoid modeling: tectonic implications. Earth and Planetary Sciences Letters, 209, 275-290.

Barka, A.A., and R. Reilinger (1997). Active tectonics of the Eastern Mediterranean region: deduced from GPS, neotectonic and seismicity data, Anal. Geofis. 6, 587–610.

Balavadze, B.K. and Mindeli, P.Sh., 1965. Earth's crustal Structure in the Black Sea basin based on geophysical data. Seism.Issled.RezultAbstr. Soviet-Bloc Res., Geophys., Astron., Space, 145: 77-78.

Belousov, V.V., Volvovsky, B.S., Arkhipov, I.V., Buryanov, V.B., Evsyukov, Y.D., Goncharov, V.P., Gordienko, V.V., Ismagilov, D.F., Kislov, G.K., Kogan, L.I., Kondyurin, A.V., Kozlov, V.N., Lebedev, L.I., Lokholatnikov, V.M., Malovitsky, Y.P., Moskalenko, V.N., Neprochnov, Y.P., Ostisty, B.K., Rusakov, O.M., Shimkus, K.M., Shlezinger, A.E., Sochelnicov, V.V., Sollogub, V.B., Solovyev, V.D., Starostenko, V.I., Starovoitov, A.F., Terechov, A.A., Volvovsky, I.S., Shigunov, A.S., Zolotarev, V.G., 1988. Structure and evolution of the Earth's crust and upper mantle the Black Sea. Bolletino di Geofisica Teorica ed Applicata 30 (117– 118), 109– 196.

Ben Avraham, Z., Tibor, G., Limanov, A.F., Leybov, M.B., Ivanov, M.K., Tokarev, M.Yu., Woodside, J.M., 1995. Structural and tectonics of the eastern Cyprus Arc. Mar. Pet. Geol. 12, 263– 271.

Ben-Avraham, Z., 1986. Multiple opening and closing of the Eastern Mediterranean and South China Basins. Tectonics, 8:5̄1362.

Ben-Avraham, Z., 1989. Multiple opening and closing of the eastern Mediterranean and south China basins. Tectonics 8, 351– 362.

Ben-Avraham, Z., and Tibor, G., 1994. Structure and tectonics of the Eastern Cyprus arc. Am. Geophys. Union, 117. (Abstract)

Ben-Avraham, Z., Ginzburg, A., Makris, J., Eppelbaum., L., 2002. Crustal Struture of the Levant basin, eastern Mediterranean. Tectonophysics, 346, 23-43.

Ben-Gai, Y., Ben-Avraham, Z., Buchbinder, B., and Kendall, C.G.S.C., 2005. Post-Messinian evolution of the Southeastern Levant Basin based on two-dimensional stratigraphic simulation, Marine Geology, 221, 359-379.

Biju-Duval B., Letouzey J., Montadert L., 1978. Structure and evolution of the Mediterranean basins, Initial Report of Deep Sea Drilling Project 42 , 951– 984.

Blakely, R.J., 1995. Potential Theory in Gravity & Magnetic Applications. Cambridge University Press, Cambridge, 441pp.

Bocaletti, M., Dainelli, P. Manetti, P., Mannori, M.R., 1988a. Tectonic framework of the Circum-Black Sea region. Bolletino di Geofisica Teorica ed Applicata 30 (117– 118), 5– 8.

Bocaletti, M., Manetti, P., 1988. The main unconformities and tectonic events in the Pontides. Bolletino di Geofisica Teorica ed Applicata 30 (117– 118), 9– 16.

Boccaletti, M., Cassinis, R., Danielli, P., Marino, C.M., Tibaldi, A., Zanchi, A., 1988b. Landsat featurews in the Black Sea Area: their tectonic significance. Bolletino di Geofisica Teorica ed Applicata 30 (117– 118), 17– 38.

Bridge, C., Calon, T. J., Hall, J., and Aksu, A. E., 2005. Salt tectonics in two convergent-margin basins of the Cyprus arc, Northeastern Mediterranean, Marine Geology, 221, 223-259.

Burton-Ferguson, R., Aksu, A. E., Calon, T. J., and Hall, J.,2005.Seismic stratigraphy and structural evolution of the Adana Basin, eastern Mediterranean, Marine Geology, 221, 189-222.

Cady, J.W., 1980. Calculation of gravity and magnetic anomalies of finite-length right polygonal prisms. Geophysics, v45, 10, 1507-1512.

Calon, T. J., Aksu, A. E., and Hall, J., 2005a. The Neogene evolution of the Outer Latakia Basin and its extension into the Eastern Mesaoria Basin (Cyprus), Eastern Mediterranean, Marine Geology, 221, 61-94.

Calon, T. J., Aksu, A. E., and Hall, J., 2005b. The Oligocene-Recent evolution of the Mesaoria Basin (Cyprus) and its western marine extension, Eastern Mediterranean, Marine Geology, 221, 95-120.

Çiftçi, G., Dondurur, D., Ergün, M., 2002. Sonar and Gihg Resolution Seismic Studies in the Eastern Black Sea.

Cooper, R.I.B., Harrison, J.C., Wilmore, P.L., 1952. Gravity measurements in the eastern Mediterranean. Phil. Trans. A, 244, 533.

Dachev, C., Stanev, V., Bokov, P., 1988. Structure of Bulgarian Black Sea Area. Bolletino di Geofisica Teorica ed Applicata 30 (117– 118), 79– 108.

Dewey, J.F., Hempton, M.R., Kidd, W.S.F., Saroğlu, F., and Şengör, A.M.C., 1986. Shortening of continental lithosphere: the Neotectonics of Eastern Anatolia: a young collision zone. Geol. Soc. Spec. Publ. London, 19-336.

Dobrin, M.B., 1981. Introduction to Geophysical Prospecting. McGraw-Hill, International Student Edition, 630pp.

Ergün, M and .Çiftçi, G., 1999. Gas saturated shallow sediments in the eastern Black Sea and geohazard effects. Offshore Technology Conference Proceedings, 621-630.

Eva, C., Riuscetti, M., Slejko, D., 1988. Seismicity of the black Sea region. Bolletino di Geofisica Teorica ed Applicata 30 (117– 118), 53– 66.

Featherstone, W.E., 2003. Comparison of different satellite altimeter-derived gravity anomaly grids with ship-borne gravity data around Australia, in: Tziavos, I.N. (ed) Gravity and Geoid 2002, Department of Surveying and Geodesy, Aristotle University of Thessaloniki, 326-331.

Finetti, I. and Morelli, C., 1973. Geophysical Exploration of the Mediterranean Sea. Bolletino di Geofisica Teorica ed Applicata, XV, 263-341.

Finetti, I., Bricchi, G., Del Ben, A., Pipan, M., Xuan, Z., 1988. Geophysical study of the Black Sea area. Bolletino di Geofisica Teorica ed Applicata 30 (117– 118), 197– 324.

Garfunkel Z., 1998. Constraints on the origin and history of the Eastern Mediterranean basin, Tectonophysics 298, 5–35.

Gass, I.G., and Masson-Smith, D., 1963. The geology and gravity anomalies of the Troodos Massif, Cyprus. Philos. Trans. R. Soc. London A, 255: 417-467.

Girdler, R.W., Harrison, J.C., 1957. Submarine gravity measurements in the Atlantic Ocean, Indian Ocean, Red Sea and Mediterannean Sea. Proc. R. SOC. London A 239, 202.

Görür, N., 1988. Timing of opening of the Black Sea. Tectonophysics 147, 247– 262.

GTOPO30, 1996. "Global 30 Arc Second Elevation Data Set". Reston: US Geological Survey.

Hall, J., Aksu, A. E., Calon, T. J., and Yasar, D., 2005a. Varying tectonic control on basin development at an active microplate margin: Latakia Basin, Eastern Mediterranean, Marine Geology, 221, 15-60.

Hall, J., Calon, T. J., Aksu, A. E., and Meade, S. R., 2005b. Structural evolution of the Latakia Ridge and Cyprus Basin at the front of the Cyprus Arc, Eastern Mediterranean Sea, Marine Geology, 221, 261-297.

Hayward, A.B., and Robertson, A.H.F., 1982. Direction of ophiolite emplacement inferred from Cretaceous and Tertiary sediments of an adjacent autochthon, the Bey Dañlar2, S.W. Turkey. Bull. Geol. Soc. Am., 93: 6875.

Hinze, W.J., 2003. Bouguer reduction density, why 2.67. Geophysics, 68, 5, 1559-1560.

Hsü, K.J., 1978. When the Black Sea was drained, Scientific American, 238, 52-63.

Hsü, K.J., Montadert, L., Bernoulli, D., Cita, M.B., Erickson, A., Garrison, R.E., Kidd, R.B., Melieres, F., Muller, C., Wright, R., 1978. History of the Mediterranean salinity crisis. In: Hsü , K., Montadert, L., et al., (Eds.), Initial Reports of the Deep Sea Drilling Project XLII, Part I. U.S. Government Printing Office, Washington, pp. 1053– 1078.

IBCM-PQ Map, 1993. Thickness of the Plio-Quaternary Sediments. Intergovermental Oceanographic Commision.

İşler, F.I., Aksu, A.E., Hall, J., Calon, T.J., Yaşar, D., 2005. Neogene development of the Antalya Basin, Eastern Mediterranean: and active fore-arc basin adjacent to an arc junction. Mar. Geol. 221, 237–265.

IOC, IHO and BODC, 2003. Centenary Edition of the GEBCO Digital Atlas, published on CD-ROM on behalf of the Intergovernmental Oceanographic Commission and the International Hydrographic Organization as part of the General Bathymetric Chart of the Oceans, British Oceanographic Data Centre, Liverpool, U.K.

Ivanov, M.K., Limonov, M.K., and Woodside, J.M., 1992. Geological and geophysical investigations in the Mediterranean and Black Seas: initial results of the "Training through Research" Cruise of RV Gelendzhik in the Eastern

Mediterranean and the Black Sea (July, 1991), UNESCO Rept. Mar. Sci., 1992.

Kazmin, V.G., Schreider, A.A., Bulychev, A.A., 2000. Early stages of evolution of the Black Sea. In: Bozkurt, E., Winchester, J.A., Piper, J.D.A. (Eds.), Tectonics and Magmatism in Turkey and 178 D.J. Meredith, S.S. Egan / Tectonophysics 350 (2002) 157–179 the Surrounding Area. Geological Society, London, Special Publications, vol. 173, pp. 235– 249.

Kempler D., Ben-Avraham Z., 1987. The tectonic evolution of the Cyprean Arc, Annal. Tecton., 1, 58–71.

Kempler D., Garfunkel Z.,1994. Structure and kinematics in the northeastern Mediterranean: a study of an irregular plate boundary, Tectonophysics, 234, 19–32.

Kılıçoğlu, A., 2005. Gravity anomaly map over the Black Sea using corrected sea surface height from ERS1, ERS2 and TOPEX/POSEIDON satellite altimetry missions. Stud. Geophys. Geod., 49, 1-12.

Krijgsman, W., Hilgen, F.J., Raffi, I., Sierro, F.J., Wilson, D.S., 1999. Chronology, causes and progression of the Messinian salinity crisis. Nature 400, 652– 655.

Le Pichon, X., 1982. Land-locked oceanic basins and continental collision: the Eastern Mediterranean as a case example, in: Hsü K. (Ed.), Mountain Building Processes, Academic Press, London, pp. 201–211.

Li, X., and Götze, H.J., 2001. Ellipsoid, geoid, gravity, geodesy, and geophysics. Geophysics, 66, 1660-1668.

Maia, M. 2006. Comparing the use of marine and satellite data for geodynamic studies. ESA Symposium "15 Years of Progress in Radar Altimetry", Venice Italy, March 13-18.

Makris, J., and Stobbe, C., 1984. Physical properties and state of the upper mantle of the Eastern Mediterranean deduced from geophysical data. In Morelli, C. (Ed.), Geological and Geodynamical Aspects of the Mediterranean. Mar. Geol., 55: 347-363.

Makris, J., Ben-Avraham, Z., Behle, A., Ginzburg, A., Giese, P., Steinmetz, L., Whitmarsh, R.B., Fleftheriou, S., 1983. Seismic refraction profiles between

Cyprus and Israel and their interpretation. Geophys. J. R. Astron. Soc. 75, 575– 591.

Makris, J., Wang, j., Odintsov, S.D., Udintsev, G.B., 1994. The magnetic ¢eld of the Eastern Mediterranean Sea, in: V.A. Krasheninnikov, J.K. Hall (Eds.), Geological Structure of the Northeastern Mediterranean (Cruise 5 of the Research Vessel `Akademik Nikolaj Strakhov'), Historical Productions- Hall Ltd, Jerusalem, pp. 75-86.

Manetti, P., Bocaletti, M., Peccerillo, A., 1988. The Black Sea: remnant of a marginal basin behind the Srednogorie-Pontides Islands-arc system during the upper Cretaceous-Eocene times. Bolletino di Geofisica Teorica ed Applicata 30 (117– 118), 39.52.

McClusky, S., S. Balassanian, A. A. Barka, C. Demir, S. Ergintav, I. Georgiev, O. Gurkan, M. Hamburger, K. Hurst, H. Kahle, K. Kastens, G. Kekelidze, R. King, V. Kotzev, O. Lenk, S. Mahmoud, A. Mishin, M. Nadariya, A. Ouzouins, D. Paradissis, Y. Peter, M. Prilepin, R. Reilinger, I. Sanli, H. Seeger, A. Tealeb, M. N. Toksöz, and G. Veis, 2000. Global positioning system constraints on plate kinematics and dynamics in the eastern Mediterranean and Caucasus, J. Geophys. Res., 105, 5695–5719.

McKenzie, D. P., 1970. The plate tectonics of the mediterranean region. Nature 226, 239-41.

Meisner, L.B., Gorshkoz., A.S., Tugolesov, D.A., 1995. Neogene- Quaternary sedimentation in the Black Sea basin. Erler, A., Ercan, T., Bingöl, E., Örçen, S. (Eds), Geology of the Black Sea Basin. General Directorate of Min. Res. And Explor., Ankara, 131-136.

Meredith, D.J. and Egan, S.S., 2002. The geological and geodynamic evolution of the eastern Black Sea basin: insights from 2-D and 3-D tectonic modeling, Tectonophysics, 350, 157– 179.

Mindeli, P.Sh., Neprochnov, Yu. P., Pataraya, E.I., 1965. Granite-free area in the Black Sea trough from DSS data seismology. Inter. Geol.Rev., 8/1:36-43.

Morelli, C., Pisani, M., Gantar, C., 1975. Geophysical studies in the Aegean Sea and in the Eastern Mediterranean. Bolletino di Geofisica Teroica ed Applicata, Vol. XVIII, 127-168.

Nabighian, M.N., Ander, M.E., Grauch, V.J.S., Hansen, R.O., LaFehr, T.R., Li, Y., Pearson, W.C., Peirce, J.W. , Phillips, J.D., Ruder M.E., 2005. Historical development of the gravity method in exploration. Geophysics, 70, 6, 63-89.

Nesteroff WD, Lort JM, Angelier J, Bonneau M, Poisson A. 1977. Esquisse structurale en Mediterranee orientale au front de d'Arc Egeen. In Symposuim on the Structural History of the Mediterranean Basin, Biju-Duval B, Montatert L (eds). Editions Technip: Paris.

Nettleton, L. L. 1942. Gravity and magnetic calculations. Geophysics, 7, 293–310.

Nikishin, A., Ziegler, P.A., Panov, D.I., Nazarevich, B.P., Brunet, M.-F., Stephenson, R.A., Bolotov, S.N., Korotaev, M.V., Tikhomirov, P.L., 2001. Mesozoic and Cenozoic evolution of the Scythian Platform – Black Sea – Caucasus domain. In: Ziegler, P.A., Cavazza, W., Robertson, A.H.F., Crasquin-Soleau, S. (Eds.), Peri-Tethys Memoir 6: Peri-Tethyan Rift/Wrench Basins and Passive Margins. Me´moires du Muse´um national d'Histoire naturelle, Paris, vol. 186, pp. 295– 346.

Nikishin, A.M., Korotaev, M.V., Ershov, A.V., Brunet, M., 2003. The Black Sea basin: tectonic history and Neogene–Quaternary rapid subsidence modeling. Sedimentary Geology, 156, 149–168

Nur, A., Ben-Avraham, Z., 1978. The eastern Mediterranean and the Levant, tectonics of continental collision. Tectonophysics 46, 297– 311.

Okay, A.I., Sahintürk, O., 1997. Geology of the Eastern Pontides. In: Robinson, A.G. (Ed.), Regional and Petroleum Geology of the Black Sea and Surrounding Region. American Association of Petroleum Geologists, Tulsa, Oklahoma, Memoir, vol. 68, pp. 291–311.

Okay, A.I., Sengor, A.M.C., Gorur, N., 1994. Kinematic history of the opening of the Black Sea and its effect on the surrounding regions. Geology 22, 267–270.

Oral, M.B., Reilinger, R.E., Toksoz, R.E., W. King, A.A. Barka, I. Kinik, O. Lenk, 1995. Global positioning system offers evidence of plate motions in eastern Mediterranean, EOS Trans. AGU.

Özelçi, H.F., 1972. Gravity anomalies of the Eastern Mediterranean. Bull. Min. Res. Explor. Inst., 80,54.

Özhan G., 1988. Sismik yansıma verileri ışığında Kuzeydoğu Akdeniz. Geol. Bul. of Turkey, 31, 51-62.

Papazachos, B.C., Papaioannou, Ch.A., 1999. Lithospheric boundaries and plate motions in the Cyprus area. Tectonophysics 308, 193– 204.

Persoglia, S., Pipan, M., Vesnaver, A., Special processing of the Black Sea seismic data. Bolletino di Geofisica Teorica ed Applicata 30 (117– 118), 67– 78.

Plouff, D., 1976. Gravity and magnetic fields of polygonal prisms and application to magnetic terrain corrections, Geophysics, 41, 727–741.

Rabinowitz, P.D., and Ryan, W.B.F., 1970. Gravity anomalies and crustal shortening in the eastern Mediterranean, Tectonophysics 10, pp. 585–608.

Rangin, C., Bader, A.G., Pascal, G., Ecevitoğlu, B., Görür, N., 2002. Deep Structure of the MİD Black Sea High (offshore Turkey) imaged by multi-channel seismic survey (BLACKSIS Cruise). Marine Geology, 18, 265-278.

Rasmussen, R. and Pedersen, L.B., 1979. End correlation in potential field modeling. Geophysical Prospecting, 27, 749-760.

Reilinger, R. E., S. C. McClusky, B. M. Oral, R. W. King, and M. N. Toksöz, 1997. Global positioning system measurements of present day crustal movements in the Arabia-Africa-Eurasia plate collision zone, J. Geophys. Res. 102, 9983–9999.

Riad, S., Refai, E., Ghalib, M., 1981. Bouguer Anomalies and Crustal Structure in the Eastern Mediterranean. Tectonophysics, 71, 253-266.

Robertson A.H.F., Kidd R.B., Ivanov M.K., Limonov A.F., Woodside J.M., Galindo-Zaldivar J., Nieto L., 1994. The scientific party of the 1993 TTR-3 Cruise, Probing continental collision in the Mediterranean Sea, EOS Transactions AGU 75, 233.

Robertson, A.H.F., 1998a. Mesozoic–Tertiary tectonic evolution of the easternmost Mediterranean area: integration of marine and land evidence. In: Robertson, A.H.F., Emeis, K.-C., Richter, C., Camerlenghi, A. (Eds.), Proceedings of the Ocean Drilling Program. Scientific Results, vol. 160, pp. 723– 782.

Robertson, A.H.F., 1998b. Tectonic significance of the Eratosthenes Seamount: a continental fragment in the process of collision with a subduction zone in the eastern Mediterranean (Ocean Drilling Program Leg 160). Tectonophysics, 298, 63-82.

Robertson, A.H.F., and Woodcock, N.H., 1979. The Mamonia Complex, south west Cyprus: the evolution and emplacement of a Mesozoic continental margin. Geol. Soc. Am. Bull., 90:651̃665.

Robertson, A.H.F., Eaton, S., Follows, E.J., Payne, A.S., 1995. Depositional processes and basin analysis of Messinian evaporitesin Cyprus. Terra Nova 7, 233– 253.

Robinson, A., Spadini, G., Cloetingh, S., Rudat, J., 1995. Stratigraphic evolution of the Black Sea: inferences from basin modeling. Marine and Petroleum Geology, Vol. 12, No. 8, pp. 821-835.

Robinson, A.G., Rudat, J.H., Banks, C.J., Wiles, R.L.F., 1996. Petroleum geology of the Black Sea. Marine and Petroleum Geology, Vol. 13, No. 2, pp. 195-223.

Robinson, A.G. (Ed.), 1997. Regional and Petroleum Geology of the Black Sea and Surrounding Region. American Association of Petroleum Geologists Memoir, 68, Tulsa, Oklahoma, 385 pp.

Ross D.A., 1974. The Black Sea. In A.Burke and Charles L. Drake, The Geology of Continental Margins, 669-682, Springer-Verlag, Berlin.

Ross D.A., Uchupi E., Prada K.E., MacIlvaine J.C., 1974. Bathymetry and microtopography of Black Sea. In: E.T. Degens and D.A. Ross, The Black Sea-Geology, Chemistry and Biology, American Association of Petroleum Geologists, Memoir, 20, Tulsa, Oklahoma, 1-10.

Rotstein, Y., Ben-Avraham, Z., 1985. Accretionary processes at subduction zones in the eastern Mediterranean. Tectonophysics 112, 551–561.

Rotstein, Y., Kafka, A.L., 1982. Seismotectonics of the southern boundary of Anatolia, eastern Mediterranean, subduction, collision, and arc jumping. J. Geophys. Res. 87, 7694-7706.

Ryan, W.B.F., 1969. The floor of the Mediterranean Sea. PhD Thesis. Columbia University, New York. 236 pp.

Ryan, W.B.F., Hsu, K.J., et al., 1973. Init. Repts. DSDP, 13 (Pts. 1 and 2): Washington (U.S. Govt. Printing Office), 1447 pp.

Sandwell, D. T., and Smith, W. H. F., 1995. Marine Gravity anomaly from satellite altimetry. Map, Geologic Data Center, Scripps Institute of Oceonography, La Jolla, CA.

Sandwell, D. T., and Smith, W. H. F., 1997. Marine gravity anomaly from Geosat and ERS 1 satellite altimetry, Journal of Geophysical Research, v. 102 , No. B5, p. 10039-10054.

Şengör A.M.C., Görür N., Saroğlu F., 1985. Strike-slip faulting and related basin formation in zones of tectonic escape: Turkey as a case study, in: Biddle K.T., Christie-Blick N. (Eds.), Strike-slip Faulting and Basin Formation, Soc. Econ. Paleontol. Mineral. Sp. Pub., 37, pp. 227–264.

Spadini, G., Robinson, A., Cloetingh, S., 1996. Western versus Eastern Black Sea tectonic evolution: pre-rift lithospheric controls on basin formation. Tectonophysics 266, 139–154.

Starostenko, V., Buryanov, V., Makarenko, I., Rusakov, O., Stephenson, R., Nikishin, A., Georgiev, G., Gerosimov, M., Dimitriu, R., Legostaeva, O., Pchelarov, V., Sava, C., 2004. Topography of the crust-mantle boundary beneath the Black Sea Basin. Tectonophysics, 381, 211-233.

Talwani, M. and Eving, M., 1960. Rapid computation of gravitational attraction of three dimensional bodies of arbitrary shape. Geophysics, 25, 203-225.

Talwani, M., Worzel, J.L., Landisman, M., 1959.Rapid gravity computations for two dimensional bodies with application to the Mendocino submarine fracture zone.. J. Geophys. Res, 64, 49-59.

Tari, E., Şahin, M., Barka, A., Reilinger, R., King, R.W., McClusky, S., Prilepin, M., 2000. Active tectonics of the Black Sea with GPS. Earth Planets Space, 52, 747–751.

Taviani M. and Rossi S., 1989. Salt-related deformations in the deep Antalya Basin: preliminary results of the Mac Gan Cruise. Mar. Geol., 87, 5-13.

Telford, W., Geldart, L.P., Sheriff, R.E., 1990. Applied Geophysics, 2en ed., Cambridge University Press, Cambridge.

Ten Veen, J.H., Woodside, J.M., Zitter, T.A.C., Dumont, J.F., Mascle, J., Volkonskaia, A., 2004. Neotectonic evolution of the Anaximander Mountains at the junction of the Hellenic and Cyprus arcs. Tectonophysics, 391, 35-65.

Tezcan, D., 2001. Seismic Stratigraphy of late Quaternary sediments on the continental shelf of Antalya Bay. M.Sc. Thesis, Institute of Marine Sciences, Middle East Technical University, Erdemli, İçel, Turkey, 62pp.

Tezcan, D., Okyar, M., 2001. Antalya Körfezi batı kıta sahanlığının geç Kuvaterner sedimanlarının sismik stratigrafisi. Türkiye Kuvaterneri Çalıştayı, Bildiri Özetleri Kitapçığı, 21-22 Mayıs. İTÜ Avrasya Yer Bilimleri Enstitüsü, Süleyman Demirel Kültür Merkezi, İTÜ, İstanbul, pp. 45.

Tezcan, D., Okyar, M., 2003. Seismic stratigraphy of late Quaternary sedimentation the continental shelf of Antalya bay. Proceeding of the "Second International Conference on Oceanography of the Eastern Mediterranean and Black Sea: Similarities and Differences of Two Interconnected Basins", 14-18 October, METU Cultural and Convention Center, Ankara, Turkey, pp 974-977.

Tezcan, D. and Okyar, M., 2006. Seismic Stratigraphy of late Quaternary deposits on the continental shelf of Antalya Bay, Northeastern Mediterranean. Continental Shelf Research, 26, 1595-1616.

Tibor, G., Ben-Avraham, Z., 2005. Late Tertiary paleodepth reconstruction of the Levant margin off Israell. Marine Geology, 221, 331-347.

Tibor, G., Ben-Avraham, Z., Steckler, M., Fligelman, H., 1992. Late Tertiary subsidence history of the southern Levant margin and its implication to the Messinian event. J. Geophys. Res. 97, 593– 614.

Tugolesov, D.A., Gorshkov, A.S., Meysner, J.B., Solovyev, V.V., Khakhalev, YE.M., 1985. The tectonics of the Black Sea Trough. Geotectonics, 19, 6, 435-445.

Turcotte, D. and Schubert, G., 2002. Geodynamics. Cambridge University Press. Second Edition, Cambridge, 456pp.

Underhill, J.R., 1989. Late Cenozoic deformation of the Hellenide foreland, western Greece. Geol. Soc. Am. Bull., 101:613-634.

Vening-Meinesz, F. A. 1934. Gravity expeditions at sea, vol. 2. Delft: J. Waltman.

Verzhbitsky, E., Kuzin, I., Lobkovsky, L., 2002. Age and Thickness of the Lithosphere within the Western and Eastern Basins of the Black Sea according to Geophysical Data. Turkish Journal of Earth Sciences (Turkish J. Earth Sci.), Vol. 11, 2002, pp. 231-242.

Vidal, N., Alvarez-Maro´n, J., Klaeschen, D., 2000. The structure of the Africa–Anatolia plate boundary in the eastern Mediterranean. Tectonics 19, 723–739.

Vidal, N., Alvarez-Marron, J., Klaeschen, D., 2000a. Internal configuration of the Levantine Basin from seismic reflection data (eastern Mediterranean). Earth and Planetary Science Letters 180, 77-89.

Vidal N, Klaeschen D, Kopf A, Docherty C, Von Huene R, Krasheninnikov VA. 2000b. Seismic images at the convergence zone from south of Cyprus to the Syrian coast, eastern Mediterranean. Tectonophysics 329: 157–170.

Vogt, P.R., Higgs, R.H., Jonshon, G.L., 1971. Hyphotesis on the origin of the Mediterranean Basin: magnetic data. J. Geophys. Res., v76, 3207-3228.

Whitechurch, H., Juteau, T., and Montigny, R., 1984. Role of the Eastern Mediterranean ophiolites (Turkey, Syria, Cyprus) in the history of the Neo-Tethys. In Dixon, J.E., and Robertson, A.H.F. (Eds.), The Geological Evolution of the Eastern Mediterranean. Geol. Soc. Spec. Publ. London, 17:301-318.

Woodcock, N.H., and Robertson, 1982. Wrench and thrust tectonics along a Mesozoic-Cenozoic continental margin: Antalya Complex, S.W. Turkey. J. Geol. Soc. London, 139:147̃163.

Woodside, J.M. and Bowin, C.O., 1970. Gravity anomalies and inferred Crustal Structure in the Eastern Mediterranean Sea. Geol. Soc. Am. Bull., 81, 1107-1122.

Woodside, J.M., 1977. Tectonic elements and crust of the eastern Mediterranean Sea. Mar. Geophys. Res. 3, 317– 354.

Woodside, J.M., and Dumont, J.F., 1997. The Anaximander Mountains area southward rifted and foundered part of the southwestern Turkish Tauruss. Terra Nova (Suppl.), 9:394. (Abstract)

Woodside, J.M., Mascle, J., Zitter, T.A.C., Limonov, A.F., Ergün, M., Volkonskaia, A., Shipboard scientists of the PRISMED II Expedition, 2002. The Florence Rise, the Western Bend of the Cyprus Arc. Marine Geology, 185, 177-194.

Yegorova, T., Starostenko, V., 1999. Large-scale 3-D gravity analysis of the lithosphere below the transition zone from western Europe to the East European Platform. Tectonophysics, 314, 83-100.

Yegorova, T., Starostenko, V., 2002. Lithosphere structure of European sedimentary basins from regional three-dimensional gravity modeling. Tectonophysics, 346, 5-21.

Zitter, T.A.C., Woodside, J.M., Mascle, J., 2003. The Anaximander Mountains: a clue to the tectonics of southwest Anatolia. Geol. J. 38, 375– 394.

Zonenshain, L.P. and Le Pichon. 1986. Deep basins of the Black Sea and Caspian Sea as remnants of Mesozoic backarc basins.Tectonophysics 123, 181-211.

e-mail: dtezcan@gmail.com

Date of Birth   25 February 1975; Germany

Education

02/2008	Ph.D., Dept. of Marine Geology and Geophysics; Institute of Marine Sciences, Middle East Technical University, Mersin, Turkey.
08/2001	M. Sc., Dept. of Marine Geology and Geophysics; Institute of Marine Sciences, Middle East Technical University, Mersin, Turkey.
09/1998	B.S., Geophysical Engineering; Ankara University, Ankara, Turkey.

Languages

    Turkish- Native,

    English- Fluent reading and writing,

    French- Fluent reading and writing,

Publications:

Tezcan D. and Okyar M., 2006. Seismic stratigraphy of Late Quaternary deposits on the continental shelf of Antalya Bay, Northeastern Mediterranean. Continental Shelf Research, Volume 26, Issue 14.